Alejandro Carrillo Lozada

Environment-induced anisotropy and the sensitivity of the radical pair mechanism in the avian compass

Anisotropia induzida pelo ambiente e a sensibilidade do mecanismo de pares radicais na orientação magnética aviária

Campinas
2013

Universidade Estadual de Campinas
Instituto de Física Gleb Wataghin

Alejandro Carrillo Lozada

Environment-induced anisotropy and the sensitivity of the radical pair mechanism in the avian compass

Orientador: Prof. Dr. Marcos Cesar de Oliveira
Co-orientador: Silvio Antonio Sachetto Vitiello

Anisotropia induzida pelo ambiente e a sensibilidade do mecanismo de pares radicais na orientação magnética aviária

Tese de Mestrado apresentada ao Programa de Pós-Graduação em Fsica do Instituto de Física Gleb Wataghin da Universidade Estadual de Campinas para obtenção do título de Mestre em Física.

Master Dissertation submitted to the Graduate Program of the Physics Institute Gleb Wataghin at Universidade Estadual de Campinas to obtain the M. Sc. degree in physics.

Este exemplar corresponde à versão final da dissertação de mestrado defendida pelo aluno Alejandro Carrillo Lozada e orientada pelo Prof. Dr. Marcos Cesar de Oliveira.

Marcos Cesar de Oliveira

Campinas
2013

FICHA CATALOGRÁFICA ELABORADA POR
MARIA GRACIELE TREVISAN – CRB8/7450 - BIBLIOTECA DO IFGW
UNICAMP

C235e

Carrillo Lozada, Alejandro, 1983-
Enviroment-induced anisotropy and the sensitivity of the radial pair mechanism in the avian compass / Alejandro Carrillo Lozada. -- Campinas, SP : [s.n.], 2013.

Orientador: Marcos Cesar de Oliveira.
Dissertação (mestrado) – Universidade Estadual de Campinas, Instituto de Física "Gleb Wataghin".

1. Navegação aviária. 2. Mecanismo par radical. 3. Anisotropia magnética. 4. Correlações quânticas. I. Oliveira, Marcos Cesar de, 1969- II. Universidade Estadual de Campinas. Instituto de Física "Gleb Wataghin". III. Título.

Informações para Biblioteca Digital

Título em inglês: Enviroment-induced anisotropy and the sensitivity of the radial pair mechanism in the avian compass
Palavras-chave em inglês:
Avian navigation
Radical par mechanism
Magnetic anisotropy
Quantum correlations
Área de Concentração: Física
Titulação: Mestre em Física
Banca Examinadora:
Marcos Cesar de Oliveira [Orientador]
Marcus Aloizio Martinez de Aguiar
Salomon Sylvain Mizrahi
Data da Defesa: 07-04-2013
Programa de Pós-Graduação em: Física

MEMBROS DA COMISSÃO JULGADORA DA DISSERTAÇÃO DE MESTRADO DE **ALEJANDRO CARRILLO LOZADA – R.A. 115265** APRESENTADA E APROVADA AO INSTITUTO DE FÍSICA "GLEB WATAGHIN", DA UNIVERSIDADE ESTADUAL DE CAMPINAS, EM 04 / 04 / 2013.

COMISSÃO JULGADORA:

Prof. Dr. Marcos Cesar de Oliveira - Orientador do Candidato
DFMC/IFGW/UNICAMP

Prof. Dr. Salomon Sylvain Mizrahi – DF/UFSCar

Prof. Dr. Marcus Aloizio Martinez de Aguiar
DFMC/IFGW/UNICAMP

A mi madre y a mi padre, por enseñarme a leer caminos entre la niebla;
por ser faros cuando no había estrellas.

A mis hermanas por su cariño, risas y verdades.

Acknowledgements

I would like to express my sincere gratitude to my advisor Prof. Marcos Cesar de Oliveira for the continuous support of my research, for his patience, motivation, enthusiasm, and immense knowledge.

Besides my advisor, I would like to thank my thesis committee: Prof. Marcus A.M. de Aguiar and Prof. Salomon Sylvain Mizrahi, for their encouragement, insightful comments, and hard questions.

To Dr. Marcio F. Cornelio for all the illuminating discussions.

I thank my fellow comrades at the group: John Lozada, Olimpio de Sá Neto, Dr. Fernando Nicácio and Frank E. S. Steinhoff for the stimulating discussions.

Abstract

Earth's magnetic field is essential for orientation of migratory birds. The most promising explanation for this orientation employs the photo-stimulated radical pair (RP) mechanism, conjectured to occur in cryptochrome photoreceptors. This last conjecture has been particularly reinforced recently by the evidence of magnetosensivity of human cryptochrome. The radicals must have an intrinsic anisotropy in order to define a reference frame for this kind of "compass". This anisotropy, when introduced through hyperfine interactions, imposes immobility of the RP formed within the eye of the bird, and implies that entanglement between the unpaired electrons of the RP is preserved over long times of hundreds of microseconds; therefore the coherence times are longer, even if the role of entanglement in the reaction remains unknown. We show that this kind of anisotropy due to hyperfine interactions is not necessary for the proper functioning of the compass. Isotropic radical pairs, i.e., molecules performing diffusional or rotational motion able to average away any anisotropy in the hamiltonian, when subjected to a fast decoherence process, are able to provide the anisotropy required for the compass to work. The environment in which the RP is immersed is then responsible for the reference frame of the compass, relaxing the immobility assumption. This significantly expands the range of applicability of the RP mechanism providing more elements for experimental search, as the candidate molecules must not be fixed within the retina. Using this external source of anisotropy, we show that entanglement is not necessary for the proper working of the compass, given that separable states can form anisotropic yields under proper conditions. Classically correlated initial conditions for the RP, or in other words, initial states without quantum correlations, can provide another source of the required anisotropy for the proper working of the compass; given that the initial state is not a perfect singlet (or triplet) state between the electronic spins and therefore is not a maximally entangled state, this new source of preferred direction in the creation of the chemical products gains relevance.

Resumo

O campo magnético da Terra é essencial na orientação de pássaros migratórios. A explicação mais promissora para esta orientação utiliza o mecanismo de pares ra-dicais (PR) criados em uma reação foto-estimulada, a qual é conjecturada ocorrer em fotor-receptores criptocromo. Esta última conjectura foi particularmente reforçada recente-mente pela evidência de sensibilidade magnética do criptocromo humano. Os radicais devem ter uma anisotropia intrínseca, a fim de definir um quadro de referência para esse tipo de "bússola". Esta anisotropia, quando introduzida através de interações hiperfinas, impõe imobilidade ao RP formado dentro do olho do pássaro, e implica na preservação do emaranhamento entre os elétrons desemparelhados do PR por tempos longos (de cente-nas de microssegundos). Consequentemente, os tempos de coerência são também longos, mesmo que o papel do emaranhamento na reação permaneça desconhecido. Mostra-se que esse tipo de anisotropia devido às interações hiperfinas não é necessário para o funcionamento da bússola. Pares radicais isotrópicos, isto é, moléculas que executam um movimento de rotação ou de difusão capaz de remover qualquer anisotropia no Hamiltoniano quando submetidos a um processo de decoerência rápida, são capazes de fornecer a anisotropia necessária para que a bússola funcione. O ambiente no qual o PR está imerso é responsável pelo referêncial da bússola, relaxando a hipótese de imobili-dade. Isto expande significativamente a gama de aplicabilidade do mecanismo de PR fornecendo mais elementos para pesquisa experimental, quanto as moléculas candidatas não devem estar fixas na retina. Utilizando esta fonte externa de anisotropia, mostramos que o emara-nhamento não é necessário para o bom funcionamento da bússola dado que estados separáveis podem formar produtos anisotrópicos sob as condições apropriadas. Condições iniciais classicamente correlacionadas para o PR, ou em outras palavras, es-tados iniciais sem correlação quântica, podem fornecer uma outra fonte da anisotropia necessária para o bom funcionamento da bússola; dado que o estado inicial não é um estado singleto (ou tripleto) perfeito entre os spins eletrônicos e portanto não é um es-tado maximamente emaranhado, esta nova fonte de direção preferencial na criação dos produtos químicos ganha relevância.

Contents

List of Figures

Chapter 1

Introduction

Magnetic fields can change the products or yields of certain molecular chemical reactions [1, 2], and even weak fields, such as the Earth's, can produce significant effects. Even though the energy involved in the interaction between the magnetic fields and the molecules is much smaller than the average thermal energy k_bT, the sensitivity in production of different reaction outcomes can still exist. This allowed in the 1960s the observation of unusual line shapes in electron paramagnetic resonance (EPR) spectra of the intermediates in radical reactions, and in the nuclear magnetic resonance (NMR) spectra of their products [3], and a consistent interpretation was made in terms of the radical pair mechanism (RPM) [4, 5]. Radical pairs involved in chemical reactions cover a wide field by their own, having applications explaining diffusive motion of molecules [6, 7], electron site exchange [8, 9] and detecting reactions occurring during photosynthesis [10]. We are interested in the means by which the magnetic field of the Earth can influence animal navigation [11]. A magnetic sense was reported in a variety of species, going from bacteria [12] to mollusks [13], fish [14], butterflies [15] and birds [16, 17]. One of the hypothesis that has been proved more consistent with experimental data in the efforts of trying to understand the avian navigation, is based on the existence of a radical pair reaction by means of an anisotropic production of chemical yields [18–22]. Although the model has existed for many years there are still fundamental questions about the physics involved. Specifically about the role of quantum correlations in the working of this sort of compass, and the possible sources of anisotropy needed. In the following two sections a summary of the most important experimental facts that give its importance to the RPM as a viable explanation for avian navigation, as well as the basics if this mechanism itself, are going to be presented. In the last section of this chapter we are

Figure 1.1: The European robin (*Erithacus rubecula rubecula*) was the first to be shown to have a magnetic compass sense.

going to present a brief summary of the most reliable candidate molecules to form the radical pair. In the next chapters we are going to set the theoretic ground to study the implications of quantum correlations and environmental effects in the working of the compass. In Chapter 2 we are going to study the terms present in the spin Hamiltonian that explain the RPM, as well as a discussion about the anisotropy in the model, specifically in the hyperfine tensor. The study of this Hamiltonian is not enough to understand the problem; we also need the influence of the environment, and in order to include it we are going to need the density matrix formalism, that will be described in Chapter 3, along with two functions that can take into account quantum correlations. Chapter 4 contains the results of our work, and in Chapter 5 are summarized the conclusions at which we arrived.

1.1 Avian navigation

The first experiments to show an avian compass were conducted in 1966 with European robins (*Erithacus rubecula rubecula*) caught in Frankfurt, Germany, and it was shown that they use the magnetic field of the Earth to orientate in the correct direction for migration [23, 24]. Several important experimental observations have been made regarding the avian compass, and based on those it was possible to build a good theoretical

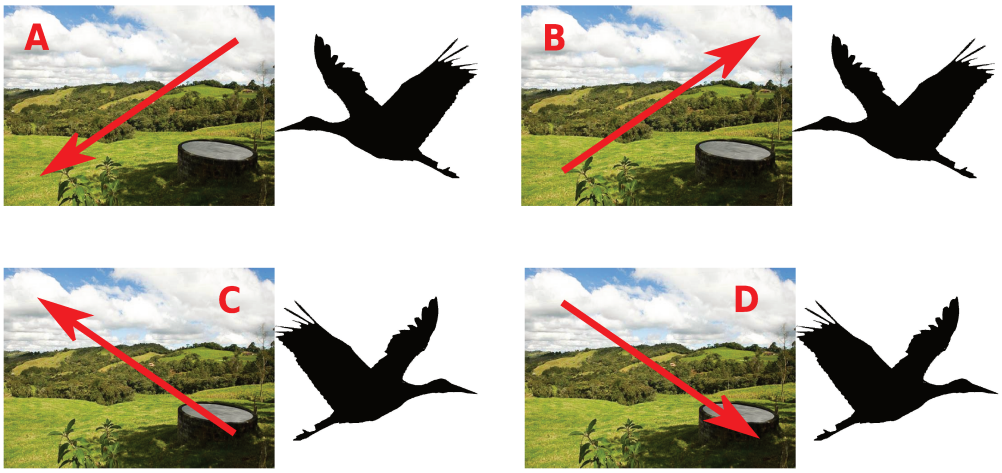

Figure 1.2: Figure adapted from [24] summarizing their findings. (A) Birds in the natural magnetic field preferred to orient in a northerly direction. (B) Using a set of Helmholtz coils to generate a small magnetic field ($46\mu T$) with opposite polarity, it was shown that these birds continued to orient in the same direction. (C) The vertical component of the magnetic field was reversed, causing the birds to orient in an incorrect, southerly direction. (D) The horizontal component of the magnetic field was reversed, causing the birds to orient in an incorrect, southerly direction.

model. The first important observation is that the magnetic *perception* is not sensitive to the polarity of the magnetic field of the Earth but only to the inclination, i.e., birds using this compass cannot distinguish North from South, but are able instead to perceive the axis of the field lines [23, 24], as is depicted in Figure 1.2. The next logic step in those experiments was to test the sensitivity of the magnetic compass of the birds to intensity and frequency of the ambient light [17, 25]. In the four species tested in those papers, the evidence showed that the light in the blue-green part of the spectrum was necessary for magnetoreception. In a different work [26] it was shown that there are other species that depend on the frequency of the light for their magnetic sense. Besides the frequency, it seems that intensity is also important, but most of the works in this sense are trying to separate a motivational effect of the ambient light from a biological effect [27, 28] without a conclusive result so far. In Figure 1.4 we can see the results of experiments that exposed the European robin to different light energies; it can be seen that when exposed to light with energies above certain threshold established near the blue-green part of the spectrum, even UV light, the birds can orientate without any problem; for yellow or red lights the orientation disappears. The results of

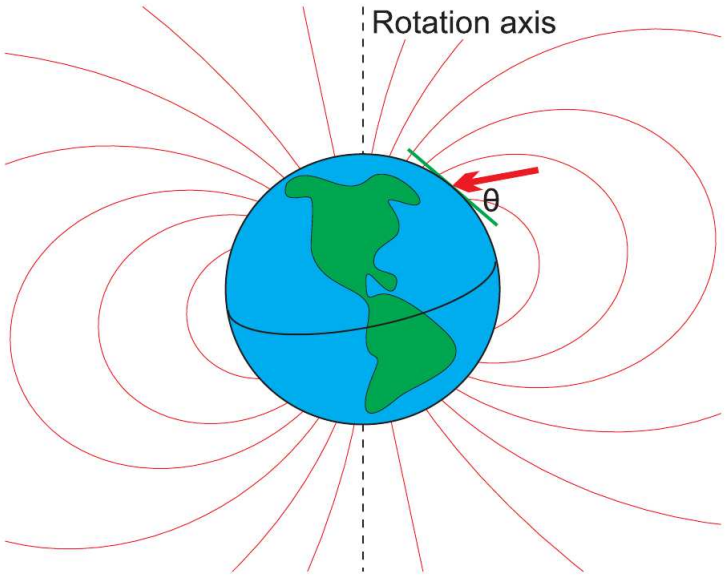

Figure 1.3: Approximate diagram of the Earth's magnetic field. The field lines make an inclination angle of θ degrees with the surface of the Earth.

the experiments conducted on light intensity can be seen in the right panel of Figure 1.5; it's shown that small intensities cannot give the underlying compass mechanism enough information for it to work properly. After learning that many migratory birds need ambient light in certain frequencies and intensities in order to navigate using the magnetic field of the Earth, a natural question arises: where in the bird this light has its effect? An experiment where a bird with its left eye covered was able to orient normally was performed, but one with the right eye covered was not [30]. Apart from the biological question regarding why this asymmetry in the compass, the experiment shows clearly that the light receptors involved in the geomagnetic sense are located in the eyes of robins. Another evidence of this was shown by measurement of genes in the brain of warblers and European robins; it was found that there are significant neural activity during night time orientation tasks in a region of the brain dubbed *cluster N* [31], and this neural activity was absent in the brains of two non-migratory species of birds. The role of *cluster N* seems promissory in the processing of neural signals in the compass, but a conclusive proof is yet to be provided [32]. After the fundamental role of light was shown, the attention turned to experiments with environmental variations of magnetic fields, such as their intensity [11, 29, 33]; European robins that can orient themselves in

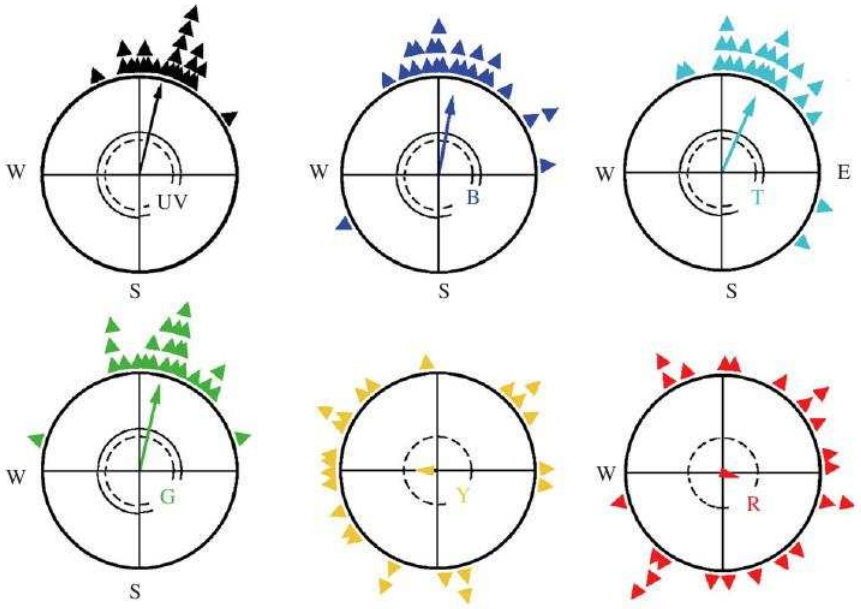

Figure 1.4: Figure from [29] with permission of The Royal Society. Letters UV, B, T, G, Y and R correspond to illumination colors, and W, S, E to directions of orientation. When the birds are exposed to light with energies above certain threshold established near the blue-green part of the spectrum the birds can orientate without problem; for yellow or red lights the orientation disappears.

the magnetic field of the Earth (which has a magnitude of $46\mu T$ in Frankfurt) cannot orient in fields of $34\mu T$ or $60\mu T$; however a continued exposure to the new magnetic field intensity, force the compass to adjust itself [29, 34] allowing the birds to navigate. Strong, short magnetic field pulses [35] were also superimposed to the magnetic field of the Earth in several species of birds. A magnetite-based compass might be realigned following the direction of the magnetic field pulse, but a radical pair mechanism should not be affected by it. However the response to the pulse depends strongly on the size and shape of the magnetite particles in an organism, and given the correct size and form (long and thin particles of magnetite), the compass may only remagnetize in the same direction in which they were originally magnetized. From the data collected a conclusion could not be extracted: in some birds within the same species the pulse appears to have no effect, in others it produces reorientation in an incorrect direction and in others it produces a reorientation in the correct direction. The final experiment conducted with external magnetic fields was the application of a radio-frequency magnetic field perpen-

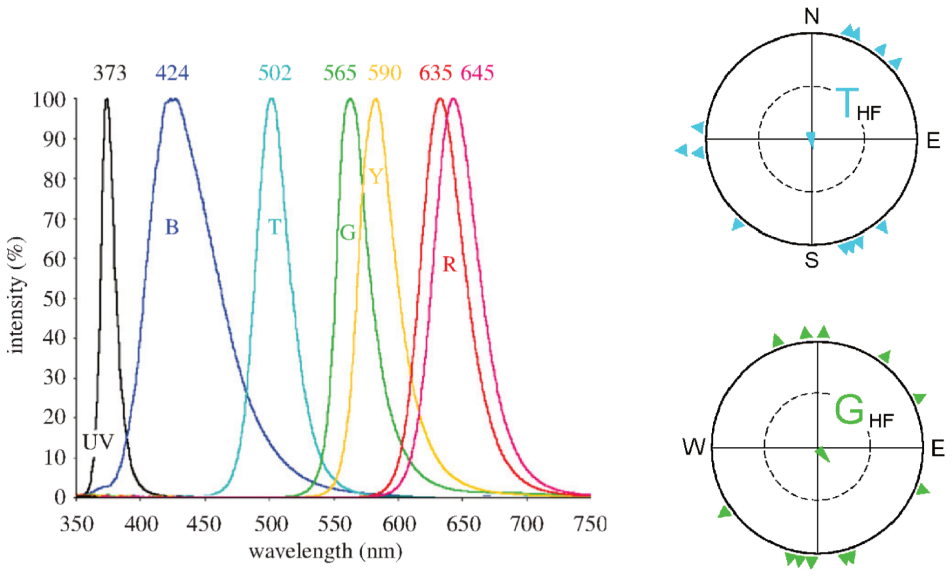

Figure 1.5: Figure from [29] with permission of The Royal Society. The Right Panel shows the average orientation with different intensities of light applied; their results show that for cyan or green light small intensity is enough, and for blue and UV light a greater intensity is necessary. The Left Panel shows experiments conducted with appropriate light, i.e., green and cyan light, when there is an external magnetic field produced by Helmholtz coils; their results showed that the magnetic orientation disappears due to the rf field.

Figure 1.6: Figure from [30] with permission of Nature Publishing Group. The European robin was subjected to monocular testing. The results of these experiments showed conclusively that the mechanism was located in the eyes of the bird.

dicular to the field of the Earth. In 2003 [36] it was found that an RF field much weaker than the magnetic field of the Earth, with a magnitude of $B = 470nT$ and a frequency of oscillation of $\omega_{rf} = 7MHz$ could disorient European robins. The relative orientation

between the applied field and the geomagnetic one was important: for parallel fields the effects were negligible; for relative orientations of 24° or 48° a perturbation was recorded, but a small orientation was still present. The complete disappearance of the compass was only accomplished when the fields were perpendicular. Similar studies, at frequency $\omega_{rf} = 1.315MHz$ and with $B = 485nT$ were conducted [37]. Once again, the robins remained oriented when fields were parallel, but they lost *some* orientation for 24° and 48°, and all orientation for perpendicular fields. As an important note, in [37] the frequency $1.315MHz$ was chosen because its the Zeeman resonance splitting for a free electron in the magnetic field of the Earth for a magnitude of $46\mu T$, which is the magnitude in Frankfurt, were the experiments were made. These results can be seen in the left panel of Figure 1.5.

1.2 Avian compass mechanism

There are several animals that use magnetoreception as a mechanism for navigation. Until now it has not been possible to determine a *magnetic organ* in any animal [28] and there are at least three viable mechanisms that can explain the existence of the compass, each of them well established in the literature and consistent with the experiments performed in several species, from fish to birds. There are however few suggestions of other mechanisms without enough experimental support [38–40]. The first of the proposed mechanisms is magnetoreception by electromagnetic induction. Some fish species are known to swim following magnetic field anomalies in the bottom of the ocean. It is suggested that they can sense the induced EMF as they swim through the magnetic field [14]. However it is known that sea water currents could also induced EMFs; this implies a difficulty trying to separate the EMFs from motion in the magnetic field of the Earth from other magnetic fields in the ocean [41, 42]. However this is unlikely to be the basis of magnetoreception in land or airborne animals. The second viable proposal is that magnetoreception is due to the response of small crystals of magnetite, Fe_3O_4 [27]. This kind of magnetoreception is responsible for the orientation of magnetotactic bacteria [12]. Magnetite deposits have been found in many animals, although it has been difficult to show a connection between these minerals and the nervous system. Until now there are two species which show the best behavioral evidence for a magnetite-based compass: trouts and pigeons [28], although recent reports suggest that these deposits

are macrophages [43] without any role in avian navigation. This mechanism also contradicts experimental evidence: a magnetite-based compass should work as a polarity detector but the navigation mechanism in the European robin cannot detect changes in polarity [29]. The third proposal is that magnetoreception operates by means of anisotropic chemical magnetic field effects on the rate or product yield of a biochemical radical pair reaction [18–20, 44–46]. From the experimental evidence this is the most viable mechanism in the case of European robins.

1.2.1 Radical pair mechanism (RPM)

Besides being established as the basis for many chemical reactions, the RPM field effects have also been observed in some interesting biological systems [47–49]. Some of these effects have been observed in the co-enzyme B_{12}[47, 50] and in modified photosynthetic reaction centers [51–53] using small magnetic fields with a magnitude of $B_0 = 1mT$, which can produce changes in the product of the singlet of O_2 [54]. A schematic view of the process can be seen in Figure 1.7. In the solid state, the RPM proceeds like this:

- A diamagnetic precursor DA reacts to form a pair of radicals, $D*$ and A: this involves an electron transfer due to a photochemical reaction. There are now two molecules each of them with a free electron.

- The creation of the two radicals happens at the same time due to the same reaction, and because of this their electronic spins are correlated. In fact, they form either singlet or triplet states. For simplicity we are going to work only with an initial singlet state, but the results are independent of which one is chosen.

- The spin state is then going to evolve under the Hamiltonian containing, at least, a Zeeman and an hyperfine term. This interconversion is going to depend strongly on the applied magnetic field magnitude and inclination angle, as well as some source of anisotropy in the system.

- There is a reaction between singlet and triplet radical pairs, and as a result different chemical yields (or the same yield at different rates) are produced. The production rates are going to be labeled as k_S and k_T.

- Finally, the yield or amount of each of the reaction products is going to vary according to the applied magnetic field inclination.

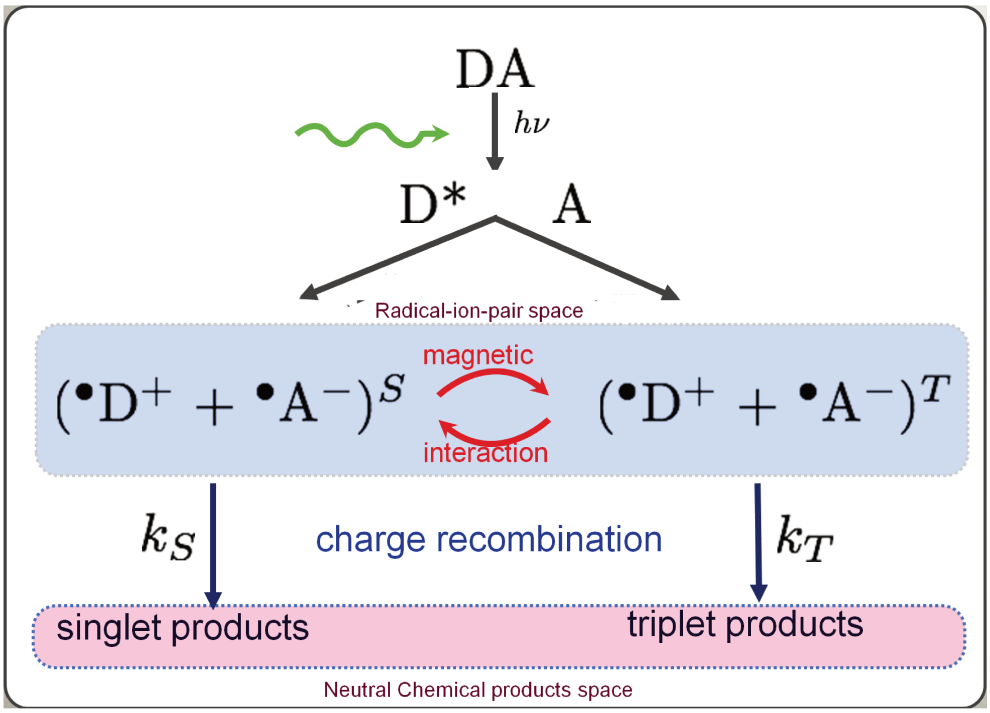

Figure 1.7: Schematic representation of a solid state radical pair mechanism. A precursor molecule DA, subjected to light influence, reacts to form a radical pair D^* A correlated by the spin; the initial state of the RP is a singlet or triplet state (S or T); the interconversion between states S or T is performed by the magnetic field, and the yields of the reaction are produced at rates k_S and k_T respectively.

1.2.2 A RPM compass

In a solid state RP we may assume that the radicals are immobile, or in other words, that they do not make significant diffusional motion nor they are able to perform significant rotations about their axis; these movements cause anisotropic hyperfine and dipolar interactions to be averaged away making the existence of a compass impossible. The RPM yields can depend on the relative alignment of the magnetic field with respect to the sample [52, 53], and from this exists the possibility of the formation of a radical pair compass. Based on the experimental evidence presented in Section 1.1, it is required blue-green light in order to initiate the formation of the radical pair by photochemically-driven electron transfer. We also know that covering the eyes disrupt the possibility of orientation; this means that this mechanism is located in the eyes of the bird; we also know that oriented radicals are necessary in order to prevent an averaging of any

anisotropic magnetic field effects. Anisotropy and its relevance will be explained in greater detail in the next chapter. If the singlet or triplet products of this chemical reaction are neurotransmitters, it is then easy to imagine transduction of the magnetic sense to the nervous system. Some studies confirm that a magnetoreceptor based in the radical pair mechanism could detect the magnetic field of the Earth, even if there is stochastic noise produced by magnetic or electric fields present in the environment or physiological temperature variations [55]. There are several molecules that can be involved in the production of the radical pairs responsible for magnetoreception [18, 38, 46, 56, 57]. The cryptochrome protein has been the most studied as it proved to form radical pairs in the human eye [58]. A schematic of the process of cryptochromes located in the retina can be seen in Figure 1.8.

1.3 Cryptochromes

Although it is not yet known which molecule is responsible for creating the radical pair that may be in charge for the magnetic sense in some birds, there is strong evidence suggesting the Cryptochromes as a candidate. Cryptochromes are a family of photoreceptor proteins that can absorb light in the blue and UV part of the spectrum, and have been found in many fungi, plants and animals [60]. In plants they regulate the growth of the hypocotyl in seedlings [61], and in mammals they have a role regulating the circadian clock [62, 63]. X-ray structures of two cryptochromes CRY-1 and CRY-3 from the mustard *Arabidopsis thaliana* have been found [64, 65]. Cryptochromes are flavoproteins, which means that they bind FAD as a catalytic cofactor, and flavins have a rich photochemistry [66, 67] and are involved in radical reactions. The cryptochrome photocycle is not clear [56, 57, 68] but it seems that cryptochromes can produce long-lived spin correlated radical pair intermediates, a necessary prerequisite for a radical pair-based compass. Cryptochromes have been isolated in the retina of the European robin [69] and in migratory garden warblers [70]. It was shown that in garden warblers the expression of retinal cryptochromes increases when birds are orienting [70, 71]. All these results point to the cryptochrome as having a photo-chemistry sensitive to the presence of a magnetic field, and that it plays a role in avian navigation, although further work is necessary to prove this unequivocally. Even if this protein proves to be the donor-acceptor molecule creating the radical pair in a photochemical reaction, nothing

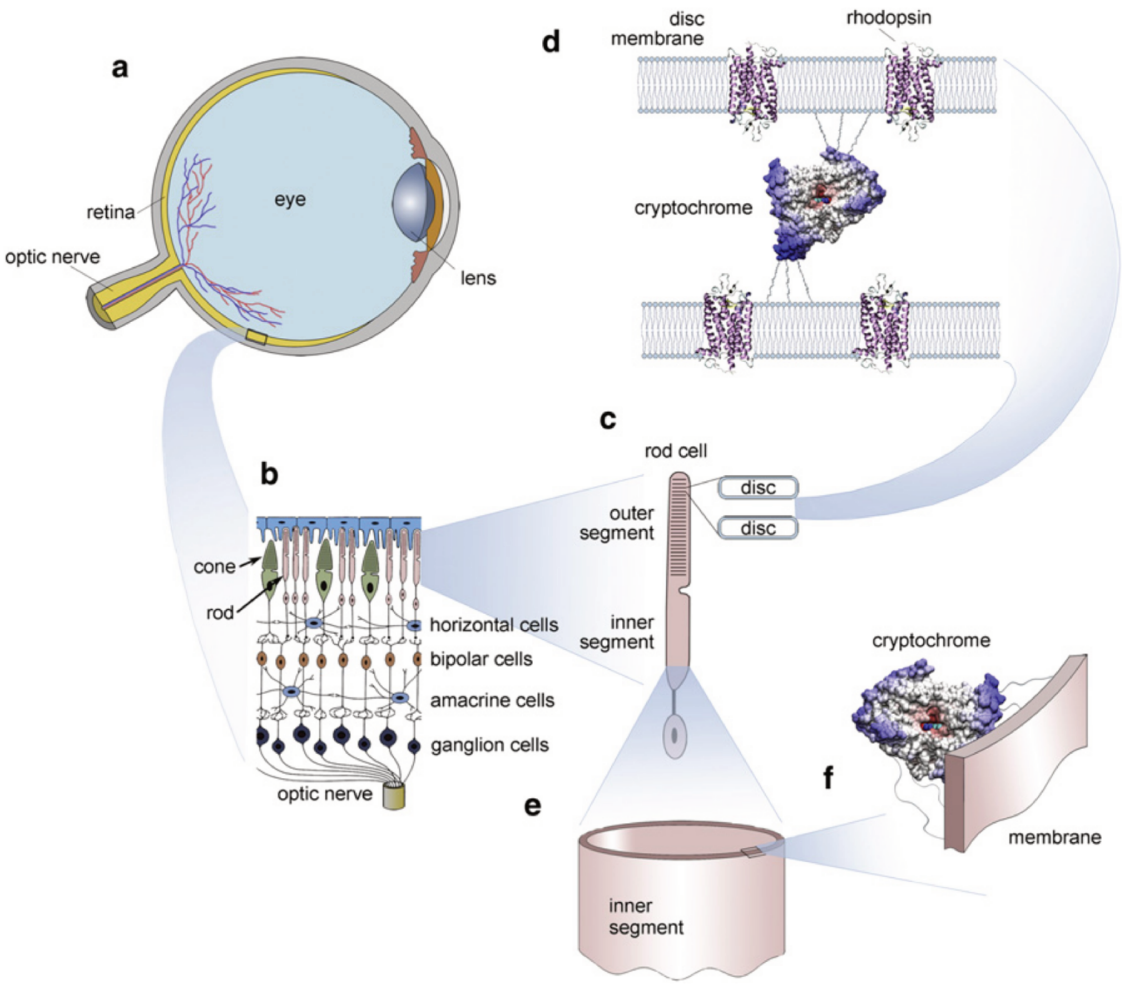

Figure 1.8: From [59] with permission of Biophysical Journal. Oriented radical pairs could be created photochemically in the retina. The cryptochrome protein is a very strong candidate to be the responsible for the creation of the RP involve in the magnetoreception.

is known about the path the message can take in the neural system of the bird, although some hypothesis have been made [72]. Even with the advances of the last decade, there is a big amount of work to be done in order to fully understand avian navigation senses.

Chapter 2

Hamiltonian for the Radical Pair

A radical pair (RP) is created due to a photochemical reaction in a molecular precursor. This implies that a RP is a molecule with a large number of nuclei and electrons in their orbits, besides two interacting unpaired electrons. As a result of the large number of degrees of freedom the dynamics of the unpaired electron spins in each pair of the radical may be incredibly complex. We can describe the RP by a general wavefunction $\Psi(\mathbf{r}_i, \mathbf{s}_i, t)$ evolving under the influence of a Hamiltonian $\hat{H}(t)$, with $\mathbf{r}$ and $\mathbf{s}$ being spatial and spin (angular momentum) coordinates for the i-th electron. The unpaired electrons will interact with all the others in the molecule, each of these interactions giving rise to a correlation. In principle there is going to be a coupling between the spatial and spin coordinates. There is no easy way to accomplish this task, even with the Born-Oppenheimer approximation.

In order to simplify this complex problem a very useful approximation is to consider the spatial and spin coordinates separately [73, 74] converting the full Hamiltonian into a spin Hamiltonian [75, 76]. With this approach we can restrict ourselves to well known Hamiltonian terms involved in spin dynamics. Using this Hamiltonian we can explain all the interactions involved in the singlet-triplet interconversion resulting in the production of anisotropic yields, that finally lead to the existence of a magnetic sense in the system. Despite this simplification the complexity of a spin Hamiltonian in a molecular reaction is still considerable. However all the fundamental features present in a RP reaction can be explained considering a radical pair formed by one proton and its unpaired electron, and an unpaired electron acting as the second radical, i.e., a one-proton radical pair. As will be clear through this Chapter, the effective hamiltonian containing all the important

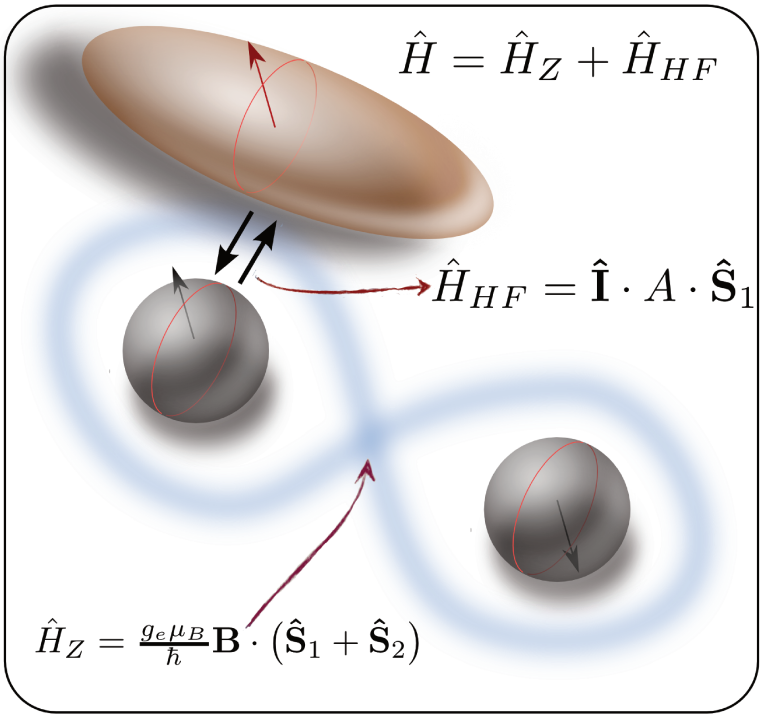

Figure 2.1: Schematic view of the one-proton radical pair where the nucleus and its unpaired electron interact by means of an anisotropic hyperfine term, and the interconversion between singlet and triplet states is mediated by the Zeeman influence of the geomagnetic field over the electronic spins.

features of this system is:

$$\hat{H} = \hat{\mathbf{I}}_\mathbf{1} \cdot A \cdot \hat{\mathbf{S}}_\mathbf{1} + \frac{g_e \mu_B}{\hbar} \mathbf{B} \cdot (\hat{\mathbf{S}}_1 + \hat{\mathbf{S}}_2), \tag{2.1}$$

where $\hat{\mathbf{S}}_\mathbf{1}$ and $\hat{\mathbf{S}}_\mathbf{2}$ are the spin operators for electron 1 and 2 respectively, $\hat{\mathbf{I}}_\mathbf{1}$ is the spin operator of the nucleus, $\mathbf{B}$ is the geomagnetic field and A is the hyperfine tensor. A general spin Hamiltonian consists of at least Zeeman, dipolar, hyperfine and exchange interactions (which is studied in Appendix (A)). In this chapter we are going to lay down the physical considerations taken over a general spin Hamiltonian that allow us to obtain this effective Hamiltonian for a one-proton RP studying each of these interactions, and to stablish why the anisotropy in the system is esential to obtain a RP-based compass. The fundamental Hamiltonian terms involved in the construction of an avian compass based on a one-proton RP can be seen in Figure 2.1.

2.1 Spin Hamiltonian

2.1.1 Zeeman interaction

An atom possesses a rotationally symmetric potential, and in such a system the Zeeman influence of a magnetic field over an electron is [77]

$$\hat{H}_Z = \mu_B\big(\hat{\mathbf{L}} + g_e\hat{\mathbf{S}}\big)\cdot\mathbf{B}, \tag{2.2}$$

where μ_B is the Bohr magneton, $\hat{\mathbf{L}}$ is the vector operator that describes the electron orbital angular momentum, g_e is the electron g-factor and $\mathbf{B}$ is the applied magnetic field. In a general molecule the rotational symmetry no longer exists (except a rotation by 2π, i.e., the identity) and as a consequence the g-factor becomes a tensor accounting for the orbit-spin couplings, allowing us to introduced the influence of $\hat{\mathbf{L}}$ in a phenomenological way [77]. However, for small organic molecules interacting with a very weak magnetic field ($46\mu T$) it is possible to assume that the g-factor is approximately constant and close to that of a free electron, allowing us to write (2.2) as

$$\hat{H}_Z = g_e\mu_B\hat{\mathbf{S}}\cdot\mathbf{B} = -\gamma_e\hbar\hat{\mathbf{S}}\cdot\mathbf{B}. \tag{2.3}$$

In the last expression $\gamma_e = -|g_e|\mu_B/\hbar$. The nuclei in the radical pairs also feel the Zeeman effect produced by the magnetic field, but due to the nuclear gyromagnetic ratios being smaller than the electronic ones, we can consider these terms negligible; even in the case of a proton there are two orders of magnitude in difference between the gyromagnetic ratios, so it is safe to leave outside our considerations the nuclear Zeeman term. This is not the case with hyperfine interactions.

2.1.2 Hyperfine interaction

The hyperfine interaction couples the unpaired electron spin with the internal magnetic field from the spins in the nuclei of the radical. There are two different contributions in this interaction [76]. The first one is the direct dipolar interaction between magnetic moments of electron and nuclei. In a liquid phase, this interaction is averaged away by the diffusive and rotational movement of the radicals; in a solid state radical pair, this term makes the hyperfine interaction anisotropic. In the next section this anisotropy is going to be discussed in more detail.

The other contribution to the hyperfine interaction is the Fermi contact interaction. This term arises from the magnetic interaction between an electron and the nuclear spin when the electronic wavefunction does not vanish in the nuclear position. This interaction is isotropic: it does not depend on the orientation of the electronic or nuclear spins respect to the molecule; in fact, it only depends on the relative orientation between spins. In this case the hyperfine interaction can be written as

$$\hat{H}_{HF} = \sum_i a_i \hat{\mathbf{S}}_i \cdot \hat{\mathbf{I}}_i, \tag{2.4}$$

where a_i is the isotropic hyperfine constant between the electronic and nuclear spins, $\hat{\mathbf{S}}_i$ and $\hat{\mathbf{I}}$, of the i-th radical. The Hamiltonian (2.4) for a one-proton radical pair will read:

$$\hat{H}_{HF} = a\big(S_1 I_1 + S_2 I_2 + S_3 I_3\big). \tag{2.5}$$

Here $\hat{\mathbf{S}} = \{S_1, S_2, S_3\}$ and $\hat{\mathbf{I}} = \{I_1, I_2, I_3\}$.

We have to consider also the Exchange interaction, but its details will be presented in Appendix (A), as well as the criteria that allow us to avoid its inclusion in the spin hamiltonian for the RPM.

2.1.3 Dipolar interaction

Owing to the magnetic field experienced by one unpaired electron due to the other one, we have to consider a dipolar interaction. This interaction is described by the Hamiltonian [78]

$$\hat{H}_D = \frac{\mu_0 \mu_B^2 g_1 g_2}{4\pi\hbar^2 r^3}\Big[\hat{\mathbf{S}}_1 \cdot \hat{\mathbf{S}}_2 - \frac{3}{r^2}\big(\hat{\mathbf{S}}_1 \cdot \mathbf{r}\big)\big(\hat{\mathbf{S}}_2 \cdot \mathbf{r}\big)\Big] = \frac{\alpha}{r^3}\Big[\hat{\mathbf{S}}_1 \cdot \hat{\mathbf{S}}_2 - \frac{3}{r^2}\big(\hat{\mathbf{S}}_1 \cdot \mathbf{r}\big)\big(\hat{\mathbf{S}}_2 \cdot \mathbf{r}\big)\Big]. \tag{2.6}$$

Here the g_i's are the electron g-factors for each radical 1 and 2, $\hat{\mathbf{S}}_\mathbf{i}$ are the spin operators for the electrons, μ_0 is the vacuum permeability and μ_B is the Bohr magneton. We have to note that Eq. (2.6) is only valid for point dipoles separated by $\mathbf{r}$. In molecules this vector can be approximated by the centers of the single occupied molecular orbits in each radical. It can be shown [79, 80] that Eq. (2.6) can be written as

$$\hat{H}_D = \frac{\alpha}{r^3}\hat{\mathbf{S}}_1 \cdot D \cdot \hat{\mathbf{S}}_2, \qquad D_{ij} = \delta_{ij} - 3\hat{r}_i\hat{r}_j \tag{2.7}$$

where D is the dipolar tensor. For strong fields the dipolar interaction goes to zero in a radical pair; however for weak fields the dipolar interaction acts to suppress the magnetic field effects [79]. As in the exchange interaction discussed in Appendix (A), the influence of Eq. (2.7) is constrained to a small separation between the *magnetic* dipoles, i.e., to a small nuclear distance which allows the formation of a bond between the atoms. For distances where the bond dissapears, where the diatomic molecule can be considered a radical pair, the strength of both interactions, dipolar and Exchange, is small. Even more, Efimova *et al.* proved that for the cryptochrome protein in a radical pair the exchange and dipolar interactions cancel each other [81]. Based on these results, in the rest of the thesis we are going to take into consideration only the hyperfine and Zeeman terms in our spin Hamiltonian to model the behavior of the radical pair.

2.2 Reduced spin Hamiltonian

If a RP reaction is to be sensitive to a magnetic field at all, there must be Zeeman influence of a magnetic field over the unpaired electron spins. Hence, we consider the hamiltonian made up with terms (2.3) and (2.5):

$$\hat{H}(\mathbf{B}) = \hat{H}_Z(\mathbf{B}) + \hat{H}_{HF}, \tag{2.8}$$

where the dependence on the magnetic field $\mathbf{B}$ has been made explicit; $\hat{H}_Z(\mathbf{B})$ is the Zeeman contribution and $\hat{H}_{HF}$ is the hyperfine contribution. The hyperfine hamiltonian between the nucleus and the electron that form a (single) radical can be written as

$$\hat{H}_{HF} = \hat{\mathbf{I}} \cdot A \cdot \hat{\mathbf{S}}, \tag{2.9}$$

with $\hat{\mathbf{I}}$ the nuclear spin operator, A the hyperfine tensor and $\hat{\mathbf{S}}$ the electronic spin operator. The dot products are taken in a x, y, z coordinate system. We can expand (2.9) as

$$\hat{H}_{HF} = A_{xx}\hat{I}_x\hat{S}_x + A_{xy}\hat{I}_x\hat{S}_y + A_{xz}\hat{I}_x\hat{S}_z + A_{yx}\hat{I}_y\hat{S}_x \ldots \tag{2.10}$$

The Zeeman effect of the magnetic field over the unpaired electron spin $\hat{\mathbf{S}}$ on one radical can be written as:

$$\hat{H}_Z = \frac{g_e\mu_B}{\hbar}\mathbf{B} \cdot \hat{\mathbf{S}}, \tag{2.11}$$

where g_e is the electron g-factor and μ_B is the Bohr Magneton; we assume that the electron g-tensor is isotropic and close to that of a free electron; care must be taken because if the molecules involved in the reaction were *greater* than the bio-molecules involved in photochemical reactions, an anisotropic geometric structure should be considered in the g-factors as well: g-tensors describing magnetic moments and spin-orbit couplings in molecules with dozens of atoms are necessarily non-diagonal; this implies that the Zeeman interaction can also be a source of anisotropy in a different kind of chemical process. Based on the considerations of the previous section, let us neglect all the other interactions such as exchange and dipolar and write the full radical pair spin Hamiltonian for our problem as a sum of terms for radicals 1 and 2,

$$\hat{H} = \hat{H}^1 + \hat{H}^2, \tag{2.12}$$

where the contribution from radical N is

$$\hat{H}^N = \left(\sum_{i=1}^{M} \hat{\mathbf{I}}_{iN} \cdot A_{iN} \cdot \hat{\mathbf{S}}_N \right) + \frac{g_e \mu_B}{\hbar} \mathbf{B} \cdot \hat{\mathbf{S}}_N, \tag{2.13}$$

in which i labels the i-th nucleus in radical N.

To gain some insight in the qualitative problems that come with the Hamiltonian (2.13) we are going to study the simplest model of a radical pair that still contains the main features of the process. This is the one-proton radical pair. For that case the Hamiltonian (2.13) can be reduced:

$$\hat{H} = \hat{\mathbf{I}}_\mathbf{1} \cdot A \cdot \hat{\mathbf{S}}_\mathbf{1} + \frac{g_e \mu_B}{\hbar} \mathbf{B} \cdot (\hat{\mathbf{S}}_1 + \hat{\mathbf{S}}_2), \tag{2.14}$$

where now $\hat{\mathbf{S}}_1$ and $\hat{\mathbf{S}}_2$ are the spin operators for radical 1 and radical 2 respectively. Radical 2 is just an electron. In the following we will omit the subindex in the nuclear spin operator.

The magnetic field is $\mathbf{B} = B_0\big(\sin\theta\cos\phi\hat{e}_x + \sin\theta\sin\phi\hat{e}_y + \cos\theta\hat{e}_z\big)$; to simplify calculations, and without loss of generality, we are going to set the angle $\phi = 0$; with this assumption the field now reads:

$$\mathbf{B}_0 = B_0\big(\sin\theta\hat{e}_x + \cos\theta\hat{e}_z\big). \tag{2.15}$$

Then the explicit form of the hamiltonian (2.14) is

$$\hat{H} = \hat{\mathbf{I}}_\mathbf{1} \cdot A \cdot \hat{\mathbf{S}}_\mathbf{1} + \omega_0\Big(\sin\theta\big(\hat{S}_{1x} + \hat{S}_{2x}\big) + \cos\theta\big(\hat{S}_{1z} + \hat{S}_{2z}\big)\Big), \tag{2.16}$$

where $\omega_0 = g\mu_B B_0/\hbar$, g is the electronic g-factor, μ_B is the Bohr magneton and B_0 is the field amplitude. The direction of the applied magnetic field with respect to the fixed axis system of our radical pair is then defined in terms of the polar angle θ.

2.2.1 Preferred basis

In order to make calculations we could use two different basis: the most obvious choice is the basis that set eigenstates for the operator $\hat{\mathbf{S}}^2$, i.e., the singlet and triplet states coming from the addition of the spin angular momenta of the two electrons in the radicals, plus spin up or down for the nucleus. In this case the ket is just $|i,j\rangle$, where $i = \{s, t_0, t_1, t_{-1}\}$ and $j = \{1/2, -1/2\}$. The action of the operator $\hat{S}_z$ over the general ket $|i,j\rangle$, given that $\hat{\mathbf{S}} = \hat{\mathbf{S}}_1 + \hat{\mathbf{S}}_2$, is:

$$\hat{S}_z|i,j\rangle = m(i)|i,j\rangle, \tag{2.17}$$

where $m(s) = 0, m(t_0) = 0, m(t_1 = 1)$ and $m(t_{-1}) = -1$. Furthermore, we can write the other cartesian components of the spin operator in terms of the ladder operators:

$$\hat{S}_x = \left(\hat{S}_+ + \hat{S}_-\right)/2 \tag{2.18}$$

$$\hat{S}_y = \left(\hat{S}_+ - \hat{S}_-\right)/2i. \tag{2.19}$$

These operators acting on our kets give:

$$\hat{S}_+|i,j\rangle = \hbar\sqrt{(i - m(i))(i + m(i) + 1)}|\{i, m(i) + 1\}, j\rangle \tag{2.20}$$

$$\hat{S}_-|i,j\rangle = \hbar\sqrt{(i + m(i))(i - m(i) + 1)}|\{i, m(i) - 1\}, j\rangle. \tag{2.21}$$

On the other side the spin operator for the nucleus acting on its eigenstate is:

$$\hat{I}_z|i,j\rangle = \pm\frac{\hbar}{2}|i,j\rangle. \tag{2.22}$$

As before, we can write $\hat{I}_x$ and $\hat{I}_y$ in terms of ladder spin operators, such that

$$\hat{I}_+|i,j\rangle = \hbar\delta_{j,-1/2}|i,1/2\rangle, \tag{2.23}$$

$$\hat{I}_-|i,j\rangle = \hbar\delta_{j,1/2}|i,-1/2\rangle. \tag{2.24}$$

In the last equation $\delta_{j,-1/2}$ and $\delta_{j,1/2}$ are Kronecker deltas. The other basis will be more useful for us in the determination of the effect of anisotropy in the energy levels

of our system. This basis will be just an eigenbasis for the operators of each of the two electronic spins and the nucleus: $\hat{S}_{1z}$, $\hat{S}_{2z}$, $\hat{S}_1^2$, $\hat{S}_2^2$, $\hat{I}_z$ and $\hat{I}^2$. This basis is just $|\pm 1/2\rangle_{\hat{S}_1} \otimes |\pm 1/2\rangle_{\hat{S}_2} \otimes |\pm 1/2\rangle_{\hat{I}} = |\pm 1/2, \pm 1/2, \pm 1/2\rangle$. In this basis the ladder operators are easy to treat:

$$\hat{S}_{1+} |i, j, k\rangle = \hbar \delta_{i,-1/2} |1/2, j, k\rangle \tag{2.25}$$

$$\hat{S}_{1-} |i, j, k\rangle = \hbar \delta_{i,1/2} |-1/2, j, k\rangle . \tag{2.26}$$

Having set the spin Hamiltonian, let us turn our attention to the function of anisotropy in the model.

2.3 Anisotropy in the RP model

As early as 1978 Shulten showed that the avian ability to sense the magnetic field, based on a RPM, should come from anisotropic yields of a chemical reaction happening in the bird itself [45], i.e., the chemical products should depend on a preferred spatial direction; to form such a compass the radical pair in the reaction should have anisotropic interactions. From the possibilities explored in the previous section we know that this anisotropy may come from different sources, such as hyperfine (in the hyperfine tensor), exchange, dipolar (in the dipolar tensor), or electron-Zeeman interactions (in the g-factor). Shulten explored these sources of anisotropy and proposed that the most likely was an anisotropic hyperfine interaction [45, 46].This idea has been revived recently [18], and several experiments have been conducted since then using radio frequency magnetic fields [36, 37] that support the idea of a solid state RPM compass.

Until today only two studies [19, 20] advanced the hypothesis of a solid state radical pair mechanism compass (i.e., radicals that due to their *confinement* can have a well defined average orientation compared to the magnetic field of the Earth) to test theoretically; if in fact the RPM was responsible for the avian navigation, the remaining question is about the identity of the biochemical substance, although the cryptochrome is a good candidate as was explained in (1.3).

In this section we are going to address the question about the suitability of the hyperfine interaction as responsible for the anisotropy necessary in the system in order to have a compass, using a simple model: a RP formed by a nucleus and its unpaired electron, and a *free* unpaired electron acting as the other radical in the pair, i.e., a one-proton radical pair.

2.3.1 Anisotropic hyperfine interaction

The hyperfine interaction between an electron and a magnetic nucleus is described, in general, by an hyperfine tensor (HFT) A which can be represented as a real, symmetric, $3x3$ matrix:

$$A = \begin{pmatrix} a_{xx} & a_{xy} & a_{xz} \\ a_{yx} & a_{yy} & a_{yz} \\ a_{zx} & a_{zy} & a_{zz} \end{pmatrix}. \tag{2.27}$$

In reactions occurring in liquid phase radical pairs, rapid rotations and diffusion of the radicals remove any anisotropic parts of the hyperfine interaction, leaving only an isotropic hyperfine coupling: in the lifespan of the RP, random orientations due to molecular movement will not produced a net preferred direction. These isotropic couplings can be characterized using a constant a, as in the hyperfine Hamiltonian defined in (2.4). In this case the hyperfine tensor can be written as

$$A = \begin{pmatrix} a & 0 & 0 \\ 0 & a & 0 \\ 0 & 0 & a \end{pmatrix} = aI, \tag{2.28}$$

where I is the 3x3 identity matrix. As was stated in section 2.1.2, hyperfine interactions can come from two sources. The anisotropic part comes from the coupling between the electron and nuclear magnetic moments if both are treated as point dipoles. Using the Born-Oppenheimer approximation, which allows us to break the wavefunction of the molecule in electronic and nuclear parts, we can state that the spatial distribution of the unpaired electron around the fixed nuclei depends on the molecular orbital that the electron is occupying. There are some computational packages that allow a relatively simple calculation of molecular orbits, and in turn allow to calculate the anisotropic part of the hyperfine tensor. The isotropic contribution comes from the breakdown of the point dipole approximation, and as we said before it is known as the Fermi contact interaction [76]. This interaction is valid when the electronic wavefunction does not vanish in the nuclear position; its strength is determined by the value of the electron's wavefunction very close to the nucleus. In this region the Coulomb interaction between the nuclear and electron charges is strong, and this implies that electron correlation effects are considerable. As a consequence the isotropic part of the hyperfine interaction is hard to calculate. Before we address the study of the energy levels of the spin Hamiltonian, let us define some quantities to make more readable the eigenvalue expressions.

2.3.2 Axiality and rhombicity of the hyperfine tensor

In order to quantify the degree of asymmetry or anisotropy in a second-rank tensor in euclidean $3-d$ space [82] without specifying its orientation, we can use three useful expressions:

$$a = \frac{1}{3}\big(a_1 + a_2 + a_3\big), \tag{2.29}$$

which is the isotropic part of the hyperfine interaction, and a_i is the i-th eigenvalue of the hyperfine tensor A. We can order the eigenvalues such that

$$|a_1 - a| \leq |a_2 - a| \leq |a_3 - a|. \tag{2.30}$$

Now we can define the anisotropic (asymmetric) part of the hyperfine interaction using two quantities: the axiality parameter

$$\sigma = \frac{1}{2}\big(a_3 - a\big) = \frac{1}{6}\big(2a_3 - a_1 - a_2\big), \tag{2.31}$$

and the rhombicity parameter

$$\xi = \frac{1}{2}\big(a_1 - a_2\big). \tag{2.32}$$

2.3.3 Zero-field energy levels

Taking $\mathbf{B} = 0$, the hyperfine tensor with entries in its diagonal $A = \mathrm{diag}(a_1, a_2, a_3)$ and projecting the Hamiltonian (2.16) with the basis kets defined in (2.25), we get a 8x8 energy matrix for the Hilbert space spanned by the three 2x2 spin spaces:

$$\left\langle \hat{H} \right\rangle = E = \frac{1+\sigma_z}{2} \otimes h + \frac{1-\sigma_z}{2} \otimes h,$$

with σ_z the usual Pauli operator, and h:

$$h = \begin{pmatrix} \frac{a_3}{4} & 0 & 0 & \frac{a_1-a_2}{4} \\ 0 & -\frac{a_3}{4} & \frac{a_1+a_2}{4} & 0 \\ 0 & \frac{a_1+a_2}{4} & -\frac{a_3}{4} & 0 \\ \frac{a_1-a_2}{4} & 0 & 0 & \frac{a_3}{4} \end{pmatrix}$$

The a_i are the eigenvalues of the hyperfine tensor A. The first case of interest is the isotropic hyperfine tensor $A = aI$, with I the $3x3$ identity matrix. In this case the eigenvalues of the matrix are $-3a_3/4 = -3a/4$ with a 2-fold degeneracy and $a_3/4 = a/4$

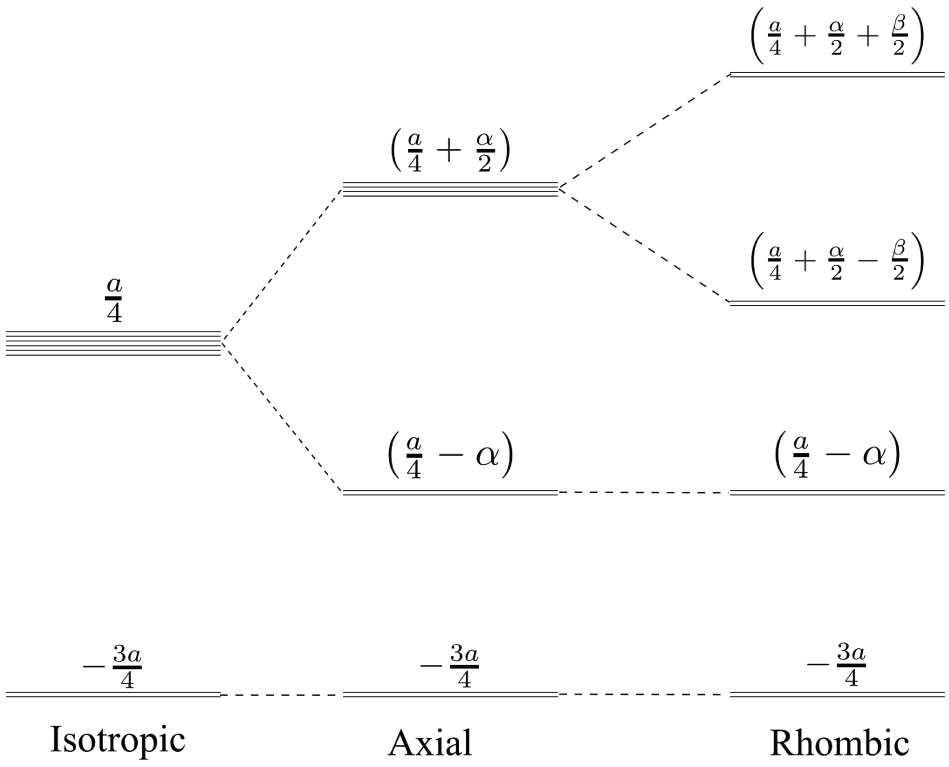

Figure 2.2: Zero-field energy levels in a one-proton radical pair for three different values of the hyperfine tensor: isotropic, *axial* and *rhombic*. Hyperfine anisotropy introduces energy level splittings not present in the isotropic case.

with a 6-fold degeneracy. If the axiality (2.31) becomes different from zero with the rhombicity (2.32) equal to zero, the 6-fold degenerate level splits into a 2-fold and a 4-fold degenerate levels: the eigenvalues are going to be $1/4(-2a_2 - a_3) = -3a/4$ with a 2-fold degeneracy, $1/4(2a_2 - a_3) = a/4 - \sigma$ with a 2-fold degeneracy and $a_3/4 = a/4 + \sigma/2$ with a 4-fold degeneracy. If we increase the anisotropy, i.e., fully rhombic, there are 4 energy levels 2-fold degenerated with eigenvalues:

$$\begin{aligned}
-\frac{1}{4}(a_1 + a_2 + a_3) &= -\frac{3a}{4} \\
\frac{1}{4}(a_1 + a_2 - a_3) &= \frac{a}{4} - \sigma \\
\frac{1}{4}(a_1 - a_2 + a_3) &= \frac{a}{4} + \frac{\sigma}{2} + \frac{\xi}{2} \\
\frac{1}{4}(-a_1 + a_2 + a_3) &= \frac{a}{4} + \frac{\sigma}{2} - \frac{\xi}{2}.
\end{aligned}$$

For a rhombic anisotropy the only degeneracy, with the magnetic field turned off, comes from the unpaired electron spin of the radical which does not contain a nuclei.

2.3.4 Energy levels considering Zeeman interaction

The consideration of a magnetic field different from zero allows the splitting of the remaining 2-fold degeneracies. To get the energy matrix we proceed as before, applying our spin Hamiltonian to the states (2.25). Setting $\phi = 0$, the resulting magnetic field is given by $\mathbf{B} = B_0\{\sin\theta, 0, \cos\theta\}$ and the energy matrix is:

$$E = \begin{pmatrix}
\frac{a_3+4\omega_{z,0}}{4} & \frac{\omega_{x,0}}{2} & 0 & \frac{a_1-a_2}{4} & \frac{\omega_{x,0}}{2} & 0 & 0 & 0 \\
\frac{\omega_{x,0}}{2} & -\frac{a_3}{4} & \frac{a_1+a_2}{4} & 0 & 0 & \frac{\omega_{x,0}}{2} & 0 & 0 \\
0 & \frac{a_1+a_2}{4} & -\frac{a_3-4\omega_{z,0}}{4} & \frac{\omega_{x,0}}{2} & 0 & 0 & \frac{\omega_{x,0}}{2} & 0 \\
\frac{a_1-a_2}{4} & 0 & \frac{\omega_{x,0}}{2} & \frac{a_3}{4} & 0 & 0 & 0 & \frac{\omega_{x,0}}{2} \\
\frac{\omega_{x,0}}{2} & 0 & 0 & 0 & \frac{a_3}{4} & \frac{\omega_{x,0}}{2} & 0 & \frac{a_1-a_2}{4} \\
0 & \frac{\omega_{x,0}}{2} & 0 & 0 & \frac{\omega_{x,0}}{2} & -\frac{a_3+4\omega_{z,0}}{4} & \frac{a_1+a_2}{4} & 0 \\
0 & 0 & \frac{\omega_{x,0}}{2} & 0 & 0 & \frac{a_1+a_2}{4} & -\frac{a_3}{4} & \frac{\omega_{x,0}}{2} \\
0 & 0 & 0 & \frac{\omega_{x,0}}{2} & \frac{a_1-a_2}{4} & 0 & \frac{\omega_{x,0}}{2} & \frac{a_3-4\omega_{z,0}}{4}
\end{pmatrix}$$

Here $\omega_0 = g\mu_B B_0/\hbar$, $\omega_{z,0} = \omega_0 \cos\theta$ and $\omega_{x,0} = \omega_0 \sin\theta$.

Figure 2.3 shows the behavior of the energy levels of the one-proton radical pair with an anisotropic (axial) hyperfine tensor; with higher values of the magnetic field the Zeeman interaction dominates the dynamics and the anisotropy of the hyperfine interaction makes little difference to the energy levels. Both the field strength and the energies are plotted in multiples of the isotropic part of the hyperfine interaction a as was defined in Equation (2.29).

In radical pair reactions occurring in a liquid phase solution, the dynamics of the radical pair yields is dictated by the low field effect (LFE) [83–85]. Knowing that the Earth's magnetic field is about $50\mu T$, we expect that the answer of any radical pair to it would be as a result of the LFE. It is known, however, that this effect arises due to the high degeneracy of the energy levels in a RP with isotropic hyperfine coupling [84]. The weak magnetic field removes this degeneracies, and hence, changes the eigenvalues of the radical pair Hamiltonian in a significant way. This implies that a weak magnetic field can have a significant effect in the singlet (or triplet) yields. However, as shown in Figure 2.2, radical pairs with axial or rhombic hyperfine tensors do not have highly degenerate states. Even if the high degeneracy present in the zero-field isotropic case is

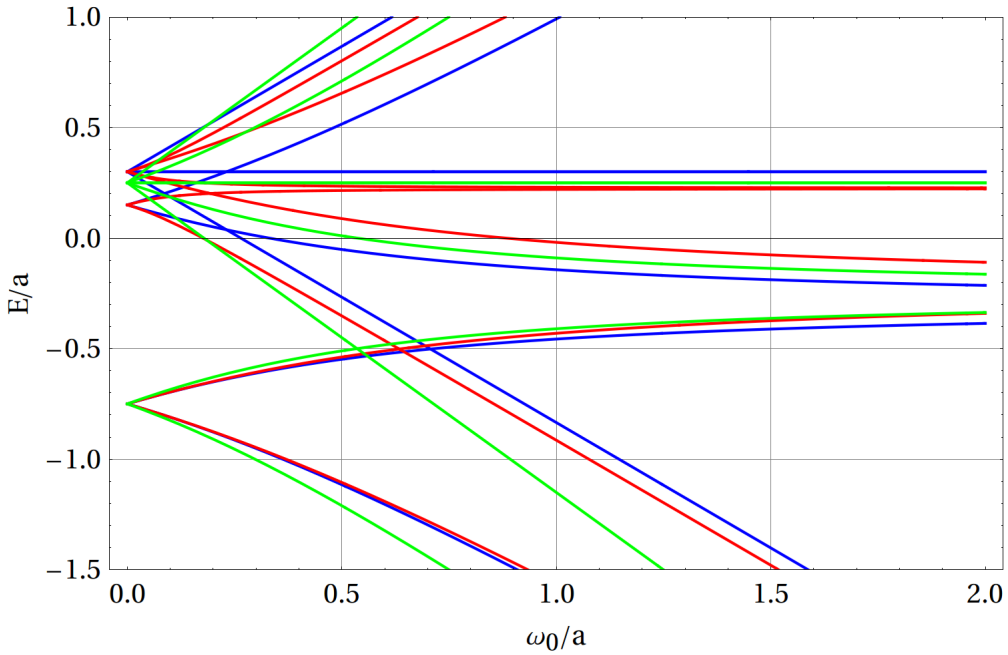

Figure 2.3: Energy levels in a one-proton radical pair, with the isotropic hyperfine coupling constant given by a; the rhombicity is $\xi = 0$. *The green curve* corresponds to an axiality $\sigma = 0$, i.e., an isotropic hyperfine tensor. The *The red curve* shows an axiality of $\sigma = a/10$ and an angle $\theta = \pi/2$. *The blue curve* shows an axiality of $\sigma = a/10$ and an angle $\theta = 0$.

lost, in Figure 2.4 we can see that radical pairs with anisotropic hyperfine interactions have several crossings of the energy levels at weak fields. In Figure 2.4 the crossings are marked with red arrows. We can associate the energy crossings with fast changes in the eigenstates of the radical pair, and consequently, in the singlet yield. There are two things to note: the first one is that the crossings occur at fields $a \gg B_0$, like the field of the Earth. The second thing to note is that the fields at which the crossings occur depend highly on their orientation, i.e., for a static field with fixed amplitude, there are going to be resonant effects on the singlet yield with some orientations, but not with others. In Figure 2.1 we can see a graphic of our model summarizing all the details described in previous sections: a one-proton radical pair where the nucleus and its unpaired electron interact by means of an anisotropic hyperfine term, and the interconversion between singlet and triplet states, which are total spin Angular momentum states, mediated by the Zeeman effect over the electronic spins.

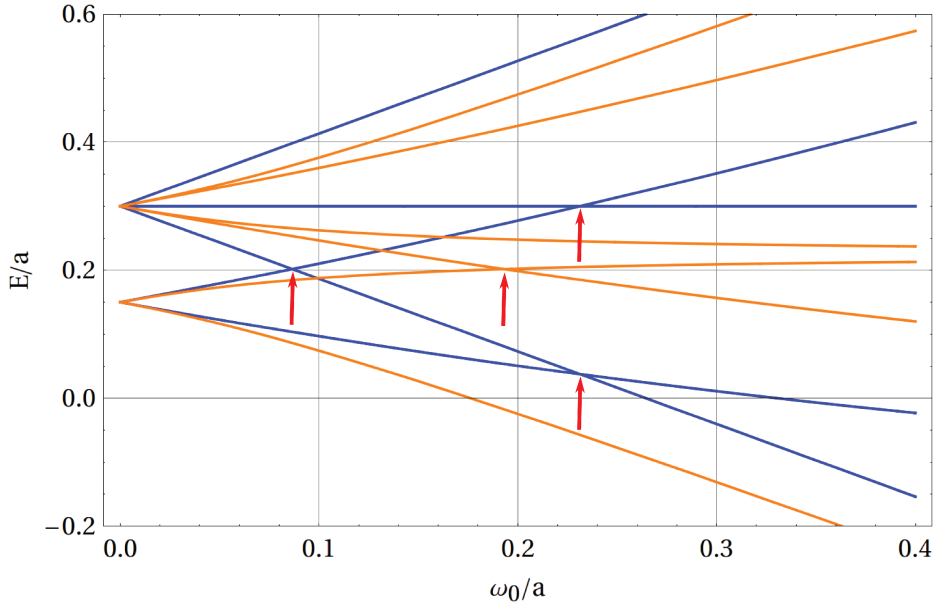

Figure 2.4: Magnified view of the energy crossings with low fields, with an axiality parameter of $\sigma = a/10$. *The blue curve* corresponds to an angle inclination of $\theta = 0$, and *the orange curve* corresponds to an angle inclination of $\theta = \pi/2$.

2.4 Radio Frequency field

Recent works have revealed that weak Radio Frequency fields (RF) of the order of nT are capable of disrupting the magnetic compass sense of European robins under certain circumstances [36, 37]. Long-lived radical pairs that can sustain a photoinduced anisotropic radical yield creation, show Zeeman resonance even in the geomagnetic field for which $B_0 \simeq 50\mu$T, setting the most appropriate frequency for the disruption.

This Zeeman resonance occurs at a radio frequency of:

$$\upsilon_{rf} = |\gamma_e| B_0 = 28.054 B_0 \text{MHz/mT},$$

where $\gamma_e = -|g_e|\mu_B/\hbar$. For an amplitude of $B_0 = 47\mu T$ the above frequency gives $\upsilon_{rf} = 1.317$ MHz. Ritz and coworkers [36, 37] showed that the choice of frequency is independent of the hyperfine structure and hence of the identity of the radical pair.

In order to describe the RF field, one can define its orientation using spherical polar coordinates; we already have (θ, ϕ) for the static $\mathbf{B}_0$ Earth's magnetic field (2.15), so we choose (φ, η) for the RF field. This approach does not provide a simple way to fix the relative orientation of RF and Earth's magnetic fields, which is vital to interpret the

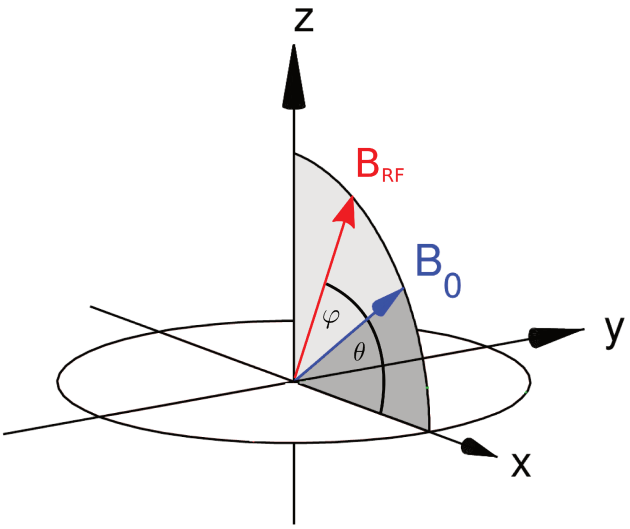

Figure 2.5: Illustration of the position in the 3D cartesian space of the magnetic field of the Earth $\mathbf{B}_0$ and the RF field $\mathbf{B}_RF$; for simplicity they are confined in the $x-z$ plane.

experiments. Given that we are not concerned with experimental set-ups, this approach will suffice. To simplify the expressions let us set one of the polar angles defining the RF field orientation as zero. In Figure 2.5 we can see a schematic representation of both fields in the 3D plane with $\phi = 0$ for $\mathbf{B}_0$ and $\eta = 0$ for the RF field, which can be written as:

$$\begin{aligned}\mathbf{B}_{rf} &= B_{rf}\cos\omega_{rf}t\big(\sin\varphi\cos\eta\hat{e}_x + \sin\varphi\sin\eta\hat{e}_y + \cos\varphi\hat{e}_z\big) \\ &= B_{rf}\cos\omega_{rf}t\big(\sin\varphi\hat{e}_x + \cos\varphi\hat{e}_z\big).\end{aligned} \tag{2.33}$$

In this equation $\omega_{rf} = 2\pi\upsilon_{rf}$ and B_{rf} is going to be in the order of nT, i.e., three orders of magnitude less than the average amplitude of the geomagnetic field.

Chapter 3

Density Matrix formalism

To give to our model a more realistic context, we need to consider the effect of the environment on the spin Hamiltonian. Although there are some ways to do this effectively, the more general description can be get using the density operator. In this chapter we are going to describe general aspects of the theory involving the density operator, as well as the fundamentals of quantum correlations measured using it. With the density matrix formalism and the hamiltonian described in the last Chapter, we can obtain a complete picture of the physics involved in the RP-based compass.

3.1 Basics

In open quantum systems, the use of the density matrix or density operator is a convenient method for describing systems whose state is not completely known. It is defined as [86–88]:

$$\rho = \sum_m p_m \left|\psi_m\right\rangle \left\langle\psi_m\right|, \tag{3.1}$$

where $|\psi_m\rangle$ are the accessible states of the quantum system, and p_m denotes the probability for the quantum state $|\psi_m\rangle$; as any probability, it fulfills $\sum_m p_m = 1$. Necessary conditions for the density matrix are that it has a trace equal to one and it is a self-adjoint, semi-positive operator [86]. The unity of the trace is proved by

$$Tr(\rho) = \sum_m p_m Tr(\left|\psi_m\right\rangle \left\langle\psi_m\right|) = \sum_m p_m = 1, \tag{3.2}$$

giving that the trace of an operator $\hat{A}$ defined in a basis $\{|\psi_n\rangle\}$ is define as $Tr(\hat{A}) = \sum_n \langle\psi_n| \hat{A} |\psi_n\rangle$. The self-adjoint condition, $\rho^\dagger = \rho$, comes directly from the definition (3.1).

To prove the semi-positivity property, let us consider the mean value with respect to an arbitrary state $|\phi\rangle$:

$$\langle\phi| \rho |\phi\rangle = \sum_m p_m \langle\phi| \psi_m\rangle \langle\psi_m| \phi\rangle = \sum_m p_m |\langle\phi| \psi_m\rangle|^2 \geq 0. \tag{3.3}$$

The density operator can also describe quantum systems whose state $|\psi\rangle$ is well known [86]. In this case $\sum_n p_n = p_1 = 1$, and the matrix reduces to $\rho = |\psi\rangle \langle\psi|$. This system is called *pure*; the equation (3.1) defines in general a *mixed* ensemble; these mixed states are a weighted sum over pure states, i.e., an statistical ensemble of pure states. In order to distinguish between these two cases, we use the square of the density matrix: a pure state has an idempotent density operator, $\rho^2 = \big(|\psi\rangle \langle\psi| \big) \big(|\psi\rangle \langle\psi| \big) = \rho$ and together with equation (3.2) we arrive at $Tr(\rho^2) = 1$. For a mixed state, it holds [88]

$$Tr(\rho^2) = \sum_{m,n} p_m p_n \langle\psi_n| \big(|\psi_n\rangle \langle\psi_n| \psi_m\rangle \langle\psi_m| \big) |\psi_n\rangle = \sum_{m,n} p_m p_n |\langle\psi_n| \psi_m\rangle|^2, \tag{3.4}$$

where we used the fact that the trace does not depend on the basis representation. Using then that $|\langle\psi_n| \psi_m\rangle|^2 < 1$ if $n \neq m$, and $\sum_m p_m = 1$, it follows that

$$Tr(\rho^2) = \sum p_n \underbrace{\sum p_m |\langle\psi_n| \psi_m\rangle|^2}_{<1} < 1. \tag{3.5}$$

This means that $Tr(\rho^2) \leq 1$, with equality only for a pure state.

Using the density operator we can also calculate the average of quantum mechanical operators $\hat{A}$ as the average over the expectation values of the accessible states:

$$\begin{aligned} \left\langle \hat{A} \right\rangle = Tr(\rho \hat{A}) &= \sum_{m,n} p_m \langle\psi_m| \psi_n\rangle \langle\psi_n| \hat{A} |\psi_m\rangle \\ &= \sum_{m,n} p_n \delta_{n,m} \langle\psi_n| \hat{A} |\psi_m\rangle \\ &= \sum_m p_m \langle\psi_m| \hat{A} |\psi_m\rangle , \end{aligned}$$

where $\delta_{n,m}$ is the Kronecker delta. Inserting unity $\mathbb{I} = \sum_a |a\rangle \langle a|$ for a complete basis $\{|a\rangle\}$ in the last equation yields:

$$\begin{aligned}\left\langle \hat{A} \right\rangle &= \sum p_m \langle \psi_m | \, \mathbb{I}\hat{A}\mathbb{I} \, | \psi_m \rangle = \sum_{m,a,b} p_m \langle \psi_m | \, a \rangle \langle a | \, \hat{A} \, | b \rangle \langle b | \, \psi_m \rangle \\ &= \sum_{m,a,b} p_m \langle b | \, \psi_m \rangle \langle \psi_m | \, a \rangle \langle a | \, \hat{A} \, | b \rangle \\ &= \sum_b \langle b | \, \Big(\sum_m p_m \, | \psi_m \rangle \langle \psi_m | \, \Big) \Big(\sum_a | a \rangle \langle a | \, \Big) \hat{A} \, | b \rangle \\ &= \sum_b \langle b | \, \rho \hat{A} \, | b \rangle = Tr\big(\rho \hat{A}\big).\end{aligned}$$

With simple rearrangement of the coefficients we obtain:

$$\left\langle \hat{A} \right\rangle = \sum_{m,a,b} p_m \langle a | \, \hat{A} \, | b \rangle \langle b | \, \psi_m \rangle \langle \psi_m | \, a \rangle \,, \tag{3.6}$$

and with this we prove that:

$$Tr\big(\rho \hat{A}\big) = Tr\big(\hat{A} \rho\big). \tag{3.7}$$

Within an orthonormal basis $\{|\phi_i\rangle\}$, the matrix elements of ρ read [89]:

$$\langle \phi_i | \, \rho \, | \phi_j \rangle = \sum_m \langle \phi_i | \, \Big(p_m \, | \psi_m \rangle \langle \psi_m | \, \Big) \, | \phi_j \rangle = \sum_m p_m \langle \phi_i | \, \psi_m \rangle \langle \psi_m | \, \phi_j \rangle \,. \tag{3.8}$$

For the diagonal elements $i = j$, the projections onto the basis states can be simplified to get $p_m |\langle \phi_i | \, \psi_m \rangle|^2$; this implies that the diagonal elements of a density matrix describe the probability of finding the system in the state $|\phi_i\rangle$ if the system is on the state $|\psi_m\rangle$. Since this state is in general not known, the elements $\langle \phi_i | \, \rho \, | \phi_j \rangle = \rho_{i,i}$ are summed over all m's; as a consequence these elements are an averaged probability of finding the system in the state $|\phi_i\rangle$. We can also say that the diagonal element $\rho_{i,i}$ is the *population* of the state ϕ_i. The off-diagonal element $\rho_{i,j}$ is the average of the cross terms; this elements express interference effects between the states ϕ_i and ϕ_j; the interference effects appear if the state ψ_m is a superposition of these states; off-diagonal elements are known as *coherences* of the density matrix. It is important to note that the diagonal elements are sums of real positive numbers, but the off-diagonal elements are sums of complex numbers.

Another important question we can address is about the possibility to learn about the state of one subsystem of a multipartite system. To answer it we refer to the reduced density operator [86]. Suppose that we have two systems A and B which can be described by a density matrix ρ_{AB} for the bipartite system. The reduced density operator of subsystem A is defined as the trace over the state space of the subsystem B [90]:

$$\rho_A = Tr_B\big(\rho_{AB}\big) = \sum_{j=1}^{N_B} \big(\mathbb{I}_A \otimes \langle\psi_j|\,\big)\rho_{AB}\big(\mathbb{I}_A \otimes |\psi_j\rangle\,\big), \tag{3.9}$$

where the states ψ_j are an orthonormal basis in the Hilbert space of subsystem B, $\mathcal{H}_B$, with dimension N_B. From a dynamical point of view, in general we cannot write down $\rho_{AB}(t) = \rho_A(t) \otimes \rho_B(t)$; this is known as the Born Approximation, and it implies that both subsystems have a sufficiently different time scale so that the evolution of one of them is not going to affect the evolution of the other. In other words, there are no correlations between A and B.

Let us consider two simple examples. First, suppose that the quantum system is in a product state of its subsystems, i.e $\rho_{AB} = \zeta_A \otimes \zeta_B$, which in turn implies that A and B are uncorrelated. To get the reduced density matrix of A we take the trace over B:

$$\begin{aligned}
\rho_A &= \sum_{j=1}^{N_B} \big(\mathbb{I}_A \otimes \langle\psi_j|\,\big)\big(\zeta_A \otimes \zeta_B\big)\big(\mathbb{I}_A \otimes |\psi_j\rangle\,\big) \\
&= \sum_{j=1}^{N_B} \big(\mathbb{I}_A \otimes \langle\psi_j|\,\big)\big(\zeta_A \otimes \zeta_B\,|\psi_j\rangle\,\big) \\
&= \zeta_A \otimes \underbrace{\sum_{j=1}^{N_B} \langle\psi_j|\,\zeta_B\,|\psi_j\rangle}_{Tr(\zeta_B)=1} = \zeta_A,
\end{aligned} \tag{3.10}$$

where we have used condition (3.2). Analogously, the trace over A is $\rho_B = \zeta_B$. Then, the reduced density matrix of a subsystem A in ρ_{AB}, without correlations, is ρ_A. For a more conclusive example, let us examine the density matrix

$$\begin{aligned}
\rho &= \left(\frac{|0_A 0_B\rangle - |1_A 1_B\rangle}{\sqrt{2}}\right)\left(\frac{\langle 0_A 0_B| - \langle 1_A 1_B|}{\sqrt{2}}\right) \\
&= \frac{1}{2}\big(\,|0_A 0_B\rangle\langle 0_A 0_B| - |0_A 0_B\rangle\langle 1_A 1_B| - |1_A 1_B\rangle\langle 0_A 0_B| + |1_A 1_B\rangle\langle 1_A 1_B|\,\big).
\end{aligned} \tag{3.11}$$

Here $|0_A 0_B\rangle = |0\rangle_A \otimes |0\rangle_B$, where $|0\rangle_A$ belongs to subsystem A, and $|0\rangle_B$ to subsystem B; $|0\rangle_A$ and $|0\rangle_B$ define orthonormal basis. According to definition (3.10), the partial trace over B is calculated as

$$\begin{aligned}
\rho_A &= \frac{1}{2} Tr_B\big(|0_A 0_B\rangle \langle 0_A 0_B| - |0_A 0_B\rangle \langle 1_A 1_B| - |1_A 1_B\rangle \langle 0_A 0_B| + |1_A 1_B\rangle \langle 1_A 1_B| \big) \\
&= \frac{1}{2}\Big(\big(\langle 0_B|\, 0_B\rangle \langle 0_B|\, 0_B\rangle + \langle 1_B|\, 0_B\rangle \langle 0_B|\, 1_B\rangle \big) |0_A\rangle \langle 0_A| \\
&\quad - \big(\langle 0_B|\, 0_B\rangle \langle 1_B|\, 0_B\rangle + \langle 1_B|\, 0_B\rangle \langle 1_B|\, 1_B\rangle \big) |0_A\rangle \langle 1_A| \\
&\quad - \big(\langle 0_B|\, 1_B\rangle \langle 0_B|\, 0_B\rangle + \langle 1_B|\, 1_B\rangle \langle 0_B|\, 1_B\rangle \big) |1_A\rangle \langle 0_A| \\
&\quad + \big(\langle 0_B|\, 1_B\rangle \langle 1_B|\, 0_B\rangle + \langle 1_B|\, 1_B\rangle \langle 1_B|\, 1_B\rangle \big) |1_A\rangle \langle 1_A| \Big) \\
&= \frac{1}{2}\big(|0_A\rangle \langle 0_A| + |1_A\rangle \langle 1_A| \big).
\end{aligned}$$

Unlike in the previous example, here it is not possible to write (3.11) as a direct product of the density operators of the subsystems, i.e., we cannot write $\rho_{AB} = |\psi_A\rangle \otimes |\psi_B\rangle \langle \psi_A| \otimes \langle \psi_B|$. It is also possible to define operators which may act on only one of the subsystems; let us suppose there is an operator that acts on the states of A, $\hat{S}_A$. The operator then can be written as $\hat{S}_{AB} = \hat{S}_A \otimes \mathbb{I}_B$ [87]. Using the partial trace we can obtain its expectation value:

$$\left\langle \hat{S_{AB}} \right\rangle = Tr_A Tr_B\Big(\rho_{AB} \hat{S}_{AB} \Big) = Tr_A\Big(Tr_B\big(\rho_{AB} \big) \hat{S}_A \Big) \Big) = Tr_A\big(\rho_A \hat{S}_A \big) = \left\langle \hat{S}_A \right\rangle . \quad (3.12)$$

Having the fundamental theoretic background to understand the properties of the density operators, let us study the evolution of a system described by $\rho(t)$.

3.2 Dynamics

3.2.1 Closed quantum systems

A closed quantum system is decoupled from its environment, i.e. there are not dissipation or noise effects due to a reservoir. A closed system can be driven by external forces, and in that case the Hamiltonian H is time-dependent [87]. Otherwise, for $H \neq H(t)$, the system's energy is going to remain a constant of motion. The Schrödinger equation $i\hbar \frac{d}{dt} |\psi(t)\rangle = \hat{H}(t) |\psi(t)\rangle$, governs the time evolution of the state $|\psi(t)\rangle$; we can express the solution of this equation in terms of unitary time evolution operators $\hat{U}(t, t_0)$, that

take the initial state $|\psi(t_0)\rangle$ in a time t_0 to a state $|\psi(t)\rangle$ in a time t:

$$|\psi(t)\rangle = \hat{U}(t,t_0)\,|\psi(t_0)\rangle\,.$$

Inserting this into the Schrödinger equation, we obtain an expression for the time-evolution operator with initial condition $\hat{U}(t_0,t_0)=1$,

$$i\hbar\frac{d}{dt}U(t,t_0) = H(t)U(t,t_0). \tag{3.13}$$

Its solution can be written as a time-ordered exponential

$$\hat{U}(t,t_0) = \hat{T}exp\Big[-\frac{i}{\hbar}\int_{t_0}^{t}\hat{H}(s)ds\Big], \tag{3.14}$$

where $\hat{T}$ is the time ordering operator.If the system is in a mixture of states we must use the density operator, and its evolution can be written as

$$\begin{aligned}\rho(t) &= \sum p_m\,|\psi_m(t)\rangle\,\langle\psi_m(t)| = \sum p_m\hat{U}(t,t_0)\,|\psi_m(t_0)\rangle\,\langle\psi_m(t_0)|\,\hat{U}^\dagger(t,t_0)\\ &= \hat{U}(t,t_0)\rho_0\hat{U}^\dagger(t,t_0).\end{aligned}$$

Therefore, the derivative of $\rho(t)$ yields for $H\neq H(t)$:

$$\begin{aligned}\partial_t\big(\hat{U}(t,t_0)\rho_0\hat{U}^\dagger(t,t_0)\big) &= \big(\partial_t\hat{U}(t,t_0)\big)\rho_0\hat{U}^\dagger(t,t_0) + \hat{U}(t,t_0)\rho_0\big(\partial_t\hat{U}^\dagger(t,t_0)\big)\\ &= -\frac{i}{\hbar}\hat{H}\rho(t) + \frac{i}{\hbar}\rho(t)\hat{H},\end{aligned} \tag{3.15}$$

and we obtain:

$$\partial_t\rho(t) = -\frac{i}{\hbar}\Big[\hat{H},\rho(t)\Big]. \tag{3.16}$$

This equation is called the von-Neumann equation, and it is also valid for a time-dependent Hamiltonian. If the density matrix commutes with the Hamiltonian, ρ does not show any explicit time-dependence and the system is stationary. Although this seems as the dynamic of operators in the Heisenberg picture, it is not the case. The former is defined as

$$d_t\hat{A}_H(t) = \partial_t\hat{A}_H(t) - \frac{i}{\hbar}\Big[\hat{A}_H,\hat{H}\Big], \tag{3.17}$$

where

$$\hat{A}_H(t) = e^{\frac{i}{\hbar}\hat{H}t}\hat{A}_S(t)e^{-\frac{i}{\hbar}\hat{H}t}. \tag{3.18}$$

The time dependence of $\hat{A}_S(t)$ can only be explicit [91]. On the other hand, since states are time-independent in the Heisenberg picture, the corresponding density matrix has to be time-independent too, i.e. $d_t\rho_H = \partial_t\rho_H = 0$. In the Schrödinger picture, the total time derivative of ρ_S vanishes, i.e. $d_t\rho_S(t) = 0$ and the density-matrix is a constant of motion (as in the case of statistical mechanics).

3.2.2 Open quantum systems

Now let us turn our attention to the situation in which a system S is coupled to an environment E [87]. The system S is called *open* if there is an exchange of energy with the environment E. If the environment has an infinite number of degrees of freedom, it is called *reservoir* or *heat bath* (a reservoir in a thermal equilibrium state). The combined system $S + E$ is closed, and as such it follows a unitary time-evolution. Due to the correlations present in the dynamics between S and E, we can no longer say that any part of the complete system $S+E$ is closed anymore. In order to learn something about the subsystem of interest S, we have to eliminate the environmental degrees of freedom. The Hilbert space of the total system $S + E$ is the tensor product of both subsystems, and we may write the total Hamiltonian as $\hat{H}(t) = \hat{H}_S \otimes \mathbb{I}_E + \mathbb{I}_S \otimes \hat{H}_E + \hat{H}_I(t)$ where $\hat{H}_S$ denotes the system's Hamiltonian, $\hat{H}_E$ the free Hamiltonian of the environment and $\hat{H}_I(t)$ the interaction between them. To get expectation values of observables in S we have to perform a partial trace over the environment eigenstates; as a result the time evolution of the system's density matrix is governed by a reduced von-Neumann-equation (3.16):

$$\partial_t\rho(t) = -\frac{i}{\hbar}Tr_E\Big(\Big[\hat{H}, \rho(t)\Big]\Big). \tag{3.19}$$

In general the right-hand side of this equation does not factorize due to the correlations between system and environment, and therefore $\rho_S(t)$ is not just a direct tensor product of the density matrices of S and E. Depending on the nature of the problem, one derives from this equation an approximate equation called master equation [87, 88, 92]. To get an useful expression we need the general formulation of the time dependence of the density matrix: the Lindblad equation. To make its structure plausible, let us start by discussing the concept of quantum operations [86]. In this context, quantum operations map a density operator to other density operator. Suppose that system and environment are initially decoupled, i.e., $\rho_{SE}(t_0) = \rho_S(t_0) \otimes \rho_E(t_0)$. This is an important

assumption and evidently not true in all situations. However we can prepare a system in a certain state that allows us to cut off all correlations between the system and the environment. We can also prepare the environment, such that at $t = t_0$ it is in the state $\rho_E(t_0) = |\epsilon_0\rangle\langle\epsilon_0|$ where $|\epsilon_k\rangle$ is an orthonormal basis for a finite-dimensional environmental state space. The needed quantum operation can be get tracing away the environmental degrees of freedom on the system $S + E$ to obtain ρ_S in a time t:

$$\begin{aligned}
\mathcal{E}(\rho) &= Tr_E\big(\rho(t)\big) \\
&= Tr_E\big(\hat{U}\{\rho_S(t_0)\otimes\rho_E\}\hat{U}^\dagger\big) \\
&= \sum_k \big(\mathbb{I}_S\otimes\langle\epsilon_k|\,\big)\hat{U}\big(\rho_S(t_0)\otimes|\epsilon_0\rangle\langle\epsilon_0|\,\big)\hat{U}^\dagger\big(\mathbb{I}_S\otimes|\epsilon_k\rangle\,\big) \\
&= \sum_k \big(\mathbb{I}_S\otimes\langle\epsilon_k|\,\big)\Big(\hat{U}\rho_S(t_0)\hat{U}^\dagger\hat{U}\,|\epsilon_0\rangle\langle\epsilon_0|\,\hat{U}^\dagger\Big)\big(\mathbb{I}_S\otimes|\epsilon_k\rangle\,\big) \\
&= \sum_k \Big(\hat{U}\rho_S(t_0)\hat{U}^\dagger\Big)\underbrace{\langle\epsilon_k|\,\hat{U}\,|\epsilon_0\rangle}_{\hat{E}_k}\underbrace{\langle\epsilon_0|\,\hat{U}^\dagger\,|\epsilon_k\rangle}_{\hat{E}_k^\dagger} = \sum_k \hat{E}_k\rho_S(t)\hat{E}_k^\dagger.
\end{aligned} \tag{3.20}$$

This is the *operator-sum* or Kraus representation. The $\hat{E}_k = \langle\epsilon_k|\,\hat{U}\,|\epsilon_0\rangle$ are the Kraus operators, which act on the state space of the principal system. Taking the trace of the operation $\mathcal{E}(\rho)$

$$Tr_S\big(\mathcal{E}(\rho)\big) = Tr_S\Big(\sum_k \hat{E}_k\rho_S(t)\hat{E}_k^\dagger\Big) = Tr_S\Big(\sum_k \hat{E}_k\hat{E}_k^\dagger\rho_S(t)\Big) = 1, \tag{3.21}$$

we obtain that

$$\sum_k \hat{E}_k\hat{E}_k^\dagger = \mathbb{I}_S. \tag{3.22}$$

From this point we can motivate the time evolution of the density matrix of the system S as a quantum operation. To do that we have to specify the timescale δt on which we are considering changes in $\rho(t)$ [87]. First and most important, δt should be greater than the time the reservoir takes to *forget* information acquired from the system; in other words, the timescale of the system must be high enough compared to that of the environment to prevent correlations appearing in the environment due to its interaction with the system. This information dissipated by the system S in the environment may even flow back, and hence we want to look at a timescale on which such a feedback is not possible. This is known as the Markov approximation. On the other hand, δt

should be small enough so that all significant changes in the system S are incorporated into the dynamics: compared to the system the environment is not changing; this is known as the Born approximation, which states that for all time t the density matrix of $S + E$ is $\rho(t) \approx \rho_S(t) \otimes \rho_E$. In this way the evolution of ρ is going only to depend on the present density matrix, and we can look for a quantum operation (equation (3.20)), which changes the initial state to order δt:

$$\rho_S(\delta t + t_0) = \mathcal{E}(\rho_0) = \sum_k \hat{E}_k \rho_0 \hat{E}_k^\dagger = \rho_0 + O(\delta t). \tag{3.23}$$

Note that due to the Born approximation this is true for any time t as initial state. This result can be obtained if one of the Kraus operators is given by $\hat{E}_0 = \mathbb{I}_S + O(\delta t)$, and the others are proportional to $\delta t^{1/2}$. Now let us assume that $\hat{E}_0$ characterizes an infinitesimal change in time due to an effective Hamiltonian $\hat{H}_{eff} = \hat{H}_S + i\hbar\hat{K}$ where $\hat{H}_S$ is the Hamiltonian of the system and $\hat{K}$ denotes the coupling to the environment. The Kraus operators can be written as:

$$\hat{E}_0 = \mathbb{I}_S - \frac{i}{\hbar}\hat{H}_{eff}\delta t = \mathbb{I}_S + \Big(\hat{K} - \frac{i}{\hbar}\hat{H}_S\Big)\delta t \tag{3.24}$$

$$\hat{E}_k = \sqrt{\delta t}\hat{L}_k, \qquad k \geq 1 \tag{3.25}$$

where $\hat{L}_k$ are the Lindblad operators. Also, from the normalization condition of the Kraus operators equation (3.22), and taking into account the hermitian nature of both $\hat{H}_S$ and $\hat{K}$, i.e., $\hat{H}_S = \hat{H}_S^\dagger$, $\hat{K} = \hat{K}^\dagger$, we obtain:

$$\begin{aligned}
\mathbb{I}_S &= \Big(\mathbb{I}_S + \hat{K}\delta t - \frac{i}{\hbar}\hat{H}_S\delta t\Big)\Big(\mathbb{I}_S + \hat{K}\delta t - \frac{i}{\hbar}\hat{H}_S\delta t\Big)^\dagger + \sum_k \hat{L}_k\hat{L}_k^\dagger\delta t + O(\delta t^2) \\
&= \mathbb{I}_S + \hat{K}^\dagger\delta t + \frac{i}{\hbar}\hat{H}_S^\dagger\delta t + \hat{K}\delta t - \frac{i}{\hbar}\hat{H}_S\delta t + \sum_k \hat{L}_k\hat{L}_k^\dagger\delta t + O(\delta t^2) \\
&= \mathbb{I}_S + 2\hat{K}\delta t + \sum_k \hat{L}_k\hat{L}_k^\dagger\delta t + O(\delta t^2).
\end{aligned}$$

Consequently

$$\hat{K} = -\frac{1}{2}\sum_k \hat{L}_k\hat{L}_k^\dagger. \tag{3.26}$$

Inserting Equations (3.24) and (3.25) into equation (3.23) yields

$$\begin{aligned}\rho_S(\delta t + t_0) &= \Big(\mathbb{I}_S + \Big(\hat{K} - \frac{i}{\hbar}\hat{H}_S\Big)\delta t\Big)\rho_0\Big(\mathbb{I}_S + \Big(\hat{K} + \frac{i}{\hbar}\hat{H}_S\Big)\delta t\Big) \\ &\quad + \sum_k \hat{L}_k\rho_0\hat{L}_k^\dagger\delta t + O(\delta t^2) \\ &= \Big(\rho_0 + \hat{K}\rho_0\delta t - \frac{i}{\hbar}\hat{H}_S\rho_0\delta t\Big)\Big(\mathbb{I}_S + \hat{K}\delta t + \frac{i}{\hbar}\hat{H}_S\delta t\Big) \\ &\quad + \sum_k \hat{L}_k\rho_0\hat{L}_k^\dagger\delta t + O(\delta t^2) \\ &= \rho_0 - \frac{i}{\hbar}\Big[\hat{H}_S, \rho_0\Big]\delta t + \Big\{\hat{K}, \rho_0\Big\}\delta t + \sum_k \hat{L}_k\rho_0\hat{L}_k^\dagger\delta t + O(\delta t^2),\end{aligned}$$

and therefore, ignoring terms of order $O(\delta t^2)$ and using Equation (3.26), we arrive at the following differential equation for any time t:

$$\partial_t\rho_S(t) = -\frac{i}{\hbar}\Big[\hat{H}_S, \rho_S(t)\Big] + \sum_k \Big(\hat{L}_k\rho_S(t)\hat{L}_k^\dagger - \frac{1}{2}\Big\{\rho_S(t), \hat{L}_k^\dagger\hat{L}_k\Big\}\Big). \tag{3.27}$$

This result is known as the Lindblad equation. As a final step we need to specify the effective Hamiltonian:

$$\hat{H}_{eff} = \hat{H}_S - \frac{i\hbar}{2}\sum_k \hat{L}_k\hat{L}_k^\dagger. \tag{3.28}$$

Building the Lindblad equation we have made strong approximations, and in order to make clear our points let us summarized them. We assumed that system and environment are initially decoupled and that the evolution of the reduced density matrix is Markovian. On the appropriate timescale, we characterized the transition from $\rho_S(t_0)$ to $\rho_S(\delta t + t_0)$ using a quantum operation of first order in δt. The change in time is formally represented by arbitrarily Kraus operators. This operators are transition elements of the initial environmental state to a final state, over which we carried out the trace. The operator $\hat{E}_0$ is an effective time evolution, which adds a slight perturbation to the initial state. With all this the Lindblad equation is represented by a commutator between the density matrix and the Hamiltonian plus a term containing the influence of the environmental operators. It can be seen that neglecting the reservoir degrees of freedom in (3.27), we obtain a von-Neumann-like equation:

$$\partial_t\rho_S(t) = -\frac{i}{\hbar}\Big(\hat{H}_{eff}\rho_S(t) - \rho_S(t)\hat{H}_{eff}^\dagger\Big). \tag{3.29}$$

In the case where there are no couplings to the environment, i.e.,$\hat{H}_{eff} = \hat{H}_S$, equation (3.27) becomes equation (3.16). For the closed system the time evolution of the density operator is

$$\rho_S(t) = \hat{U}_{eff}(t,t_0)\rho_0\hat{U}^{\dagger}_{eff}(t,t_0) = e^{-i\hat{H}_{eff}(t-t_0)/\hbar}\rho_0 e^{i\hat{H}^{\dagger}_{eff}(t-t_0)/\hbar}. \tag{3.30}$$

There is however a fundamental difference with the previous results; here we cannot expect neither the effective Hamiltonian to be hermitian nor the evolution to be unitary given that our approach actually consists in ignoring information about the overall system, specifically the one belonging to the environment. The effective evolution in the Lindblad equation characterizes an evolution according to $\hat{H}_{eff}$ [87]. Let us suppose for example that the system is in a pure state with a density matrix $\rho(t) = |\psi(t)\rangle\langle\psi(t)|$. From equation (3.29) we see that $|\psi(t+\delta t)\rangle = \left(1 - \frac{i}{\hbar}\hat{H}_{eff}\delta t\right)|\psi(t)\rangle$. We can then write an operator containing this evolution:

$$\hat{L} = \sum_k \hat{L}_k\rho\hat{L}^{\dagger}_k = \sum_k \left(\hat{L}_k|\psi(t)\rangle\right)\left(\langle\psi(t)|\hat{L}^{\dagger}_k\right) = \sum \left|\bar{\psi}_k(t)\right\rangle\left\langle\bar{\psi}_k(t)\right|. \tag{3.31}$$

These are the projections -or jumps- from the state $|\psi_k(t)\rangle$ to one of the possible $\left|\bar{\psi}_k(t)\right\rangle$ states. Together both contributions preserve the unity of the trace.

The Lindblad equation (3.27) may also be written formally as [87]:

$$\partial_t\rho_S(t) = \mathcal{L}(t)\rho_S(t), \tag{3.32}$$

where $\mathcal{L}(t)$ contains the right side of (3.27). Its solution can be written as the action of a time evolution operator:

$$\rho_S(t) = \hat{T}exp\Big[\int_{t_0}^{t}\mathcal{L}(s)ds\Big]\rho_0. \tag{3.33}$$

With the theory developed so far we can solve the dynamics of our spin Hamiltonian using the Lindblad equation in order to take into account the influence of the environment over the radical pairs. Before we address our RP Hamiltonian with the tools presented here, it is necessary to talk about quantum correlations and to describe tools to measure it.

3.3 Entanglement

The generation of a radical pair due to a photochemical reaction sets the initial state of the electronic spins of the radicals in a singlet (or triplet) state, and this state is a maximal entangled one. Some discussions have been given recently about the importance of entanglement in the magneto-perception process [93, 94], but this still remains obscure. In this section we are going to define entanglement and a way to measure it.

A pure state is separable if $|\psi_{AB}\rangle = |\psi_A\rangle \otimes |\psi_B\rangle$ where $|\psi_A\rangle$ and $|\psi_B\rangle$ are the states of the quantum subsystems A and B [95, 96]. This state only can show classical correlation between its subsystems, which means that the state $|\psi_{AB}\rangle$ contains the same information that there is in the subsystem's states $|\psi_A\rangle$ and $|\psi_B\rangle$. As discussed in section 3.1, tracing over one of the subsystems yields the density-matrix of the other subsystem and it is therefore clear that they do not have influence on each other.

Let us define the state $|\psi_{AB}\rangle$ as:

$$|\psi_{AB}\rangle = a\,|0_A 0_B\rangle + b\,|0_A 1_B\rangle + c\,|1_A 0_B\rangle + d\,|1_A 1_B\rangle\,. \tag{3.34}$$

In order to (3.34) be a separable state, we require that $ad - bc = 0$. If we cannot write $|\psi_{AB}\rangle$ as a tensor product of its subsystems, then it is an entangled state. An example of such a state is:

$$|\psi\rangle = \frac{1}{\sqrt{2}}\big(\,|H_A H_B\rangle + |V_A V_B\rangle\,\big) = \frac{1}{\sqrt{2}}\big(\,|HH\rangle + |VV\rangle\,\big). \tag{3.35}$$

The density matrix of this system can be written as:

$$\rho \equiv \frac{1}{2}\big(\,|HH\rangle + |VV\rangle\,\big)\big(\,\langle HH| + \langle VV|\,\big) = \frac{1}{2}\begin{pmatrix} 1 & 0 & 0 & 1 \\ 0 & 0 & 0 & 0 \\ 0 & 0 & 0 & 0 \\ 1 & 0 & 0 & 1 \end{pmatrix}. \tag{3.36}$$

As discussed in subsection 3.1, the off-diagonal elements $\rho_{41} = \langle VV|\,\rho\,|HH\rangle$ and $\rho_{14} = \langle HH|\,\rho\,|VV\rangle$, i.e., the coherences, characterize the quantum correlation between the states $|HH\rangle$ and $|VV\rangle$.

In general, the density matrix of an entangled, mixed state cannot be written as

$$\rho = \sum_i p_i\big(\rho_{A,i} \otimes \rho_{B,i}\big), \tag{3.37}$$

To measure the *degree* of Entanglement there are few theoretic tools, depending on the dimensions of the subsystems. We can measure entanglement if the Hilbert space of the total system is $\mathcal{H} = \mathcal{H}_A^2 \otimes \mathcal{H}_B^2$ or $\mathcal{H} = \mathcal{H}_A^2 \otimes \mathcal{H}_B^3$, i.e., when we have two qubits or one qubit and a qutrit interacting. In the last case it is possible to use the *negativity* [97, 98]; however we are going to work with the two spin space defined by the electron in each radical. In this case we can use the Concurrence, which is a quantitative measure for entanglement [99]. To obtain it, one starts by computing the *spin-flip* matrix of the complex conjugated density matrix $\tilde{\rho}$:

$$\tilde{\rho} = \big(\sigma_y \otimes \sigma_y\big)\rho^*\big(\sigma_y \otimes \sigma_y\big), \big(\sigma_y = \{\{0, i\}, \{i, 0\}\}\big). \tag{3.38}$$

With this is possible to determine the non-hermitian matrix $\rho\tilde{\rho}$; using the square roots of its eigenvalues λ_i we can then calculate the Concurrence, which is defined as:

$$C(\rho) = max\Big\{0, \lambda_1 - \lambda_2 - \lambda_3 - \lambda_4\Big\}. \tag{3.39}$$

The square roots of this eigenvalues are ordered as $(\lambda_1 > \lambda_2 > \lambda_3 > \lambda_4)$. For the pure state (3.34) the Concurrence is given by $C(\rho) = 2|ad - bc|$. Maximal entanglement is reached for $a = d = 1/\sqrt{2}, b = c = 0$ or $b = c = 1/\sqrt{2}, a = d = 0$. Either choose of parameters yields the maximum value $C(\rho) = 1$, i.e., a Bell state. On the other hand, a disentangled state, like $a = b = c = d = 1/2$, has $C(\rho) = 0$. In conclusion, the Concurrence lies in between 0 and 1 with maximal entanglement for $C(\rho) = 1$. To illustrate the procedure consider the density matrix [90]

$$\rho = \frac{1}{8}\begin{pmatrix} 3 & 0 & 0 & 2 \\ 0 & 1 & 0 & 0 \\ 0 & 0 & 1 & 0 \\ 2 & 0 & 0 & 3 \end{pmatrix}. \tag{3.40}$$

First, we compute the spin-flip matrix $\tilde{\rho} = \big(\sigma_y \otimes \sigma_y\big)\rho^*\big(\sigma_y \otimes \sigma_y\big)$

$$\begin{aligned}
\tilde{\rho} &= \left(\begin{pmatrix} 0 & -i \\ i & 0 \end{pmatrix} \otimes \begin{pmatrix} 0 & -i \\ i & 0 \end{pmatrix} \right) \rho^* \left(\begin{pmatrix} 0 & -i \\ i & 0 \end{pmatrix} \otimes \begin{pmatrix} 0 & -i \\ i & 0 \end{pmatrix} \right) \\
&= \begin{pmatrix} 0 & 0 & 0 & -1 \\ 0 & 0 & 1 & 0 \\ 0 & 1 & 0 & 0 \\ -1 & 0 & 0 & 0 \end{pmatrix} \rho^* \begin{pmatrix} 0 & 0 & 0 & -1 \\ 0 & 0 & 1 & 0 \\ 0 & 1 & 0 & 0 \\ -1 & 0 & 0 & 0 \end{pmatrix} \\
&= \frac{1}{8} \begin{pmatrix} 3 & 0 & 0 & 12 \\ 0 & 1 & 0 & 0 \\ 0 & 0 & 1 & 0 \\ 2 & 0 & 0 & 3 \end{pmatrix}.
\end{aligned}$$

The eigenvalues of this matrix are $\{5/8, 1/8, 1/8, 1/8\}$, and the Concurrence therefore reads

$$C(\rho) = max\Big\{0, 5/8 - 1/8 - 1/8 - 1/8\Big\} = \frac{1}{4}. \tag{3.41}$$

There is another interesting quantity that can allow us to say something about the quantum correlations in our system beyond entanglement, and it is known as the *Quantum discord*.

3.3.1 Quantum discord

Any measurement made in quantum mechanics perturbs the systems. In general the state of a system is not known, and the result of any measurement only says to us the collapsed state product of the interaction of the system and our apparatus. This is not true in a classical system, when the measure of the canonical variables does not perturb the system and defines without uncertainty its state. The idea of Quantum discord [100] is to take advantage of the disturbance made by measurements as a test to the presence of quantum correlations in a bipartite two-level quantum system living in the Hilbert space $\mathcal{H} = \mathcal{H}_A^2 \otimes \mathcal{H}_B^2$. The mutual information function is used to monitor the effects of measurement in the system, and is defined as:

$$I_{AB} = S_A + S_B - S_{AB}, \tag{3.42}$$

S_x is the von Neumann entropy of system x such that $S(\rho) = -Tr\big(\rho \log_2 \rho\big)$. This function measures the amount of information shared between the subsystems A and B. It can be seen as the amount of correlation between them, either classical or quantum.

The next step is to perform a measurement on one of the subsystems, and looking the effect this measurement has on the mutual information it is possible to tell if there are quantum correlations in the total system AB. To achieve this it is sufficient to compare both functions, after and before the measurement. This is the most difficult part of the process, since the measurement that can be made is no unique and it is necessary to make an optimization over all possible measurements. We can define all the set of measurements (or projectors) acting on one of the subsystems, say B, as Π_x^B; the measurement-induced mutual information takes the form:

$$J_{\overleftarrow{AB}} = \max_{\{\Pi_x^B\}} \left[S(\rho_A) - \sum_x p_x S(\rho_A^x) \right],$$

where $p_x = Tr_A\{\Pi_x^B \rho_{AB} \Pi_x^B\}$ is the probability of obtaining the result x from the measure and $\rho_A^x = Tr_B\{\Pi_x^B \rho_{AB} \Pi_x^B\}/p_x$ is the density matrix of the system after the measurement is applied. The maximum is taken over the positive measurements $\{\Pi_x^B\}$ made over the system B.

The final form of the Quantum discord is then:

$$\delta_{\overleftarrow{AB}} = I_{AB} - J_{\overleftarrow{AB}}. \tag{3.43}$$

Computation of $\delta_{\overleftarrow{AB}}$ is in general a non-trivial effort due to the big amount of possible measurements that can be performed; only some systems have an analytic solution (see for example [101, 102]). In our radical pair system an analytic solution is no possible, and only numeric results can be obtained.

With the description of the density matrix formalism and the two measures of quantum correlations, we are ready to face the spin Hamiltonian and discuss the physics involved in the radical pair mechanism.

Chapter 4

Results

4.1 Basic features of the model

To get a better understanding of the RP system we are going to analyze the implications of its anisotropy by studying a simplified case, i.e., the free evolution of the master equation; this means that we need to consider only the Liouville von-Neumann equation (3.16). To get the full reaction (the end the singlet-triplet interconversion process), we need the influence of the environment in the form of a *measurement* process. These two features are going to be presented in this section. We are going to use three different designations for spins *up* and *down* to ease the reading equations: $|1/2\rangle = |\uparrow\rangle = |\alpha\rangle$ for spin *up* and $|-1/2\rangle = |\downarrow\rangle = |\beta\rangle$ for spin *down*. We are going to use angular frequency units used in nuclear magnetic resonance problems and express the units of the hyperfine tensor in mT for brevity.

4.1.1 Closed problem

The spin hamiltonian for a one-proton radical pair (2.14), with $\phi = 0$ in the magnetic field is:

$$\hat{H} = \hat{\mathbf{I}}_\mathbf{1} \cdot A \cdot \hat{\mathbf{S}}_\mathbf{1} + \omega_0 \Big(sin\theta \big(\hat{S}_{1x} + \hat{S}_{2x} \big) + cos\theta \big(\hat{S}_{1z} + \hat{S}_{2z} \big) \Big). \tag{4.1}$$

Using this Hamiltonian we can write down the Liouville-von Neumann equation (3.16):

$$\begin{aligned}\partial_t\rho(t) &= -i\Big[\hat{H},\rho(t)\Big] \\ &= -i\Bigg(\Big\{\hat{\mathbf{I}}_{\mathbf{1}}\cdot A\cdot\hat{\mathbf{S}}_{\mathbf{1}}+\omega_0\Big(\sin\theta\big(\hat{S}_{1x}+\hat{S}_{2x}\big)+\cos\theta\big(\hat{S}_{1z}+\hat{S}_{2z}\big)\Big)\Big\}\rho \\ &\quad -\rho\Big\{\hat{\mathbf{I}}_{\mathbf{1}}\cdot A\cdot\hat{\mathbf{S}}_{\mathbf{1}}+\omega_0\Big(\sin\theta\big(\hat{S}_{1x}+\hat{S}_{2x}\big)+\cos\theta\big(\hat{S}_{1z}+\hat{S}_{2z}\big)\Big)\Big\}\Bigg),\end{aligned} \tag{4.2}$$

where A is the hyperfine tensor and $\hat{S}_i$ and $\hat{I}_i$ are the cartesian components of the electronic and nuclear spins. To make further simplifications let us assume that our hyperfine tensor has a rhombicity $\xi = 0$, which means that the eigenvalues are $a_1 = a_2 \neq a_3$. In the following we are going to ignore the subindex in the nuclear spin operator. With all of the above we get

$$\begin{aligned}\partial_t\rho(t) = -i\Bigg(&\Big\{a_x\big(\hat{I}_x\hat{S}_x+\hat{I}_y\hat{S}_y\big)+a_z\hat{I}_z\hat{S}_z \\ &+\omega_0\Big(sin\theta\big(\hat{S}_{1x}+\hat{S}_{2x}\big)+cos\theta\big(\hat{S}_{1z}+\hat{S}_{2z}\big)\Big)\Big\}\rho \\ &-\rho\Big\{a_x\big(\hat{I}_x\hat{S}_x+\hat{I}_y\hat{S}_y\big)+a_z\hat{I}_z\hat{S}_z \\ &+\omega_0\Big(sin\theta\big(\hat{S}_{1x}+\hat{S}_{2x}\big)+cos\theta\big(\hat{S}_{1z}+\hat{S}_{2z}\big)\Big)\Big\}\Bigg).\end{aligned} \tag{4.3}$$

. Express the spin operators as a sum of ladder operators we get:

$$\begin{aligned}\partial_t\rho(t) = -i\Bigg(&\Big\{\frac{a_x}{2}\big(\hat{I}_+\hat{S}_{1-}+\hat{I}_-\hat{S}_{1+}\big)+a_z\hat{I}_z\hat{S}_z \\ &+\omega_0\Big(sin\theta\big(\hat{S}_{1x}+\hat{S}_{2x}\big)+cos\theta\big(\hat{S}_{1z}+\hat{S}_{2z}\big)\Big)\Big\}\rho \\ &-\rho\Big\{\frac{a_x}{2}\big(\hat{I}_+\hat{S}_{1-}+\hat{I}_-\hat{S}_{1+}\big)+a_z\hat{I}_z\hat{S}_z \\ &+\omega_0\Big(sin\theta\big(\hat{S}_{1x}+\hat{S}_{2x}\big)+cos\theta\big(\hat{S}_{1z}+\hat{S}_{2z}\big)\Big)\Big\}\Bigg).\end{aligned} \tag{4.4}$$

To solve the problem using the Liouville-von Neumann equation requires to find the system of coupled differential equations containing expressions for each entry in the density matrix. A general state for the three-spin system read $|i\rangle_I \otimes |n\rangle_{S_1} \otimes |p\rangle_{S_2} = |i,n,p\rangle$, where $\{i,n,p\}$ can take the values α or β; for example the matrix element corresponding to the diagonal element where the nucleus and both electrons are in the *up* spin state will read:

$$\langle\alpha\alpha\alpha|\,\rho\,|\alpha\alpha\alpha\rangle = \langle\uparrow\uparrow\uparrow|\,\rho\,|\uparrow\uparrow\uparrow\rangle \equiv \rho^{\alpha\alpha\alpha}_{\alpha\alpha\alpha} = \rho^{\uparrow\uparrow\uparrow}_{\uparrow\uparrow\uparrow}, \tag{4.5}$$

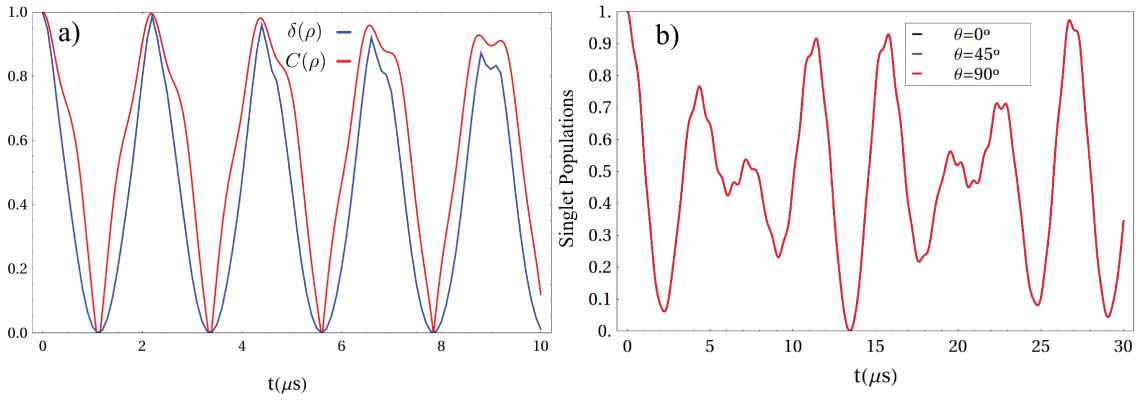

Figure 4.1: Dynamics of the closed isotropic ($a_1 = a_2 = a_3$) one-proton spin Hamiltonian. (a) the evolution of Quantum discord (blue curve) and Concurrence (red curve). (b) the evolution of the population of the singlet state.

and a general matrix element will read

$$\langle jmq|\,\rho\,|inp\rangle \equiv \rho_{inp}^{jmq}. \tag{4.6}$$

Using this notation we can express Equation (4.4) using the base states $|i, n, p\rangle$, and in this way we can write a generic equation for each of the matrix elements. Although this is not a useful form to make analytical calculations it can give some insight in the general behavior of the system. The general matrix entry reads:

$$\begin{aligned}\partial_t \rho_{inp}^{jmq} = -\frac{i}{2}\Big(& a_1\Big(\delta_{j\alpha}\delta_{m\beta}\rho_{inp}^{\beta\alpha q} + \delta_{j\beta}\delta_{m\alpha}\rho_{inp}^{\alpha\beta q} - \delta_{i\alpha}\delta_{n\beta}\rho_{\beta\alpha p}^{jmq} \\ & + \delta_{i\beta}\delta_{n\alpha}\rho_{\alpha\beta p}^{jmq}\Big) + B_x\Big(\delta_{m\alpha}\rho_{inp}^{j\beta q} + \delta_{m\beta}\rho_{inp}^{j\alpha q} + \delta_{q\alpha}\rho_{inp}^{jm\beta} \\ & + \delta_{q\beta}\rho_{inp}^{jm\alpha} - \delta_{n\alpha}\rho_{i\beta p}^{jmq} - \delta_{n\beta}\rho_{i\alpha p}^{jmq} - \delta_{p\alpha}\rho_{in\beta}^{jmq} - \delta_{p\beta}\rho_{in\alpha}^{jmq}\Big) \\ & - \Big(2B_z(p - q + n - m) + a_3\big(ni - mj\big)\Big)\rho_{inp}^{jmq}\Big).\end{aligned} \tag{4.7}$$

Here $B_x = g\mu_B B_0 \sin\theta$ and $B_z = g\mu_B B_0 \cos\theta$ are x and z components of the magnetic field, $a_1 = a_2 \neq a_3$ are the three diagonal entries of the hyperfine tensor and $\delta_{\alpha\beta}$ are the Kronecker deltas between the states. In the following we are going to use as initial condition a singlet state for the two electrons. This state is defined as $|s, 0\rangle =$

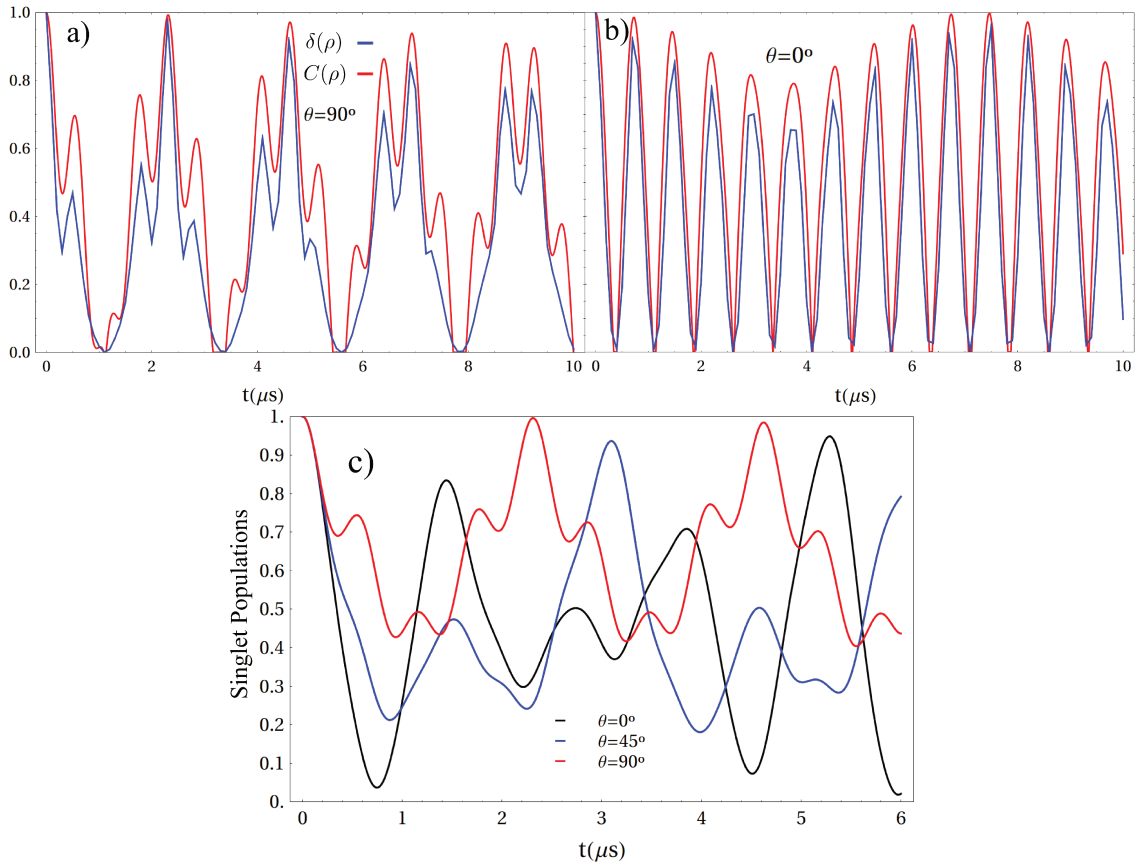

Figure 4.2: Dynamics of the closed anisotropic ($a_1 = a_2 \neq a_3$) one-proton spin Hamiltonian. (a) and (b) the evolution of Quantum discord (blue curve) and Concurrence (red curve) for $\theta = \pi/2$ and $\theta = 0$ respectively. The variation of the angle now changes the behavior of quantum correlations. (c) Dynamics of the closed anisotropic ($a_1 = a_2 \neq a_3$) one-proton spin Hamiltonian. The singlet population for three different angles.

$\frac{1}{\sqrt{2}}\big(\,|1/2\rangle\,|-1/2\rangle - |-1/2\rangle\,|1/2\rangle\,\big) = \frac{1}{\sqrt{2}}\big(\,|\uparrow\downarrow\rangle - |\downarrow\uparrow\rangle\,\big)$. So, the initial condition reads:

$$\rho_0 = |s,0\rangle\,\langle s,0| = \left(\frac{1}{\sqrt{2}}\Big(\,|\uparrow\downarrow\rangle - |\downarrow\uparrow\rangle\,\Big)\right)\left(\frac{1}{\sqrt{2}}\Big(\,\langle\uparrow\downarrow| - \langle\downarrow\uparrow|\,\Big)\right) \tag{4.8}$$

$$= \frac{1}{2}\Big(\,|\uparrow\downarrow\rangle\,\langle\uparrow\downarrow| - |\downarrow\uparrow\rangle\,\langle\uparrow\downarrow| - |\uparrow\downarrow\rangle\,\langle\downarrow\uparrow| + |\downarrow\uparrow\rangle\,\langle\downarrow\uparrow|\,\Big). \tag{4.9}$$

As we are interested in the influence of the magnetic field on the singlet products, we can trace out the nuclear spin to get the dynamic between the two unpaired electrons:

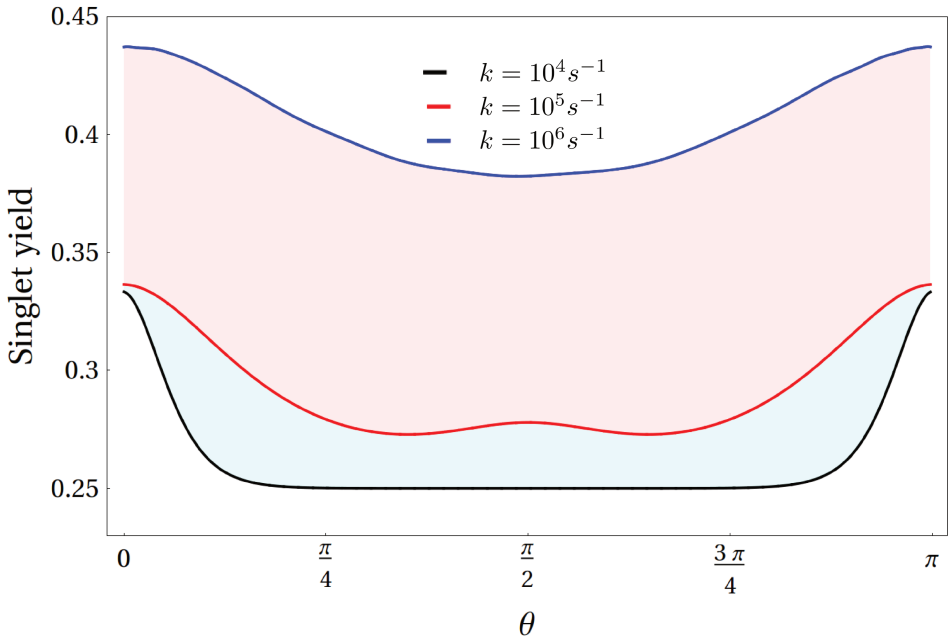

Figure 4.3: Angle variation of the magnetic field using an axial hyperfine tensor $\big(g_e\mu_B/\hbar\big)A = \big(g_e\mu_B/\hbar\big)diag(a_1, a_1, a_2)$, with $a_2 = 2a_1$. A difference in the strength of the measurement process can affect the singlet production. *Black curve*: $k = 1$MHz; the singlet and triplet states with short time to interact, and the reaction is going to finish in $\sim 50\mu s$. *Red curve*: with $k = 0.1$MHz the radical pair have a lifetime of $\sim 150\mu s$. *Blue curve*: with $k = 0.01$MHz the radical pair have a life time of $\sim 1000\mu s$.

$$\partial_t \rho = \partial_t \begin{pmatrix} \rho^{\alpha\alpha}_{\alpha\alpha} & 0 & 0 & 0 \\ 0 & \rho^{\alpha\beta}_{\alpha\beta} & \left(\rho^{\alpha\beta}_{\beta\alpha}\right)^* & 0 \\ 0 & \rho^{\alpha\beta}_{\beta\alpha} & \rho^{\beta\alpha}_{\beta\alpha} & 0 \\ 0 & 0 & 0 & \rho^{\beta\beta}_{\beta\beta} \end{pmatrix}.$$

If the hyperfine tensor is axial, i.e., $a_1 = a_2 \neq a_3$ all terms created by the action of the operator $\hat{S}_x$ in the Zeeman term are going to disappear and the only remaining angular dependence is due to the $\hat{S}_z$. If the hyperfine tensor is isotropic all angular dependencies introduced by the Zeeman term disappear. In Figure 4.1 the dynamics of the closed isotropic ($a_1 = a_2 = a_3$) one-proton spin Hamiltonian is summarized. In (4.1) (a) the evolution of Quantum discord (blue curve) defined in (3.3.1) and Concurrence (red curve) defined in (3.3) is depicted. There is a periodic appearance of maxima and minima in both $C(\rho)$ and $\delta(\rho)$. This is an obvious consequence of the lack of environmental influence

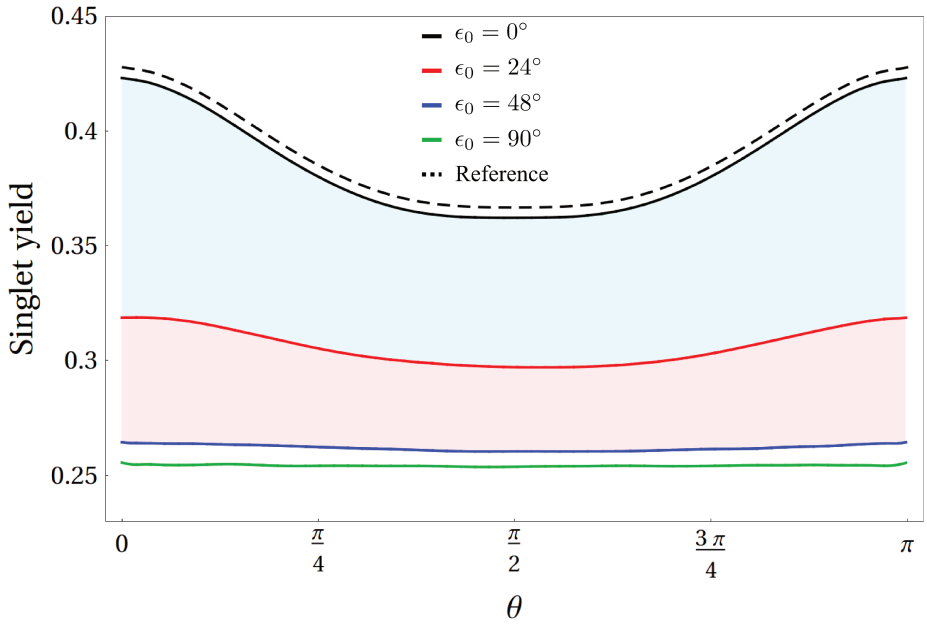

Figure 4.4: Influence of the RF field over the singlet yield production. The frequency of the RF field is $\upsilon_{rf} = \omega_{rf}/2\pi = 1.317$ MHz and its magnitude is $B_{rf} = 150$nT; the magnitude of the magnetic field of the Earth is $B_0 = 47\mu$T. The difference between the inclination angles of $\mathbf{B}_0$ and $\mathbf{B}_{rf}$ is denoted by ϵ_0. The dashed line is the reference singlet production without RF field (lifted by 0.005 in order to be able to differentiate it from the parallel case).

on the system. The quantity that contains the information about the yield production is the population of the singlet state; we can write it as:

$$\rho_{ss}(t) = \frac{1}{2}\left(\rho_{\uparrow\downarrow}^{\uparrow\downarrow} + \rho_{\downarrow\uparrow}^{\downarrow\uparrow} - \rho_{\downarrow\uparrow}^{\uparrow\downarrow} - \rho_{\uparrow\downarrow}^{\downarrow\uparrow}\right). \tag{4.10}$$

However in a closed system it is not possible to talk about singlet yield since the chemical reaction never ends and the chemical products will recombine over and over again. In (4.1) (b) we can see the evolution of the population of the singlet state.

If we consider an anisotropic hyperfine tensor with $a_1 = a_2 \neq a_3$ the sensitivity with the magnetic field inclination is clear. In Figure 4.2 (a) and (b), we plot the evolution of Quantum discord (blue curve) and Concurrence (red curve) for $\theta = \pi/2$ and $\theta = 0$ respectively, in order to observe the behavior of quantum correlations. The variation of the angle affects the behavior of the quantum correlations: for a small angle there are going to be more sudden deaths of entanglement [103] and maxima of the concurrence

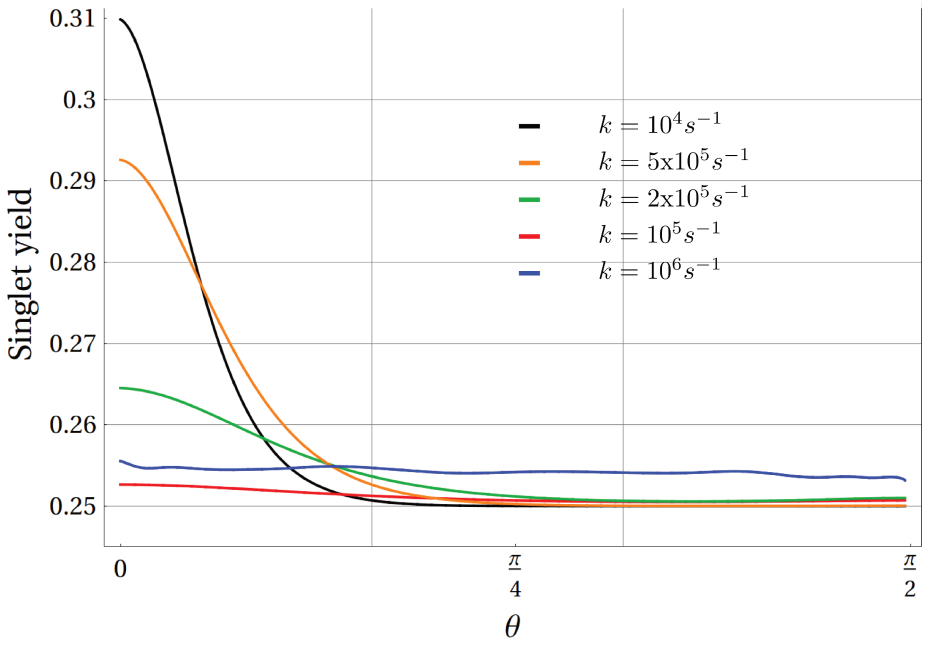

Figure 4.5: Influence of the RF field over the singlet yield production of one-proton RP subjected using different rates k.

and discord. For $\theta = \pi/2$ not only the minima and maxima have a longer period, but there are now local minima and maxima. In (4.2) (c) the singlet population for three different angles is plotted. Now it can be seen how in a closed system with an axial hyperfine tensor the populations as well as quantum correlations are affected by changes in the inclination of the magnetic field. To complete the description of a radical pair reaction we need to take into account the influence of the environment; due to its intervention the chemical reaction can end and it will be possible to talk about (singlet or triplet) yields.

4.1.2 Measurement process

To model the scape rates from singlet and triplet states to form singlet or triplet yields, i.e., to show how the singlet-triplet interconversion ends allowing the formation of anisotropic chemical products that will carry the information of the magnetic sense, we add two new *states* $|S\rangle$ and $|T\rangle$ [94] that will reduce our 8x8 density matrix for the three spins to a 2x2 density matrix with the total population of singlet states S in one of the entries of the diagonal, and the total triplet state population T in the other one.

These new states will allow us to use projector operators P_n to take the general kets $|i,n,p\rangle$ with $\{i,n,p\}$ being either $\downarrow$ or $\uparrow$, into the states $|S\rangle$ or $|T\rangle$. In other words, these projectors will allow us to make a *measurement* of the amount of singlet yield (chemical product) in the reaction. To define them we need to use the singlet-triplet base for the electronic spins defined in (3.1): $\big\{\,|s\rangle\otimes|j\rangle\,,|t_0\rangle\otimes|j\rangle\,,|t_{-1}\rangle\otimes|j\rangle\,,|t_1\rangle\otimes|j\rangle\,\big\}$, where $|j\rangle$ is the nuclear spin state $\{\uparrow,\downarrow\}$ and

$$
\begin{aligned}
&|S=0,m_S=0\rangle=|s\rangle=\frac{1}{\sqrt{2}}\Big(\,|\uparrow\downarrow\rangle-|\downarrow\uparrow\rangle\,\Big)\\
&|S=1,m_S=-1\rangle=|t_{-1}\rangle=|\uparrow\uparrow\rangle\\
&|S=1,m_S=0\rangle=|t_0\rangle=\frac{1}{\sqrt{2}}\Big(\,|\uparrow\downarrow\rangle+|\downarrow\uparrow\rangle\,\Big)\\
&|S=1,m_S=+-\rangle=|t_1\rangle=|\downarrow\downarrow\rangle\,,
\end{aligned}
$$

are the electronic spin states, where the state with total spin $S=0$ is described by $|s\rangle$ and the states with total spin $S=1$ are described by $|t_i\rangle$. In this notation i is the projection for each state $m_S=\{-1,0,1\}$. The projectors are then:

$$
\begin{aligned}
&P_{S\uparrow}=|S\rangle\langle s,\uparrow|\\
&P_{S\downarrow}=|S\rangle\langle s,\downarrow|\\
&P_{T_{-1}\uparrow}=|T\rangle\langle t_{-1},\uparrow|\\
&P_{T_0\uparrow}=|T\rangle\langle t_0,\uparrow|\\
&P_{T_1\uparrow}=|T\rangle\langle t_1,\uparrow|\\
&P_{T_{-1}\downarrow}=|T\rangle\langle t_{-1},\downarrow|\\
&P_{T_0\downarrow}=|T\rangle\langle t_0,\downarrow|\\
&P_{T_1\downarrow}=|T\rangle\langle t_1,\downarrow|\,.
\end{aligned}
$$

The strength of the process is modulated by a factor k, given in angular frequency units. If it is of the order of tens of MHz the process will end fast avoiding the interconversion; if it is less than kHz the system will be almost closed, giving unrealistic long radical pair lifetimes. Using a Lindblad-like operator we can write the measurement process as:

$$
\mathcal{L}(\rho)=\sum_{n=\{S,T\}}\frac{k}{2}\big(2P_n\rho(t)P_n^\dagger-P_n^\dagger P_n\rho(t)-\rho(t)P_n^\dagger P_n\big). \tag{4.11}
$$

As with any projector it is easy to show that $P_n^\dagger P_n = P_n P_n^\dagger = P_n$, and the previous equation is now:

$$\mathcal{L}(\rho) = \sum_{n=\{S,T\}} \frac{k}{2}\big(2P_n\rho(t)P_n^\dagger - P_n\rho(t) - \rho(t)P_n\big), \tag{4.12}$$

and the master equation is:

$$\partial_t\rho(t) = -i\Big[\hat{H}, \rho(t)\Big] + \mathcal{L}(\rho(t)). \tag{4.13}$$

As was done in the previous section we use generic states of the tripartite system on $\mathcal{L}(\rho)$ to get a generic equation that can be added to (4.7) to solve the dynamic; a matrix element for our Lindblad-like operator is:

$$\begin{aligned}\mathcal{L}(\rho)^{jmq}_{inp} = (k/8)\Big(&2(1+4pn)\Big(\delta_{q\beta}\delta_{m\alpha}\rho^{j\beta\alpha}_{inp} + \delta_{q\alpha}\delta_{m\beta}\rho^{j\alpha\beta}_{inp}\Big)\\ &+ 2\delta_{p\beta}\delta_{n\alpha}\Big(2\delta_{q\beta}\delta_{m\alpha}\rho^{j\beta\alpha}_{i\beta\alpha} + 2\delta_{q\alpha}\delta_{m\beta}\rho^{j\alpha\beta}_{i\beta\alpha} + (1+4qm)\rho^{jmq}_{i\beta\alpha}\Big)\\ &+ 2\delta_{p\alpha}\delta_{n\beta}\Big(2\delta_{q\beta}\delta_{m\alpha}\rho^{j\beta\alpha}_{i\alpha\beta} + 2\delta_{q\alpha}\delta_{m\beta}\rho^{j\alpha\beta}_{i\alpha\beta} + (1+4qm)\rho^{jmq}_{i\alpha\beta}\Big)\\ &+ (-3+4pn+4q(1+4pn)m)\rho^{jmq}_{inp}\Big).\end{aligned} \tag{4.14}$$

Using both Eq. (4.7) and Eq. (4.14) we can now talk about a *singlet yield*. In Figure 4.3 we can see the result of the angle variation of the field using an axial hyperfine tensor $\big(g_e\mu_B/\hbar\big)A = \big(g_e\mu_B/\hbar\big)diag(a_1, a_1, a_2)$, with $a_2 = 2a_1$; first we choose one angle θ, solve the master equation, and pick the singlet population when the dynamic has arrived at the steady state. This steady state represents the end of the interconversion process (the end of the chemical reaction leaving only triplet and singlet chemical products). In Figure 4.3 we can see how a difference in the strength of the measurement process can affect the singlet production. We used three different decay rates k in MHz. If the decay rate is $k = 1$MHz the singlet and triplet states are going to have little time to interact, and the reaction is going to end soon, being the time of singlet production $\sim 50\mu s$; the yields are going to be produced faster and there is no angular sensitivity to talk about: the remains are insensitive products that are going to start a neurophisiological travel in order to say to the brain of the bird that the inclination of the field is different. It is necessary the emphasize that the amount of singlet yield is not as important as the difference of it with different angles. These results are opposite to those presented in

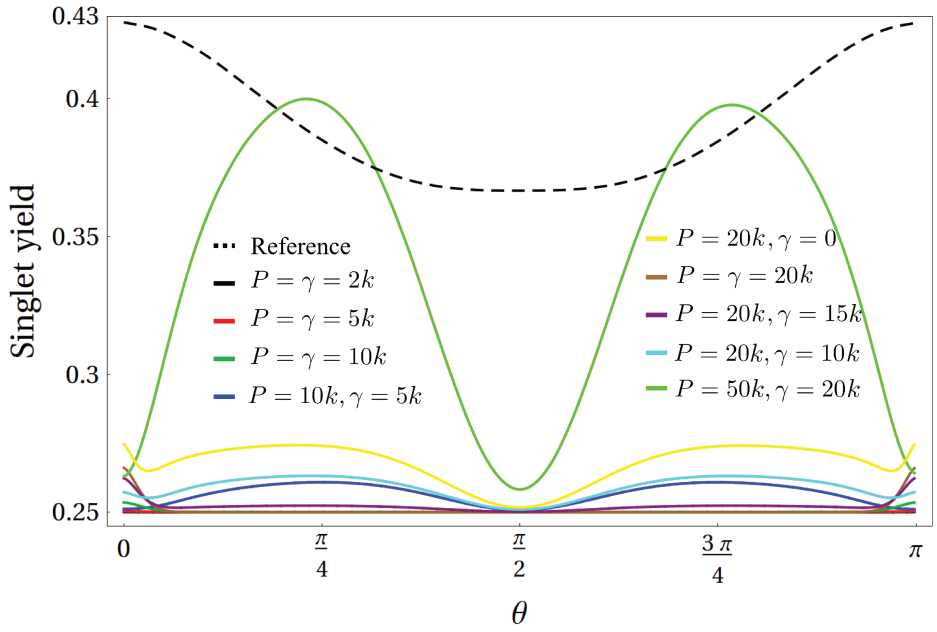

Figure 4.6: One-proton RP subject to a RF field using different rates P and γ. The dashed line represents the yield production of the system without environmental noise, using a rate $k = 0.001$MHz for the measurement process in all the cases, $B_{rf} = 150$nT, $B_0 = 47\mu$T and $\upsilon_{rf} = 1.317$MHz.

[94], where the authors found that a bigger decay rate k implied a singlet production more sensitive to changes in the inclination angle. The other two measurement rates depicted in the Figure, $k = 0.1$MHz and $k = 0.01$MHz, have a lifetime of $\sim 150\mu s$ and $\sim 1000\mu s$ respectively. We can only suppose that there is enough time for orientation-sensitive yields being produced at the end of the reaction; to be sure we can use one of the experimental discoveries described in Chapter 1 and Section 2.4: the elimination of the magnetic sense applying a radio frequency magnetic field [36, 37]. Using the Earth's magnetic field given by Eq. (2.15) and the RF field in EQ. (2.33) the new Zeeman term became

$$\begin{aligned}\hat{H}_Z &= \frac{g_e\mu_B}{\hbar}\mathbf{B}\cdot(\hat{\mathbf{S}}_1+\hat{\mathbf{S}}_2)\\ &= \frac{g_e\mu_B}{\hbar}\Big(B_0\big(\sin\theta\hat{e}_x+\cos\theta\hat{e}_z\big)\\ &+ B_{rf}\cos\omega_{rf}t\big(\sin\varphi\hat{e}_x+\cos\varphi\hat{e}_z\big)\Big)\cdot(\hat{\mathbf{S}}_1+\hat{\mathbf{S}}_2).\end{aligned}$$

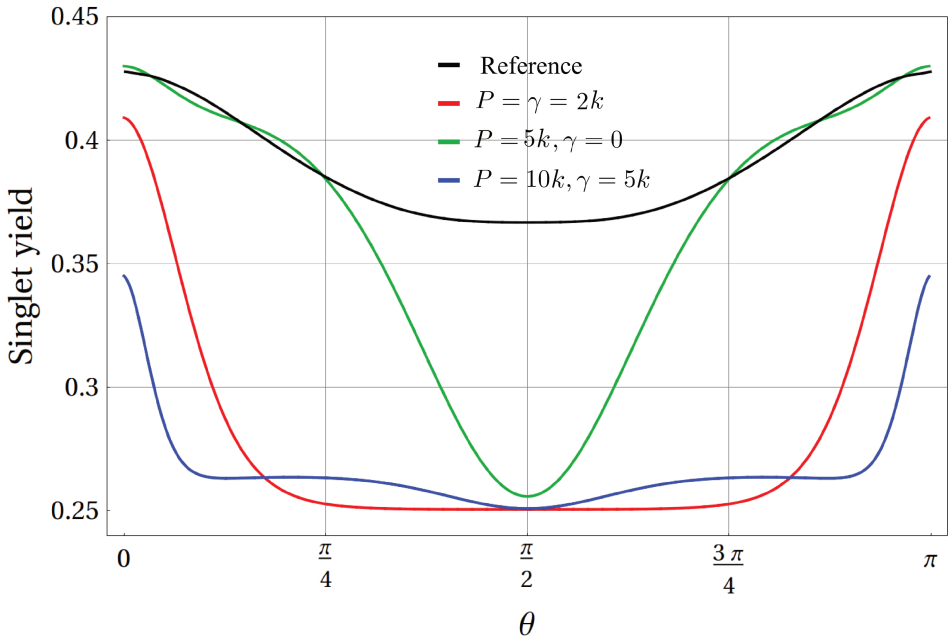

Figure 4.7: Angle sensitivity of isotropic hamiltonians with $k = 0.01$MHz caused by environmental-induced asymmetries. We used different strengths for the decoherence process: *Green curve*: decoherence rates of $P = 0, \gamma = 5k$. *Red curve*: $P = \gamma = 2k$ and *Blue curve*: $P = 10k, \gamma = 5k$. In absence of anisotropies in the hamiltonian a decoherence process or environmental noise can give the asymmetries the compass needs to work correctly. The *Black curve* in the Figure is a reference state: a singlet initial conditions with anisotropic hyperfine tensor, measurement rate $k = 0.01$MHz and $P = \gamma = 0$.

In Figure 4.4 the influence of the RF field over the singlet yield production is shown. The frequency of the RF field is $\varphi_{rf} = \omega_{rf}/s\pi = 1.317$ MHz and its magnitude is $B_{rf} = 150$nT; the magnitude of the magnetic field of the Earth is $B_0 = 47\mu$T. The difference between the inclination angles of $\mathbf{B}_0$ and $\mathbf{B}_{rf}$ (see Figure 2.5) is denoted by ϵ_0. For angle differences of $\epsilon_0 = 48°$ or $\epsilon_0 = 90°$ there are no variations in the singlet yield for any inclination angle of $\mathbf{B}_0$. For $\epsilon_0 = 24°$ there are less sensitivity but the disruption of the compass is not complete. Finally, when both fields are parallel the RF field does not exert any influence over the yield sensitivity.

This is a useful experimental fact: any model proposed have to be in agreement with the disruption of the magnetic sense when a RF field with the appropriate frequency and inclination angle is applied. In Figure 4.5 the one-proton radical pair is subjected to a RF

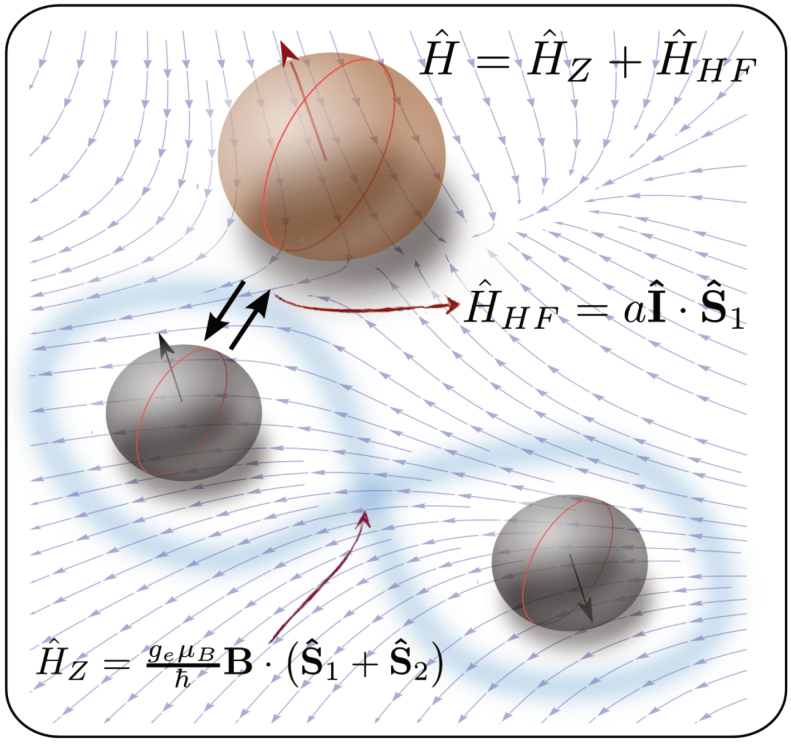

Figure 4.8: Schematic view of the one-proton radical pair where the nucleus and its unpaired electron interact by means of an isotropic hyperfine term, and the interconversion between singlet and triplet states is mediated by the Zeeman influence over the electronic spins. The anisotropy needed by the RP is induced by environmental noise.

field using different rates k. For measurement processes with rates over $k = 10^5 s^{-1}$ the sensitivity in the yield production to changes in the inclination angle does not disappear, in contradiction with the experiment; in all the following calculations we are going to use $k = 10^5 s^{-1}$ for the measurement process rate. It is possible to obtain a graphic representation of the anisotropy in the RP model expanding the singlet yield as a sum of spherical harmonics. The coefficients of such a expansion may have relevant information about the behavior of the asymmetry in the avian compass. In Appendix (B) the steps to obtain the spherical harmonic expansion of the singlet yield are shown, as well as the polar representation of the anisotropy in the compass for four sets of different parameters.

4.2 Alternative sources of anisotropy

One of the main results of our work was to show that there are reliable sources of anisotropy *outside* the Hamiltonian; given any of these sources we could get a magnetic sense in a one-proton radical pair with an *isotropic* hyperfine tensor.

4.2.1 Environmental noise

In an open environment such as the eye of the bird, it seems natural to have a faster decoherence than that suspected in previous works [93, 94, 104]. We can model the environmental influence, e.g., dipole interactions, distance fluctuations between the radical pairs or any other spin-related interaction, proposing a suitable noise processes that leaves untouched the energy of the system. We proposed the operator $\hat{R}$, defined as:

$$\hat{R} = \hat{S}_{+1} \otimes \hat{S}_{-2} \otimes \mathbb{I}, \tag{4.15}$$

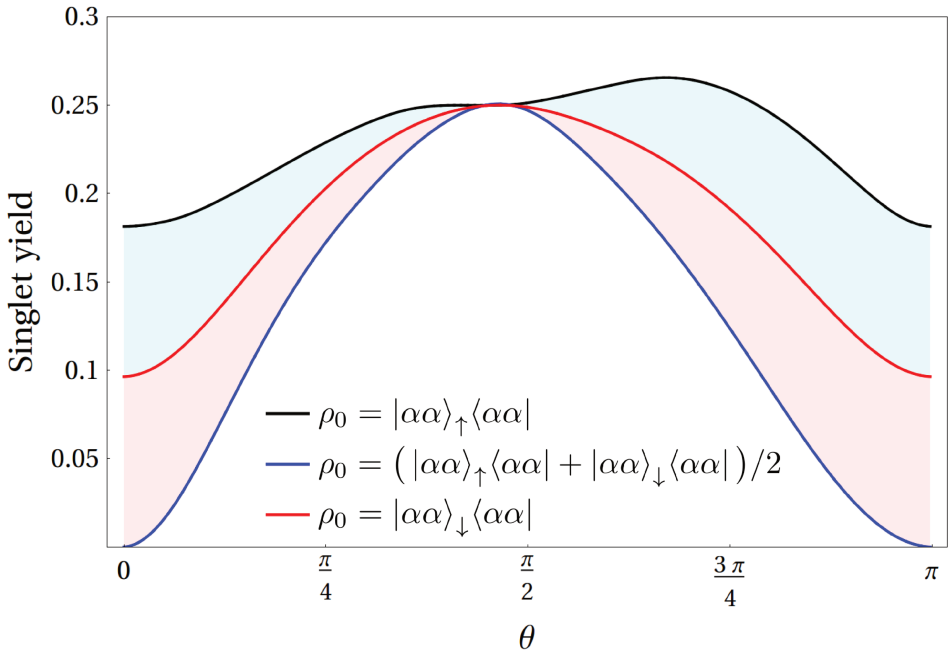

Figure 4.9: Angle sensitivity for non singlet or triplet initial conditions, specifically $\rho_0 = |\alpha\alpha\rangle\langle\alpha\alpha|$. Black: nuclear spin initially set to $|\uparrow\rangle$. Blue: nuclear spin initially set to a mixed state $\left(|\uparrow\rangle + |\downarrow\rangle\right)/\sqrt{2}$. Red: nuclear spin initially set to $|\downarrow\rangle$.

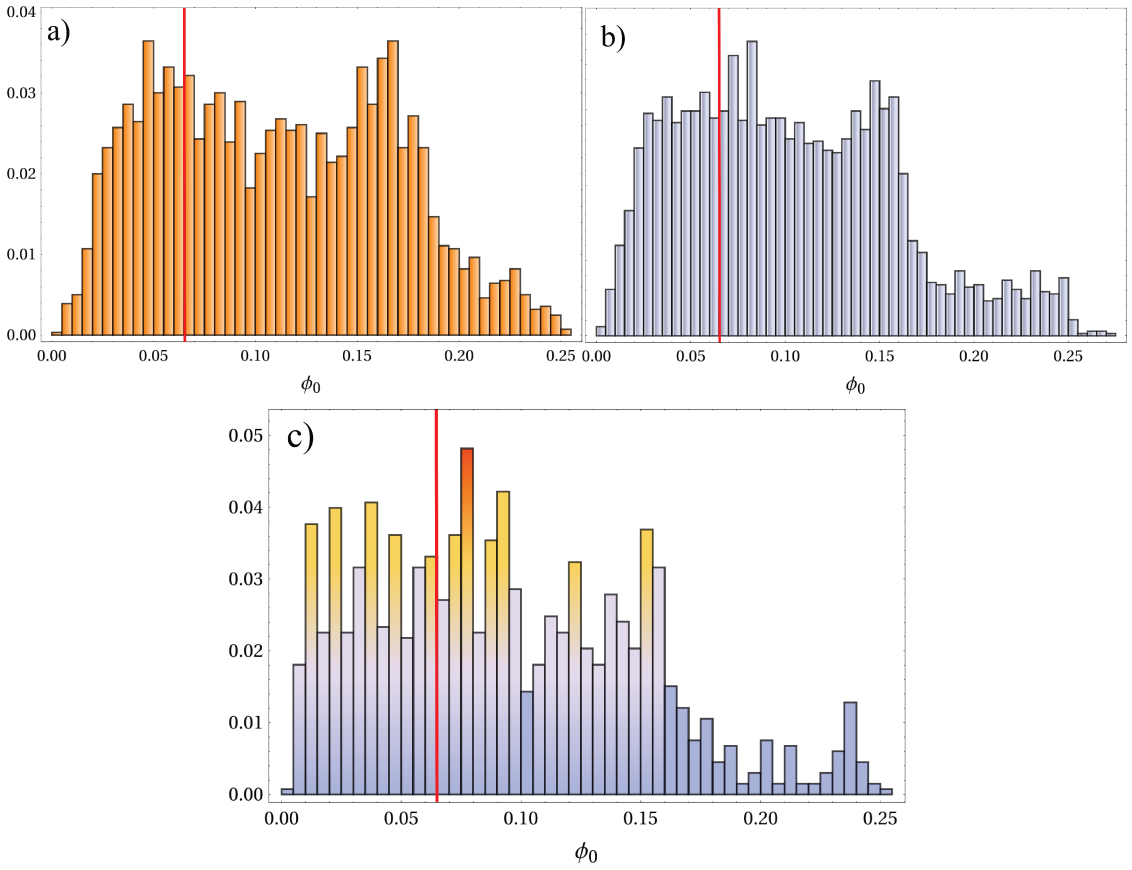

Figure 4.10: Histogram of thousands of random initial conditions. The evolution was driven by an anisotropic hyperfine tensor in Equation (4.18), and environmental anisotropy was avoid setting the decoherence processes off, i.e., $P = \gamma = 0$. a) Real off-diagonal entries in ρ_0. b) Complex off-diagonal entries in ρ_0. c) Random populations or diagonal entries in ρ_0.

where $\hat{S}_{\pm,\{1,2\}}$ are the ladder operators for spins 1 and 2 respectively, tensored with the 2x2 identity matrix of the nuclear spin space. The role of this operator is to flip spins $|{\downarrow\uparrow}\rangle \leftrightarrow |{\uparrow\downarrow}\rangle$, making the states $|{\uparrow\uparrow}\rangle$ and $|{\downarrow\downarrow}\rangle$ zero. In this way we can intensify the interconversion between singlet and triplet states introducing an environment-induced asymmetry previously inexistent. One of the advantages of using a master equation formalism is that we can add in a simple way any environmental influence using a

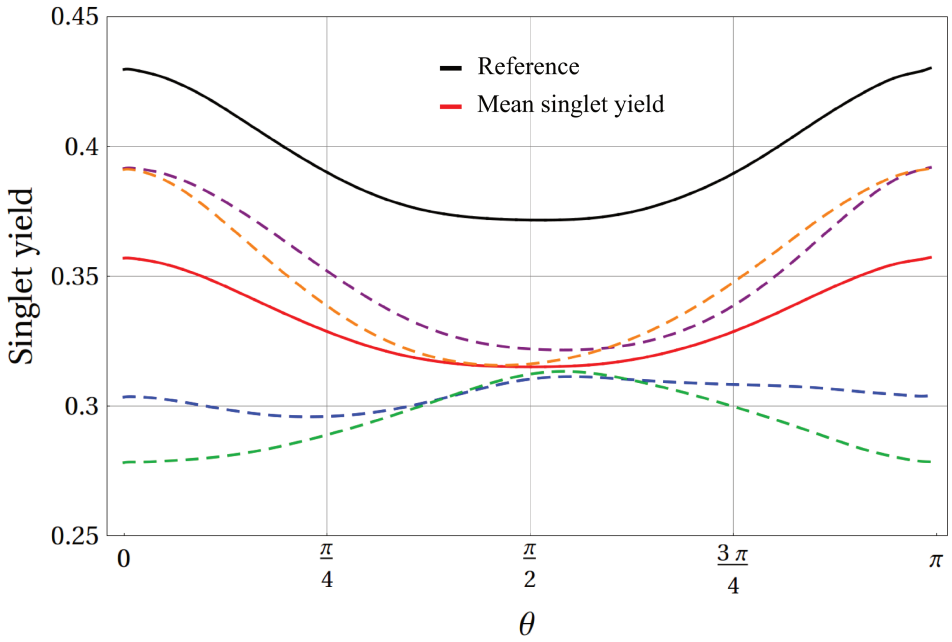

Figure 4.11: Perturbations in a singlet initial condition with an anisotropic hyperfine tensor without environmental noise. The red curve represents the mean of several hundreds of perturbed singlet initial conditions compared with the unperturbed singlet initial condition (black curve). The dashed lines are four random yields taken from the sample.

Lindblad superoperator (3.32) [86, 87]:

$$\begin{aligned}\mathcal{L}_1(\rho) = &\frac{P}{2}\left(2\hat{R}^\dagger\rho(t)\hat{R} - \hat{R}\hat{R}^\dagger\rho(t) - \rho(t)\hat{R}\hat{R}^\dagger\right) \\ &+ \frac{\gamma}{2}\left(2\hat{R}\rho(t)\hat{R}^\dagger - \hat{R}^\dagger\hat{R}\rho(t) - \rho(t)\hat{R}^\dagger\hat{R}\right).\end{aligned} \tag{4.16}$$

Equation (4.16) has the form of a *decay* process mediated by the rate P plus a *pumping* process mediated by the rate γ, both in frequency units. In this way we avoid a drastic preferred direction of the interconversion between singlet and triplet states. When both rates are equal only the coherences in the reduced density matrix are going to be affected; if they are different, there is going to be a small contribution to the populations $\rho^{\alpha\beta}_{\alpha\beta}$ and $\rho^{\beta\alpha}_{\beta\alpha}$. A matrix element for our Lindblad-like operator $\mathcal{L}_1(\rho)$ is:

$$\begin{aligned}\mathcal{L}_1(\rho)^{jmq}_{inp} = &\frac{P}{2}\left(2\delta_{p\alpha}\delta_{n\beta}\delta_{q\alpha}\delta_{m\beta}\rho^{i\alpha\beta}_{j\alpha\beta} - \delta_{q\beta}\delta_{m\alpha}\rho^{inp}_{j\alpha\beta} - \delta_{p\beta}\delta_{n\alpha}\rho^{i\alpha\beta}_{jmq}\right) \\ &+ \frac{\gamma}{2}\left(2\delta_{p\beta}\delta_{n\alpha}\delta_{q\beta}\delta_{m\alpha}\rho^{i\beta\alpha}_{j\beta\alpha} - \delta_{q\alpha}\delta_{m\beta}\rho^{inp}_{j\beta\alpha} - \delta_{p\alpha}\delta_{n\beta}\rho^{i\beta\alpha}_{jmq}\right).\end{aligned} \tag{4.17}$$

Finally, taking into account the one-proton Hamiltonian (2.14) and the Lindblad operators (4.12) and (4.16) we arrive at our final master equation:

$$\begin{aligned}\partial_t\rho(t) &= -i\Big[\hat{H},\rho(t)\Big] + \mathcal{L}(\rho(t)) + \mathcal{L}_1(\rho(t)) \\ &= -i\Big[\hat{H},\rho(t)\Big] + \sum_n \frac{k}{2}\big(2P_n\rho(t)P_n - P_n\rho(t) - \rho(t)P_n\big) \\ &\quad + \frac{P}{2}\big(2\hat{B}^\dagger\rho(t)\hat{B} - \hat{B}\hat{B}^\dagger\rho(t) - \rho(t)\hat{B}\hat{B}^\dagger\big) \\ &\quad + \frac{\gamma}{2}\big(2\hat{B}\rho(t)\hat{B}^\dagger - \hat{B}^\dagger\hat{B}\rho(t) - \rho(t)\hat{B}^\dagger\hat{B}\big).\end{aligned} \tag{4.18}$$

In Figure 4.6 we test the allowed values of the rates P and γ applying a RF field to the radical pair model. The dashed line represents the yield production of the system without environmental noise, using a rate $k = 0.001$MHz for the measurement process. As with the measurement process the expected behavior is the insensitivity of the singlet yield production under changes in the inclination angle of the magnetic field. Whenever the rates are equal, i.e. $P = \gamma$, the sensitivity will only be there for few angles. A most interesting behavior emerges when both rates are different, indicating an asymmetric production of singlet (or triplet) yield. The asymmetry in the rates transforms the maxima of singlet yield in $\theta = 0$ and $\theta = \pi$ into minima, and two new maxima appear at $\theta = \pi/4$ and $\theta = 3\pi/4$. A similar behavior of incorrect orientation was observed under two different circumstances: continued exposure to red light [105] and application of pulsed magnetic fields [35]. A substantial orientation only appears when the difference between the rates is of at least $10k$; any choice of rates P and γ under this assumption will produce a behavior in agreement with experimental data. When there is a fast enough decoherence process present in the master equation, like the processes mediated by P and γ, the angular sensitivity of the radical pair yield production is strengthen. If the hamiltonian is isotropic, with singlet or triplet initial conditions, the expected behavior is an absence of change in the production rates of the yields and there is going to be sensitivity only if there is a decoherence process present. This can be understood as another class of anisotropy induced by the environment, which chooses a preferred direction for the system through the dissipation. This can open the search of a suitable chemical species responsible for the RP creation, because the molecule does not need to have anisotropic hyperfine or Zeeman interactions, and the degree of entanglement is not going to be crucial; in other words, the molecule originating the radical pair

can be subjected to rotational or diffusional motion, given that the preservation of the anisotropy of the hyperfine tensor is not a requirement anymore. The only requirement for the correct functionality of the compass is then the decoherence, which is a must in such an open system. In Figure 4.7 the singlet yield production with an isotropic hyperfine tensor and different values for the rates P and γ can be seen. In Figure 4.8 we can see a schematic view of the system in the presence of environmental noise with an isotropic hyperfine tensor.

4.2.2 Classical correlated initial conditions

Following the discussion in Ref. [93] the initial state in the radical pair mechanism is not a perfect singlet (or triplet) state. However, due to the nature of the reaction itself it will not start in a complete uncorrelated state. This raises the question about the robustness of the mechanism when this inherent randomness in the initial state is taking into account. Using initial separable states in the radical pair master equation (4.18) with only *classical correlations*, as well as an isotropic hyperfine tensor, we showed that the inclination sensitivity of the singlet yield will be still present. As an example, an initial state without coherences, such as:

$$\rho_0 = \frac{1}{2}\big(|\alpha\beta\rangle \langle\alpha\beta| + |\beta\alpha\rangle \langle\beta\alpha| \big), \tag{4.19}$$

gives an appreciable change in the yields (and therefore allows sensitivity) for different angles θ. This can be seen in the blue curve in Figure 4.9. In the absence of either an explicit anisotropy in the hyperfine tensor, in the g electronic factor or an anisotropy produced by the environment, the sensitivity depends on the *inhomogeneity* of the populations in the density matrix. An initial state like $\rho_0 = |\alpha\alpha\rangle \langle\alpha\alpha|$, where the state $|\alpha\alpha\rangle$ belongs to the space of the two electronic spins $\mathcal{H}_1 \otimes \mathcal{H}_2$, will produce a lower but still appreciable angle sensitivity. More interesting is that it generates a different distribution for the singlet yield depending on the nuclear spin state, as it is shown in the red and black curves in Figure 4.9. This implies a preferred direction of the reaction path based on the states of the spins prior to the beginning of the yield production, and shows us that the randomness in the singlet (or triplet) initial state will strengthen rather than weaken the inclination angle sensitivity of the radical pair. To get a better idea of the robustness of the asymmetric yield production of the radical pair mechanism, we generate several thousands of the 8x8 initial density matrix; in the evolution we let

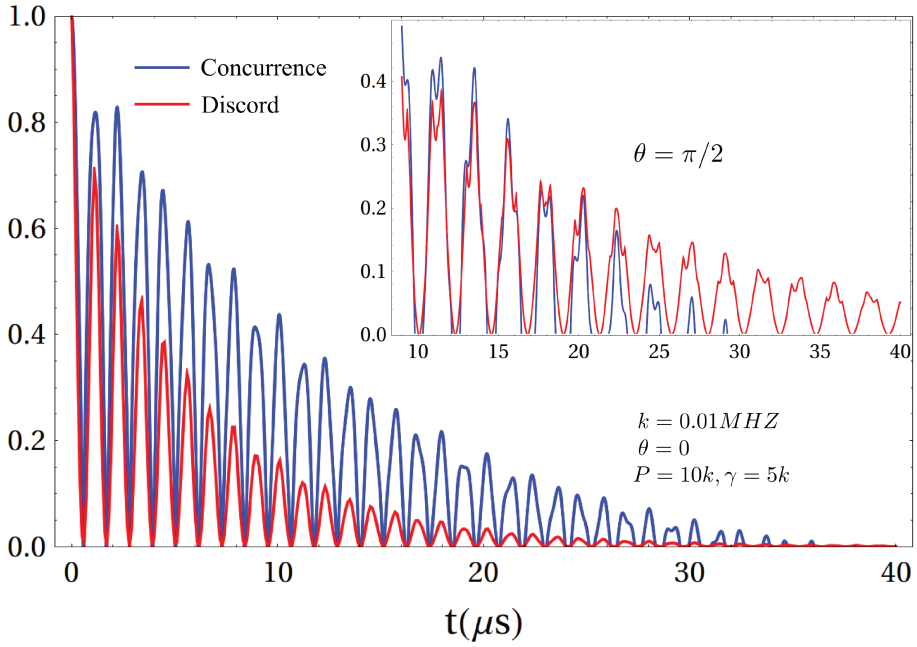

Figure 4.12: Concurrence an Quantum Discord evolution for different values of the magnetic field inclination angles. Measurement rate $k = 0.01MHz$, and dissipation rates $P = 10k$, $\gamma = 2k$, with and angle $\theta = 0$; in the inset an angle of $\theta = \pi/2$ was used.

the hyperfine tensor in Equation (4.18) to be anisotropic, and to avoid environmental anisotropy we set the decoherence processes off, i.e., $P = \gamma = 0$. To quantify the *amount* of sensitivity we define a simple quantity ϕ_0, as:

$$\phi_0 = \max(\Phi_s) - \min(\Phi_s), \tag{4.20}$$

where Φ_s is the singlet yield for a specific set of initial conditions. The results can seen in the Histogram (4.10). The red line in the three graphics represents the difference ϕ_0 generated by a radical pair with anisotropic hyperfine tensor and singlet initial condition. In the three sets of initial density matrices we can see that the sensitivity is the most usual phenomena; this is not entirely surprising, as we already saw that even an unentangled initial state without explicit anisotropies can generate yield asymmetries; moreover, this reinforces the idea that the working of the compass will be strengthen by a non-entirely quantum correlated initial state. A more realistic approach would be to make perturbations in a singlet initial condition with an anisotropic hyperfine tensor and without environmental noise. In this way we can model a great number of

non-interacting radical pairs to average the singlet yield production. The red curve in Figure 4.11 represent the mean of several hundreds of perturbed singlet initial conditions. We can verify that the mechanism is not susceptible to disturbance of the initial state, as the differences in the yield production remain unchanged when compared with the unperturbed singlet radical pair (black curve in the Figure). The dashed lines are four random yields taken from the sample. Its interesting to note that even if some of them are not symmetric about $\theta = \pi/2$, like the green and blue curves in the Figure, the mean is still symmetric, i.e., insensitive to polarization changes in the magnetic field of the Earth. These numeric experiments lead us to the final topic of this Chapter: the role of quantum correlations in the avian compass.

4.3 Quantum correlations in the Avian Compass

The sources of *anisotropy* found in the previous section will help us answer one of the most elusive questions about the radical pair model: the role of quantum correlations in the working of the avian compass. This question arises in biological systems that can be explained by means of quantum mechanics, such as the test of quantumness and role of entanglement in photosynthesis [106–108]. Some of the measures of quantum correlations between the unpaired electrons of the radical pair mechanism have shown that entanglement is preserved over times of hundreds of microseconds [93, 94]. However, it seems natural to have a faster decoherence if we take into account the very likely wildness of the environment surrounding the RP. A simple test to our hypothesis was made using the process defined in Section 4.2.1 with two sets of parameters in the system: a measurement rate $k = 0.1MHz$ and dissipation rates $P = \gamma = 2k$, and a measurement rate $k = 0.01MHz$ and dissipation rates $P = 10k$, $\gamma = 2k$; the measures of Quantum Discord and Concurrence for the two sets of parameters can be seen in Figures 4.13 and 4.12. The fast loss of coherence evident in the Figures 4.13 and 4.12 is not a surprise - having an open environment like the one we can expect in the eye of the bird, should lead naturally to a fast loss of quantum correlations. Moreover, given that there is not only one radical pair producing yields at any time, using several perturbed initial singlet states as in Figure 4.11 the behavior we get is a complete lost of quantum correlations in hundreds of nano seconds. It is worth to note that the inclination angle of the magnetic field also affects the amount of quantum correlations measured by the Quantum Discord

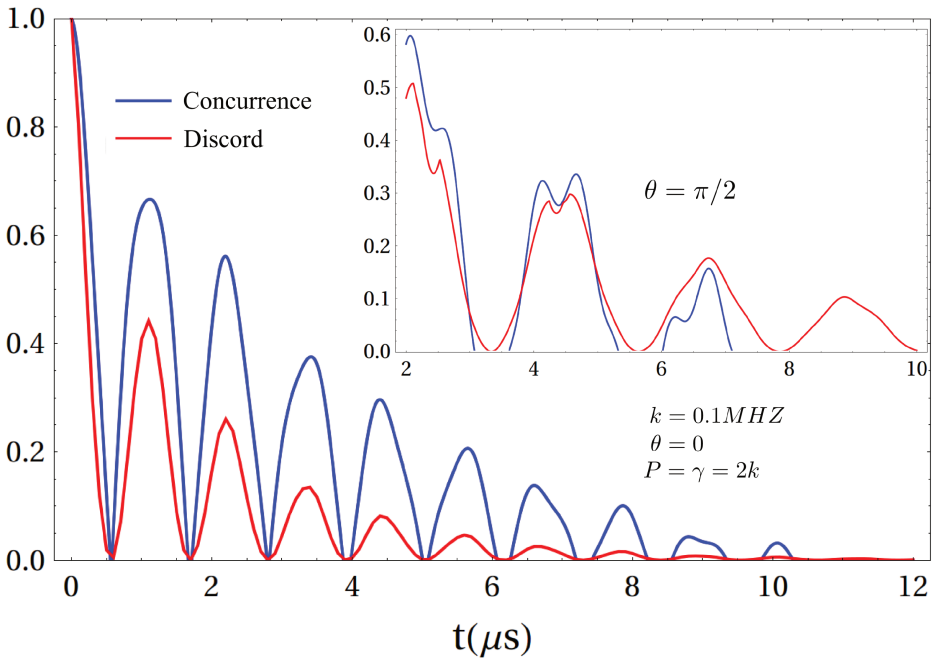

Figure 4.13: Concurrence an Quantum Discord evolution for different values of the magnetic field inclination angles. Measurement rate $k = 0.01MHz$, and dissipation rates $P = 10k$, $\gamma = 2k$, with and angle $\theta = 0$; in the inset an angle of $\theta = \pi/2$ was used. Measurement rate $k = 0.1MHz$, and dissipation rates $P = \gamma = 2k$, with and angle $\theta = 0$; in the inset an angle of $\theta = \pi/2$ was used.

and the Concurrence; for smaller angles the Concurrence values are not only higher, but predict the same time of decoherence as the Discord; however, for higher angles the entanglement is less important than the classical correlations, making the Quantum Discord to be higher and to predict longer correlation times. This can be seen more clearly in Figure 4.14, where the change of Concurrence with time and inclination angle, for P and γ fixed in the Lindblad operator (4.16), is shown. For angles less than $\theta = \pi/4$ there are going to be more collapses and revivals of entanglement, and for angles near $\pi/4$, the decoherence time are shorter than for angles near 0 and $\pi/2$. Having shown that the decoherence times are expected to be two orders of magnitude less than suspected in previous works, the remaining question is about the role of quantum correlations in the working of the compass. The discussion of the previous Section regarding classical correlated states like (4.19) gives us a hint of an answer: entanglement is not important in the production of anisotropic yields; we know that the radical pair is created in a

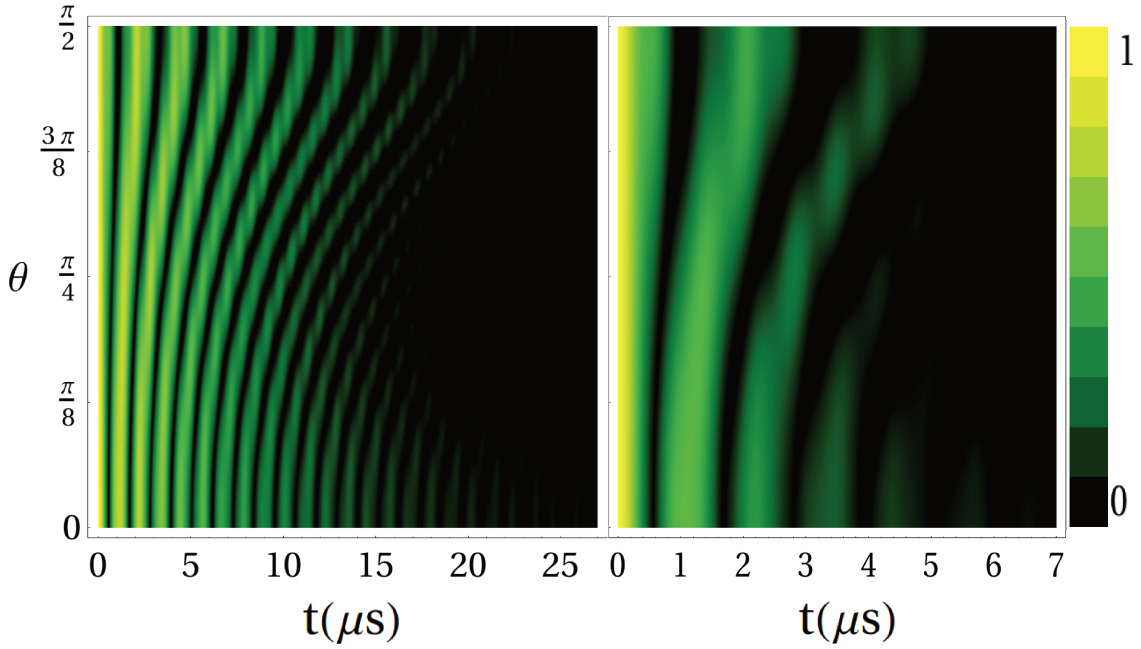

Figure 4.14: Entanglement density for different values of the rates P, γ and k, varying the angles θ of inclination of the magnetic field of the Earth ($47\mu T$). The entanglement was measured by the use of Concurrence. In the left panel, the rate values are $k = 0.01MHz$, $P = \gamma = 10k$, and in the right panel the values are $k = 0.05MHz$, $P = 10k$, $\gamma = 5k$. It's interesting to note that with smaller angles there are more entanglement sudden deaths and revivals, and that for angles around $\pi/4$ the decoherence time is shorter.

single event by a photoinduced chemical reaction, which causes the entanglement of the unpaired electronic spins of the initial state to be a consequence of the physics involved in its creation; but the sensitivity to changes in the inclination angle does not depend on the presence of quantum correlations. Even more, the difference of yields produced by states as the ones plotted in Figure 4.9, which evolve under an isotropic hamiltonian and without correlations in the initial condition, either quantum or classical, reinforce this statement. The other two numerical experiments performed in section 4.2 confirm our suspicions. In the first one, summarized in Figure 4.10 we used thousands of random initial density matrices; the conclusion is that the sensitivity to changes in the inclination angle of the magnetic field of the Earth is a more common phenomenon than the insensitivity to angle variations of the geomagnetic field. The generation of these initial conditions was thorough letting us to assure that each one was a plausible physical state. The other one, summarized in Figure 4.11 is more realistic since contains

the average yield production of several perturbed singlet initial states; this perturbation causes the initial density matrix not to be a maximal entangled one. We must emphasize that the amount of singlet production is not the important feature of the system, but the difference in that amount when a change in the inclination is performed. Considering this we see that the mean difference in the yield production remains the same, showing us that the sensitivity is robust under perturbations of the (entangled) initial state.

Chapter 5

Conclusions

The underlying mechanism that allows the existence of a magnetic sense in some birds has been debated for many years. In the $70's$ Schulten proposed that the avian compass is based on a radical pair reaction, and that a fundamental feature of such a compass would be the existence of some kind of anisotropy in the hamiltonian [45]; the most likely candidate to give the necessary anisotropy is the nuclear-electronic hyperfine interaction, which would give a dependence of the yield on the relative orientation of the magnetic field of the Earth respect to the radical pair [46].

Over the years numerous experimental evidence were found about the properties of the compass, but the underlying mechanism still remains a mystery [17, 23–25, 27, 28, 30].

In a work published in 2000, Ritz and coworkers [18] proposed the radical pair mechanism as a suitable responsible for the existence of the compass, and with that model almost all the experimental data collected over the years could be explained.

However there were some unsolved questions regarding the role of quantum correlations in the working of the compass. It was not clear at what extent the fact that the radical pair reaction started with a singlet (or triplet) state between the electronic spins could influence the generation of a compass through the production of anisotropic chemical products; works on other biological systems had shown that entanglement could be vital in the success of some biochemical reactions, such as quantum transport in photosynthesis [106–108]; this led to several works trying to solve the issue in the radical pair mechanism [93, 94, 104], but the involvement of entanglement on it remained obscure.

Facing this question we could stablish that quantum correlations are not important in the production of anisotropic yields, showing how initial states like the ones described

in Figure 4.9, evolving under an isotropic hamiltonian (i.e., without explicit anisotropies either on the hyperfine tensor or in the $g-$factor) and without correlations in the initial condition, either quantum or classical, could produce significant sensitivity in the yield when the inclination of the geomagnetic field was varied. The entanglement of the unpaired electronic spins of the initial state is a consequence of the physics involved in the creation of the pair; in other words, it is a consequence of the photochemical process involved in the creation of the pair, but the sensibility to changes in the inclination angle does not depend on the presence of quantum correlations, but on the existence of a strong enough anisotropy.

The other open question was about suitable sources of anisotropy external to the radical pair itself, i.e., due to the environment. We found two reliable sources of this anisotropy, the first one being a direct dissipation process. When there is a fast enough decoherence process, which we can make explicit in the master equation, like the processes mediated by P and γ introduced in Chapter 4, we showed that the angular sensitivity of the radical pair yield is strengthen. This class of anisotropy induced by the environment chooses a preferred direction for the system through the dissipation, making that a RP with isotropic hyperfine tensor with a singlet initial condition can produce yields that depend on the inclination of the Earth's magnetic field.

The second was based on the observation that the initial state of the system is not a perfect singlet (or triplet) state [93]. We found that any kind of correlation in the initial condition, quantum or classical, is sufficient to give an anisotropic yield production in the radical pair mechanism if the molecule has an anisotropic HF tensor; we also found that a molecule with an isotropic HF tensor can have sensitivity for variations in the field *even* if it has classically correlated, separable initial conditions. Furthermore, even if they lack any kind of correlation but have an *anisotropic* HF tensor, giving an unbalanced weight to some populations over others, we can also expect a working compass.

These two observations lead us as to an important conclusion. As discussed in [52, 53], the anisotropy present in a molecule can be averaged away if it has significant diffusive motion, or even rotations. Our findings of unexpected sources of anisotropy relax this immobility requirement opening the search for suitable molecules that can be anywhere in the eye of the bird, and that are not constrained to be fixed in the retina.

Along with this, molecules with isotropic HF tensors have proven to be more robust to environmental effects; in the presence of a RF field the control experimental data

[36, 37] shows that the compass will no longer work. However, if there is a strong enough dissipation the compass will work normally [94]. An isotropic molecule can handle higher noise magnitudes than an anisotropic one without jeopardizing control experimental data; this reinforce our proposal of an isotropic molecule with the necessary anisotropy being provided by the environmental influence or the non-perfect singlet initial condition.

Appendix A

Exchange interaction

We normally think of the radicals in a RP as separate entities. But we know that within each of them there are Coulombic forces between the electrons and their nuclei. These forces are going to determine the geometry of the radicals and their electronic structure, and are going to generate contributions to the spin Hamiltonian, characterized in the g-factor and hyperfine tensors. However this is not the whole story: for a complete treatment, we should consider also the Coulombic interactions between the electrons and nuclei on one of the radicals to the electrons and nuclei in the other, giving rise to the Exchange interaction.

To better understand what happens, let us make a simple example using a radical pair composed by two hydrogen atoms H^* [80]: When the hydrogen atoms are very close, their (electronic) wavefunctions overlap and their interaction produces two molecular orbits, known in atomic physics as bonding $1\sigma_g$ and anti-bonding $2\sigma_u^*$ states; these states are, in short, the ground states for separated electrons when the corresponding nuclei are too far apart, setting the necessary symmetry about the midpoint in the internuclear line. These are one-electron molecular wavefunctions. Now, depending on the orbital approximation, the wavefunction for the RP which is now a n-electron wavefunction, is given by a symmetrized product of these molecular orbitals. The lower energy for these configurations occurs when both electrons are in the $1\sigma_g$ molecular orbital, but according to Pauli principle this is only possible when the spins of the electrons are in a state ${}^1\Sigma_g{}^+$. The Σ states are the *zero* projection of the total electronic angular momentum on the internuclear axis. The Σ^+ states for the diatomic molecule describe the wavefunction when it is left unchanged under reflection in the plane containing the nuclei; the states Σ^- describe the wavefunction that changes sign under that operation.

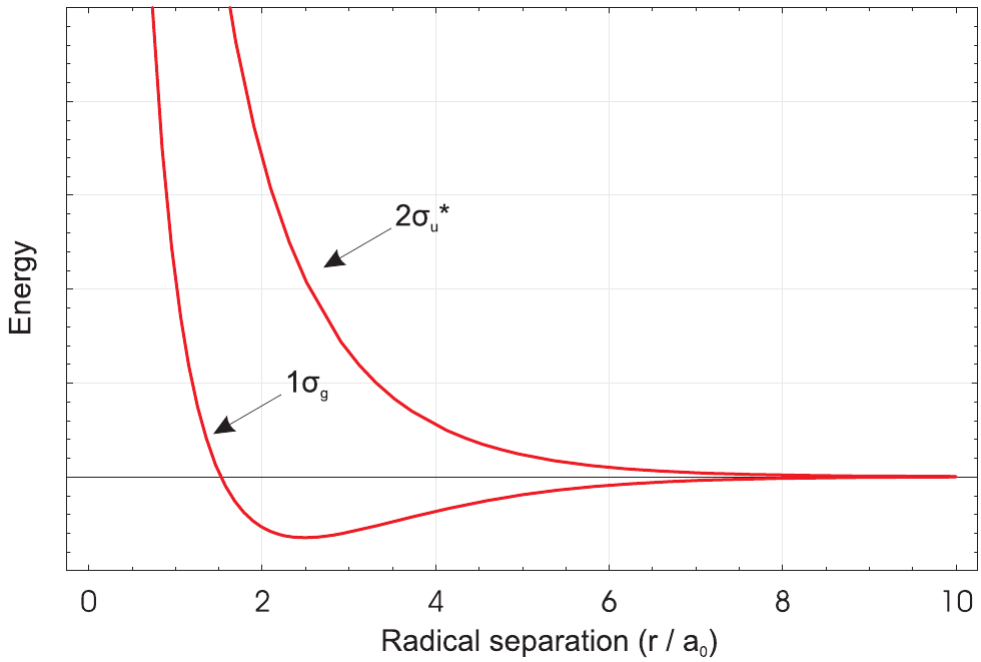

Figure A.1: First two linear combinations of atomic orbital energies for the hydrogen ion as a function of the separation between nuclei in a first approximation. See [109].

Now, for the electrons the next possible state is the $2\sigma_u^*$ molecular orbit, and the Pauli principle admits the states ${}^3\Sigma_u{}^+$ (*triplet*) and ${}^1\Sigma_u{}^+$ (*singlet*) for the diatomic molecule. We show the graphics for the energies of molecular and electronic energies for each state in Figures (A.1) and (A.2). In order to describe the spin evolution of the radical pair when the separation between radicals is enough for electron correlation and bonding effects to take place, restricting ourselves to the states mentioned before, we use the Heisenberg-Dirac-van Vleck Hamiltonian [110] for spin electronic operators in radicals 1 and 2 as

$$\hat{H}_{ex} = -J\hat{\mathbf{S}}_1 \cdot \hat{\mathbf{S}}_2, \tag{A.1}$$

where J, an empirical parameter, is such that the energy separation of the eigenstates of (A.1) is the same as the energy separation for the ground and first excited state when the Schödinger equation is solved for the molecule comprising both radicals. From Figure A.2, J is the energy between the singlet and lower triplet states. Experimental calculations of J have been made [110] even in intermolecular J [111]. However the experimental difficulty is enormous, and only some chemical species have known J values

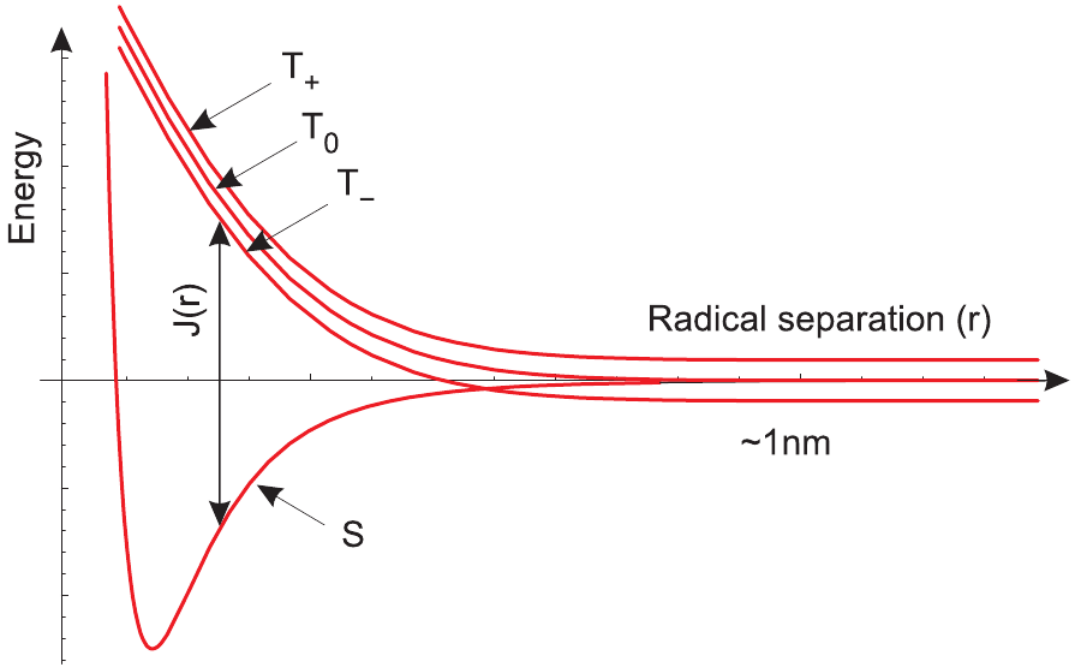

Figure A.2: Energies for the states $3\Sigma_u{}^+$ and $1\Sigma_u{}^+$ (*triplet* and *singlet*) of two hydrogen atoms varying the separation between their nuclei. If r is small, the two atoms are an effective H_2 molecule; at greater distances the radical pair description is more suitable; the splits in the triplet states are due to the Zeeman effect. See [109].

[112]. A good approximation to J is to suppose it decreases exponentially with increasing distance between the radicals in the RP and to suppose that it is independent of the relative orientation of the radicals. Within small distances this energy dominates the spin Hamiltonian's Zeeman and hyperfine terms; in other words, for small distances the Exchange interaction prevents the singlet-triplet interconversion and as a result we are going to have a *molecule* and not a radical pair. As a consequence no magnetic field effects can take place. This restricts the application of Exchange interaction, but due to the exponential decay of J with the internuclear distance, it is safe to assume it is not involved in a radical pair reaction.

Appendix B

Spherical harmonic representation

The singlet yield anisotropy, which we are going to call ρ_{SS}^{an} is obtained by subtracting from the singlet yield ρ_{SS} the spherical average singlet yield:

$$\tilde{\rho}_{SS} = \int_0^{2\pi} \int_0^{\pi} \rho_{SS} \sin\theta d\theta d\phi. \tag{B.1}$$

Using the expressions for the singlet yield anisotropy in terms of the polar angles we can get visually striking plots; this plots have a complicated structure and by eye it is not easy to find something important about the system. One way to overcome this is to decompose the singlet yield in a weighted sum of spherical harmonics, and then use the coefficients to extract information about the physics involved in the yield production. The spherical harmonics $\mathrm{Y}_l^m(\theta,\phi)$ are a well known family of special functions [113, 114] that arise naturally in physics as the angular part of solutions to Laplace's equation in spherical coordinates. They are also the eigenfunctions of the orbital angular momentum operator L^2 with eigenvalue $l(l+1)\hbar^2$, and are defined for integer values of l and m as [114]:

$$\mathrm{Y}_l^m(\theta,\phi) = e^{im\phi}\sqrt{(2l+1)\frac{(l-m)!}{(l+m)!}}P_l^m(\cos\theta). \tag{B.2}$$

Here the $P_l^m(\cos\theta)$ is the associated Legendre polynomial. The spherical harmonics form a complete orthonormal set of functions over the spherical polar coordinates (θ,ϕ) [114]:

$$\sum_{l=0}^{\infty}\sum_{m=-l}^{m=l}\left(\mathrm{Y}_l^m(\theta,\phi)\right)^*\mathrm{Y}_l^m(\theta',\phi') = \delta(\theta-\theta')\delta(\cos\phi-\cos\phi'). \tag{B.3}$$

After integration the above equation reads:

$$\int_0^{2\pi}\int_0^{\pi}\left(\mathrm{Y}_l^m(\theta,\phi)\right)^*\mathrm{Y}_{l'}^{m'}(\theta,\phi)=\delta_{ll'}\delta_{mm'}. \tag{B.4}$$

Using both results we get that an arbitrary square integrable function may be expanded as a weighted sum of spherical harmonics. We can then expand the singlet yield as:

$$\rho_{SS}=\sum_{l=0}^{\infty}\sum_{m=-l}^{m=l}a_l^m\mathrm{Y}_l^m(\theta,\phi). \tag{B.5}$$

The a_l^mh are complex numbers which can be determined by

$$a_l^m=\int_0^{2\pi}\int_0^{\pi}\left(\mathrm{Y}_l^{m'}(\theta,\phi)\right)^*\rho_{SS}. \tag{B.6}$$

The singlet yield is then completely described by the coefficients a that weight contributions from different spherical harmonics. One way to extract the coefficients (B.6) from a set of sampled singlet yield values is to use the spherical harmonic orthogonality integral. Using (B.5) and the orthogonality relation we get:

$$\begin{aligned}&\int_0^{2\pi}\int_0^{\pi}\left(\mathrm{Y}_l^m(\theta,\phi)\right)^*\rho_{SS} \\ &\qquad=\sum_{l'=0}^{\infty}\sum_{m'=-l'}^{m'=l'}a_{l'}^{m'}\left(\mathrm{Y}_l^m(\theta,\phi)\right)^*\mathrm{Y}_{l'}^{m'}\sin\theta d\theta d\phi) \\ &\qquad=\sum_{l'=0}^{\infty}\sum_{m'=-l'}^{m'=l'}a_{l'}^{m'}\delta_{ll'}\delta_{mm'}=a_l^m.\end{aligned} \tag{B.7}$$

To approximate this result we use the spherical mean function [115] and approximate the integral as a Riemann sum; a general function f will be

$$\bar{f}=\frac{1}{4\pi}\int_0^{2\pi}\int_0^{\pi}f(\theta,\phi)\sin\theta d\theta d\phi)\approx\sum_k w_k f(\theta_k,\phi_k). \tag{B.8}$$

Using this the coefficient a will read:

$$a_l^m\approx\sum_k w_k\left(\mathrm{Y}_l^m(\theta_k,\phi_k)\right)^*\rho_{SS}(\theta_k,\phi_k). \tag{B.9}$$

To get a good approximation we must evaluate this formula for each coefficient until they become negligible; this happens fast for the set of hyperfine tensors we used, becoming of

order 10^{-5} for $l = 34$. However the computational cost is considerable: for each pair of angles (θ, ϕ) we have to calculate the singlet yield until the reaction is finished and there are not any more oscillations; for a rough grid of $(90, 180)$ this implies 16200 systems of differential equations, each one consisting of 36 coupled equations.

A possible use to the coefficients a_l^m could be create a statistic to measure anisotropy with changes of the magnetic field. As was said in Chapter 1, the European robin is able to orientate with field strengths near to that of the Earth (50μT), but fail to orientate with 34μT and 60μT [25]. So, trying to understand the amount of anisotropy by means of the coefficients a_l^m under variations of the field could be possible. Knowing that $\langle \hat{L}^2 \rangle = l(l+1)\hbar^2$, we can consider the quantity

$$\langle \hat{l}^2 \rangle = \sum_{lm} |a_l^m|^2 l(l+1). \tag{B.10}$$

This could be useful because spherical harmonics are an irreducible representation of the rotation group, and this implies that $\sum_m |a_l^m|^2$ is invariant under rotations. However any calculation of this statistic would imply an incredible amount of computational time, and its results are beyond the purpose of this these.

In Figure B.1 we can see the polar plots obtain for four different sets of hyperfine tensors. In c) the hyperfine tensor was (in mT):

$$A = \begin{pmatrix} .248 & 0 & 0.05 \\ 0 & 0.2 & 0.01 \\ 0 & 0.09 & 0.252 \end{pmatrix}. \tag{B.11}$$

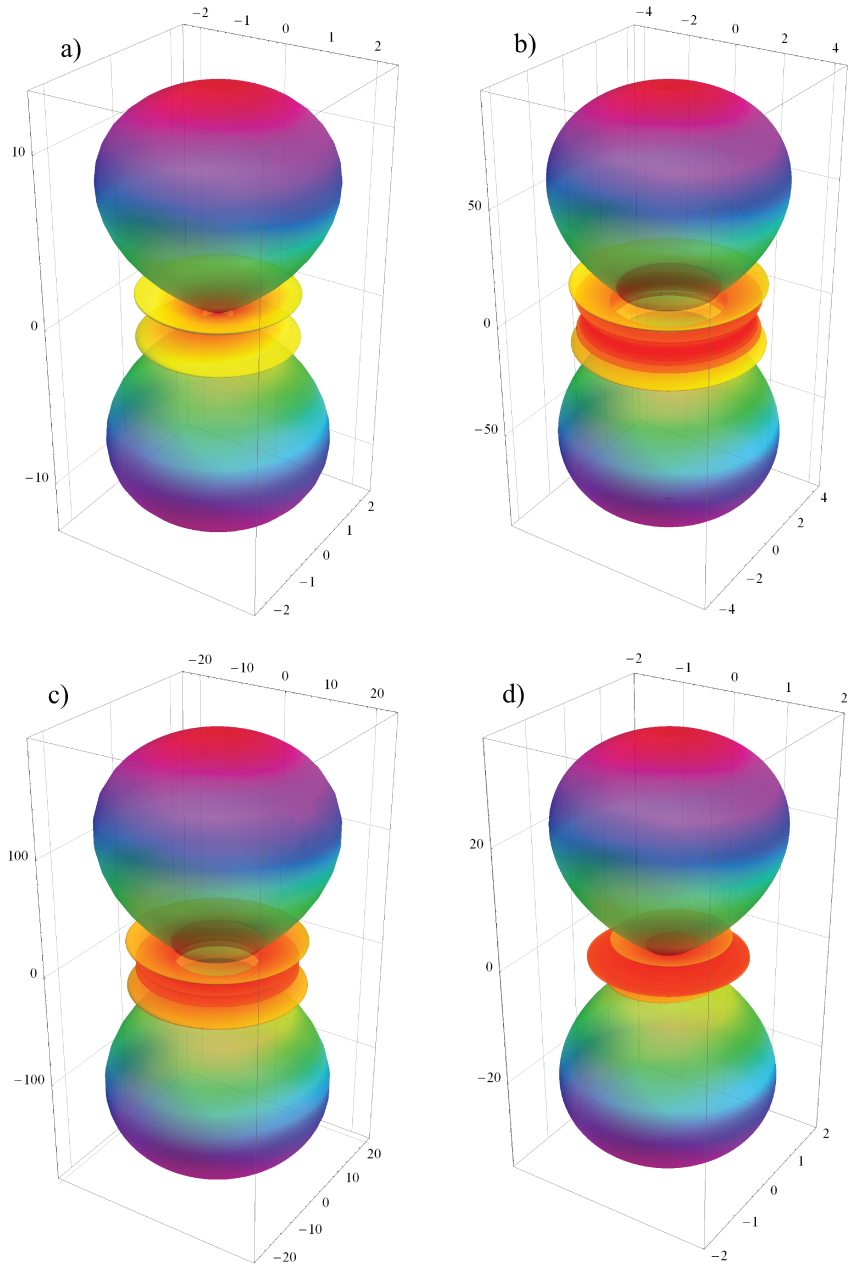

Figure B.1: Spherical harmonic decomposition plots for four sets of hyperfine tensor. In a) the hyperfine tensor was axial, with values $a_1 = a_2 = 0.1$ mT and $a_3 = 0.2$mT. In b) the hyperfine tensor was rhombic, with $a_1 = 0.1, a_2 = 0.2$ and $a_3 = 0.3$ mT. In c) the hyperfine tensor is written down in (B.11). In d) the hyperfine tensor was rhombic, with $a_1 = 0.248, a_2 = 0.2$ and $a_3 = 0.252$mT.

Bibliography

[1] U. E. Steiner and T. Ulrich. Magnetic field effects in chemical kinetics and related phenomena. *Chem. Rev.*, 89(1):51–147, 1989.

[2] H. Hayashi. *Introduction to Dynamic Spin Chemistry: Magnetic Field Effects on Chemical and Biochemical Reactions*, volume 8 of *World Scientific Lecture and Course Notes in Chemistry*. World Scientific.

[3] J. Bargon. The discovery of chemically induced dynamic polarization (cidnp). *Helvetica Chimica Acta*, 89(10), 2006.

[4] R. Kaptein and J.L. Oosterhoff. Chemically induced dynamic nuclear polarization ii: (relation with anomalous esr spectra). *Chem. Phys. Lett.*, 4(4):195 – 197, 1969.

[5] G. L. Closs. Mechanism explaining nuclear spin polarizations in radical combination reactions. *J. Am. Chem. Soc.*, 91(16):4552–4554, 1969.

[6] F. J. Adrian. Role of diffusion-controlled reaction in chemically induced nuclear-spin polarization ii. general theory and comparison with experiment. *J. Chem. Phys.*, 54(9):3912–3917, 1971.

[7] J. B. Pedersen. Diffusional aspects of spin selective reactions; fundamental quantities and relations. In *Spin Chemistry: Spin Polarization and Magnetic Field Effects in Photochemical Reactions*. The Oji International Conference on Spin Chemistry.

[8] M. Justinek, G. Grampp, S. Landgraf, P. J. Hore, and N. N. Lukzen. Electron self-exchange kinetics determined by mary spectroscopy: Theory and experiment. *J. Am. Chem. Soc.*, 126(17):5635–5646, 2004.

[9] G. Grampp, M. Justinek, and S. Landgraf. Magnetic field effects on the pyrene-dicyanobenzene system: determination of electron self-exchange rates by mary spectroscopy. *Mol. Phys.*, 100(8):1063–1070, 2002.

[10] M. K. Bowman, D. E. Budil, G. L. Closs, A. G. Kostka, C. A. Wraight, and J. R. Norris. Magnetic resonance spectroscopy of the primary state, pf, of bacterial photosynthesis. *P. Natl. Acad. Sci. USA*, 78(6):3305–3307, 1981.

[11] R. Wiltschko and W. Wiltschko. *Magnetic orientation in animals*. Springer-Verlag, Berlin, 1995.

[12] R. Blakemore. Magnetotactic bacteria. *Science*, 190(4212):377–379, 1975.

[13] J. H. Wang, S. D. Cain, and K. J. Lohmann. Identification of magnetically responsive neurons in the marine mollusc tritonia diomedea. *J. Exp. Biol.*, 206(2): 381–388, 2003.

[14] A. J. Kalmijn. Electric and magnetic field detection in elasmobranch fishes. *Science*, 218(4575):916–918, 1982.

[15] L. Brower. Monarch butterfly orientation: missing pieces of a magnificent puzzle. 199(1):93–103, 1996.

[16] R. Wiltschko and W. Wiltschko. Avian navigation: from historical to modern concepts. *Animal Behaviour*, 65(2):257 – 272, 2003.

[17] W. Wiltschko and R. Wiltschko. Magnetic orientation and magnetoreception in birds and other animals. *Journal of Comparative Physiology A: Neuroethology, Sensory, Neural, and Behavioral Physiology*, 191:675–693, 2005.

[18] T. Ritz, S. Adem, and K. Schulten. A model for photoreceptor-based magnetoreception in birds. *Biophysical journal*, 78:707 – 718, 2000.

[19] F. Cintolesi, T. Ritz, C. W. M. Kay, C. R. Timmel, and P. J. Hore. Anisotropic recombination of an immobilized photoinduced radical pair in a 50-[mu]t magnetic field: a model avian photomagnetoreceptor. *Chemical Physics*, 294(3):385 – 399, 2003.

[20] C.R. Timmel, F. Cintolesi, B. Brocklehurst, and P.J. Hore. Model calculations of magnetic field effects on the recombination reactions of radicals with anisotropic hyperfine interactions. *Chemical Physics Letters*, 334(4-6):387 – 395, 2001.

[21] T. Ritz, R. Wiltschko, P.J. Hore, C. T. Rodgers, K. Stapput, T. Thalau, C. R. Timmel, and W. Wiltschko. Magnetic compass of birds is based on a molecule with optimal directional sensitivity. *Biophys. J.*, 96(8):3451 – 3457, 2009.

[22] K. Maeda, K. B. Henbest, F. Cintolesi, I. Kuprov, , C. T. Rodgers, P. A. Liddell, D. Gust, C. R. Timmel, and P. J. Hore. Chemical compass model of avian magnetoreception. *Nature*, 453:387 – 390, 2008.

[23] W. Wiltschko and F. W. Merkel. Orientierung zugunruhiger rotkehlchen im statischen magnetfeld. *Verh. dt. zool. Ges*, 59:362367, 1966.

[24] W. Wiltschko and R. Wiltschko. Magnetic compass of european robins. *Science*, 176(4030):62–64, 1972.

[25] W. Wiltschko and R. Wiltschko. Magnetic compass orientation in birds and its physiological basis. *Naturwissenschaften*, 89:445–452, 2002.

[26] M.E. Deutschlander, J.B. Phillips, and S.C. Borland. The case for light-dependent magnetic orientation in animals. *J. Exp. Biol.*, 202(8):891–908, 1999.

[27] J. L. Kirschvink, M. M. Walker, and C. E. Diebel. Magnetite-based magnetoreception. *Current Opinion in Neurobiology*, 11(4):462 – 467, 2001.

[28] S. Johnsen and K. J. Lohmann. The physics and neurobiology of magnetoreception. *Nat Rev Neurosci*, 6(9):703–712, 2005.

[29] R. Wiltschko, K. Stapput, P. Thalau, and W. Wiltschko. Directional orientation of birds by the magnetic field under different light conditions. *J. R. Soc. Interface.*, 7(Suppl 2):S163–S177, 2010.

[30] W. Wiltschko, J. Traudt, O. Gunturkun, H. Prior, and R. Wiltschko. Lateralization of magnetic compass orientation in a migratory bird. *Nature*, 419:467 – 470, 2002.

[31] H. Mouritsen, G. Feenders, M. Liedvogel, K. Wada, and E. D. Jarvis. Night-vision brain area in migratory songbirds. 102(23):8339–8344, 2005.

[32] M. Liedvogel, G. Feenders, K. Wada, N. F. Troje, E. D. Jarvis, and H. Mouritsen. Lateralized activation of clustern in the brains of migratory songbirds. *Eur. J. Neurosci.*, 25(4):1166–1173, 2007.

[33] W. Wiltschko, K. Stapput, P. Thalau, and R. Wiltschko. Avian magnetic compass: fast adjustment to intensities outside the normal functional window. *Naturwissenschaften*, 93:300–304, 2006.

[34] T. Ritz. Quantum effects in biology: Bird navigation. *Proc. Chem.*, 3(1):262–275, 2011.

[35] W. Wiltschko and R. Wiltschko. Migratory orientation of european robins is affected by the wavelength of light as well as by a magnetic pulse. *Journal of Comparative Physiology A*, 177:363369, 1995.

[36] T. Ritz, P. Thalau, J. B. Phillips, R. Wiltschko, and W. Wiltschko. Resonance effects indicate a radical-pair mechanism for avian magnetic compass. *Nature*, 429: 177–180, 2004.

[37] P. Thalau, T. Ritz, K. Stapput, R. Wiltschko, and W. Wiltschko. Magnetic compass orientation of migratory birds in the presence of a 1.315mhz oscillating field. *Naturwissenschaften*, 92:86–90, 2005.

[38] M. J. M. Leask. A physicochemical mechanism for magnetic field detection by migratory birds and homing pigeons. *Nature*, 267(5607):144–145, 1977.

[39] A.R. Liboff and K.A. Jenrow. New model for the avian magnetic compass. *Bioelectromagnetics*, 21(8):555–565, 2000.

[40] D. T. Edmonds. A sensitive optically detected magnetic compass for animals. *Proceedings of the Royal Society of London. Series B: Biological Sciences*, 263 (1368):295–298, 1996.

[41] J. C. Montgomery and M. M. Walker. Orientation and navigation in elasmobranchs: Which way forward? *Environmental Biology of Fishes*, 60:109–116, 2001.

[42] M.G. Paulin. Electroreception and the compass sense of sharks. *Journal of Theoretical Biology*, 174:325–339(15), 1995.

[43] C. D. Treiber, M. C. Salzer, J. Riegler, N. Edelman, C. Sugar, M. Breuss, P. Pichler, H. Cadiou, M. Saunders, M. Lythgoe, J. Shaw, and D. Keays. Clusters of iron-rich cells in the upper beak of pigeons are macrophages not magnetosensitive neurons. *Nature*, 484:367 – 370, 2012.

[44] H.-J. Werner, Z. Schulten, and K. Schulten. Theory of the magnetic field modulated geminate recombination of radical ion pairs in polar solvents: Application to the pyrene–n,n-dimethylaniline system. *The Journal of Chemical Physics*, 67(2): 646–663, 1977.

[45] K. Schulten, C. E. Swenberg, and A. Weller. A biomagnetic sensory mechanism based on magnetic eld modulated coherent electron spin motion. *Zeitschrift fuer Physikalische Chemie Neue Folge*, 111:1–5, 1978.

[46] K. Schulten and A. Windemuth. Model for a physiological magnetic compass. In J. Kiepenheuer G. Maret and N. Boccara, editors, *Biophysical effects of steady magnetic elds*, volume 25, page 99106. Springer-Verlag, 1986.

[47] C. B. Grissom. Magnetic field effects in biology: A survey of possible mechanisms with emphasis on radical-pair recombination. *Chemical Reviews*, 95(1):3–24, 1995.

[48] B. Brocklehurst. Magnetic fields and radical reactions: recent developments and their role in nature. *Chem. Soc. Rev.*, 31:301–311, 2002.

[49] B. Brocklehurst and K. A. McLauchlan. Free radical mechanism for the effects of environmental electromagnetic fields on biological systems. *Int. J. Radiat. Biol.*, 69:3–24, 1996.

[50] J. M. Canfield, R. L. Belford, and P. G. Debrunner. Calculations of earth-strength steady and oscillating magnetic field effects in coenzyme b12 radical pair systems. *Molecular Physics*, 89, 1996.

[51] S. G. Boxer, C. E. D. Chidsey, and M. G. Roelofs. Magnetic field effects on reaction yields in the solid state: An example from photosynthetic reaction centers. *Annual Review of Physical Chemistry*, 34(1):389–417, 1983.

[52] S. G. Boxer, C. E. D. Chidsey, and M. G. Roelofs. Dependence of the yield of a radical-pair reaction in the solid state on orientation in a magnetic field. *Journal of the American Chemical Society*, 104(9):2674–2675, 1982.

[53] S. G. Boxer, C. E. D. Chidsey, and M. G. Roelofs. Anisotropic magnetic interactions in the primary radical ion-pair of photosynthetic reaction centers. *Proceedings of the National Academy of Sciences*, 79(15):4632–4636, 1982.

[54] Y. Liu, R. Edge, K. Henbest, C. R. Timmel, P. J. Hore, and P. Gast. Magnetic field effect on singlet oxygen production in a biochemical system. *Chem. Commun.*, (2):174–176, 2005.

[55] J. C. Weaver, T. E. Vaughan, and R. D. Astumian. Biological sensing of small field differences by magnetically sensitive chemical reactions. *Nature*, 405(6787): 707–709, 2000.

[56] A. Sancar. Structure and function of dna photolyase and chryptochrome blue-light photoreceptors. *Chem. Rev.*, 103(6):22032238, 2003.

[57] C. L. Partch and A. Sancar. Photochemistry and photobiology of cryptochrome blue-light photopigments: The search for a photocycle. *Photochemistry and Photobiology*, 81(6):12911304, 2005.

[58] L. E. Foley, R. J. Gegear, and S. M. Reppert. Human cryptochrome exhibits light-dependent magnetosensitivity. *Nat. Commun.*, 2(356), 2011.

[59] I. A. Solovyov, H. Mouritsen, and K. Schulten. Acuity of a cryptochrome and vision-based magnetoreception system inbirds. *Biophys. J.*, 99(1):40–49, 2010.

[60] A. R. Cashmore, J. A. Jarillo, Y.-J. Wu, and D. Liu. Cryptochromes: Blue light receptors for plants and animals. *Science*, 284(5415):760–765, 1999.

[61] M. Ahmad, P. Galland, T. Ritz, R. Wiltschko, and W. Wiltschko. Magnetic intensity affects cryptochrome-dependent responses in arabidopsis thaliana. *Planta*, 225:615–624, 2007. ISSN 0032-0935.

[62] M. S. Freedman, R. J. Lucas, B. Soni, M. von Schantz, M. Muoz, Z. David-Gray, and R. Foster. Regulation of mammalian circadian behavior by non-rod, non-cone, ocular photoreceptors. *Science*, 284(5413):502–504, 1999.

[63] A. Sancar. Regulation of the mammalian circadian clock by cryptochrome. *J. Biol. Chem.*, 279(33):34079–34082, 2004.

[64] Y. Huang, R. Baxter, B. S. Smith, C. L. Partch, C. L. Colbert, and J. Deisenhofer. Crystal structure of cryptochrome 3 from arabidopsis thaliana and its implications for photolyase activity. *P. Natl. Acad. Sci. USA*, 103(47):17701–17706, 2006.

[65] C. A. Brautigam, B. S. Smith, Z. Ma, M. Palnitkar, D. R. Tomchick, M. Machius, and J. Deisenhofer. Structure of the photolyase-like domain of cryptochrome 1 from arabidopsis thaliana. *P. Natl. Acad. Sci. USA*, 101(33):12142–12147, 2004.

[66] F. Müller. Free flavins: synthesis, chemical and physical properties. In F. Müller, editor, *The Chemistry and Biochemistry of Flavoenzymes*, volume 1, page 171. CRC Press, Boca Raton, 1991.

[67] P. F. Heelis. The photochemistry of flavins. In F. Müller, editor, *The Chemistry and Biochemistry of Flavoenzymes*, volume 1, page 171193. CRC Press, Boca Raton, 1991.

[68] B. Giovani, M. Byrdin, M. Ahmad, and K. Brettel. Light-induced electron transfer in a cryptochrome blue-light photoreceptor. *Nat. Struct. Mol. Biol.*, 10(6):489 – 490, 2003.

[69] A. Möller, S. Sagasser, W. Wiltschko, and B. Schierwater. Retinal cryptochrome in a migratory passerine bird: a possible transducer for the avian magnetic compass. *Naturwissenschaften*, 91:585–588, 2004. ISSN 0028-1042.

[70] H. Mouritsen, U. Janssen-Bienhold, M. Liedvogel, G. Feenders, J. Stalleicken, P. Dirks, and R. Weiler. Cryptochromes and neuronal-activity markers colocalize

in the retina of migratory birds during magnetic orientation. *P. Natl. Acad. Sci. USA*, 101(39):14294–14299, 2004.

[71] H. Mouritsen, G. Feenders, M. Liedvogel, K. Wada, and E. D. Jarvis. Magnetoreception and its use in bird navigation. *P. Natl. Acad. Sci. USA*, 102(23):8339–8344, 2005.

[72] T. Ritz, M. Ahmad, H. Mouritsen, R. Wiltschko, and W. Wiltschko. Photoreceptor-based magnetoreception: optimal design of receptor molecules, cells, and neuronal processing. *J. R. Soc. Interf.*, 7(Suppl 2):S135–S146, 2010.

[73] A. Abragam and M. H. L. Pryce. Theory of the nuclear hyperfine structure of paramagnetic resonance spectra in crystals. *Proc. Roy. Soc. A*, 205(1080):135–153, 1951.

[74] M. H. L. Pryce. A modified perturbation procedure for a problem in paramagnetism. *Proc. Roy. Soc. A*, 63(1):25, 1950.

[75] M. H. Levitt. *Spin Dynamics: Basics of Nuclear Magnetic Resonance*. Wiley, 2001.

[76] P.W. Atkins and R.S. Friedman. *Molecular Quantum Mechanics*. Oxford Unversity Press, 1997.

[77] N. M. Atherton. *Principles of Electron Spin Resonance*. Ellis Horwood Series in Physical Chemistry, 1993.

[78] R. R. Ernst, G. Bodenhausen, and A. Wokaun. *Principles of Nuclear Magnetic Resonance in One and Two Dimensions*. Oxford Unversity Press, 7 edition, 1988.

[79] A. R. O'Dea, A. F. Curtis, N. J. B. Green, C. R. Timmel, and P. J. Hore. Influence of dipolar interactions on radical pair recombination reactions subject to weak magnetic fields. *J. Phys. Chem. A*, 109(5):869–873, 2005.

[80] B. H. Bransden and C. J. Joachain. *Physics of Atoms and Molecules*. Longman Scientific and Technical, 1991.

[81] P.J. Efimova, O.; Hore. Role of exchange and dipolar interactions in the radical pair model of the avian magnetic compass. *Biophys. J.*, 94:1565 – 1574, 2008.

[82] D. M. Brink and G. R. Satchler. *Angular Momentum*. Oxford University Press, 3 edition, 1994.

[83] B. Brocklehurst. Spin correlation in the geminate recombination of radical ions in hydrocarbons. part 1.-theory of the magnetic field effect. *J. Chem. Soc., Faraday Trans. 2*, 72:1869–1884, 1976.

[84] C. R. Timmel, U. Till, B. Brockelehurst, K. A. Mclauchlan, and P. J. Hore. Effects of weak magnetic fields on free radical recombination reactions. *Mol. Phys.*, 95: 71–89, 1998.

[85] V. O. Saik, A. E. Ostafin, and S. Lipsky. Magnetic field effects on recombination fluorescence in liquid iso-octane. *J. Chem. Phys.*, 103(17), 1995.

[86] M. A. Nielsen and I. L. Chuang. *Quantum Computation and Quantum Information: 10th Anniversary Edition*. University Press, Cambridge, 2010.

[87] H.P. Breuer and F. Petruccione. *The theory of open quantum systems*. Oxford University Press, 2002.

[88] C. Gardiner and P. Zoller. *Quantum Noise*. Springer Berlin - Heidelberg, 2004.

[89] U. Weiss. *Quantum Dissipative Systems*. World Scientific, 1999.

[90] W.H. Steeb and Y. Hardy. *Problems and Solutions in Quantum Computing and Quantum Information*. World Scientific, 2004.

[91] C. H. Blanchard. Density matrix and energy–time uncertainty. *American Journal of Physics*, 50(7):642–645, 1982.

[92] M. O. Scully and M. S. Zubairy. *Quantum Optics*. Cambridge University Press, 1997.

[93] J. Cai, G. G. Guerreschi, and H. J. Briegel. Quantum control and entanglement in a chemical compass. *Phys. Rev. Lett.*, 104(22):220502, 2010.

[94] E. M. Gauger, E. Rieper, J. J. L. Morton, S. C. Benjamin, and V. Vedral. Sustained quantum coherence and entanglement in the avian compass. *Phys. Rev. Lett.*, 106 (4):040503, 2011.

[95] J. Gruska and H. Imai. Power, puzzles and properties of entanglement. In *Machines, Computations, and Universality*, volume 2055 of *Lecture Notes in Computer Science*, pages 25–68. Springer Berlin Heidelberg, 2001.

[96] F. Mintert, A.R.R. Carvalho, M. Kuś, and A. Buchleitner. Measures and dynamics of entangled states. *Physics Reports*, 415(4):207 – 259, 2005.

[97] K. Zyczkowski, P. Horodecki, A. Sanpera, and M. Lewenstein. Volume of the set of separable states. *Phys. Rev. A*, 58(2):883–892, 1998.

[98] G. Vidal and R. F. Werner. Computable measure of entanglement. *Phys. Rev. A*, 65(3):032314, 2002.

[99] W. K. Wootters. Entanglement of formation of an arbitrary state of two qubits. *Phys. Rev. Lett.*, 80(10):2245–2248, 1998.

[100] H. Ollivier and W. H. Zurek. Quantum discord: a measure of the quantumness of correlations. *Phys. Rev. Lett.*, 88(1):017901, 2001.

[101] G. Adesso and A. Datta. Quantum versus classical correlations in gaussian states. *Phys. Rev. Lett.*, 105:030501, 2010.

[102] S. Luo. Quantum discord for two-qubit systems. *Phys. Rev. A*, 77:042303, 2008.

[103] M. P. Almeida, F. de Melo, M. Hor-Meyll, A. Salles, S. P. Walborn, P. H. Souto Ribeiro, and L. Davidovich. Environment-induced sudden death of entanglement. *Science*, 316(5824):579–582, 2007.

[104] J. Cai, F. Caruso, and M. B. Plenio. Quantum limits for the magnetic sensitivity of a chemical compass. *Phys. Rev. A*, 85:040304, 2012.

[105] W. Wiltschko, A. Möller, M. Gesson, C. Noll, and R. Wiltschko. Light-dependent magnetoreception in birds: analysis of the behaviour under red light after pre-exposure to red light. *J. Exp. Biol.*, 207(7):1193–1202, 2004.

[106] M. Sarovar, A. Ishizaki, G. R. Fleming, and K. B. Whaley. Quantum entanglement in photosynthetic light-harvesting complexes. *Nat. Phys.*, 6:462 – 467, 2010.

[107] C.-M. Li, N. Lambert, Y.-N. Chen, G.-Y. Chen, and F. Nori. Witnessing quantum coherence: from solid-state to biological systems. *Nat. Phys.*, 2, 2012.

[108] M. M. Wilde, J. M. McCracken, and A. Mizel. Could light harvesting complexes exhibit non-classical effects at room temperature? *Proc. R. Soc. A*, 466(2117): 1347–1363, 2010.

[109] P. Atkins and J. de Paula. *Atkins Physical Chemistry*. Oxford Unversity Press, 7 edition, 2002.

[110] F. Illas, I. P. R. Moreira, C. de Graaf, and V. Barone. Magnetic coupling in biradicals, binuclear complexes and wide-gap insulators: a survey of ab initio wave function and density functional theory approaches. *Theoretical Chemistry Accounts*, 104:265–272, 2000.

[111] J. Abe, T. Sano, M. Kawano, Y. Ohashi, M. M. Matsushita, and T. Iyoda. Epr and density functional studies of light-induced radical pairs in a single crystal of a hexaarylbiimidazolyl derivative. *Angewandte Chemie International Edition*, 40 (3):580–582, 2001.

[112] L. E. Sinks, E. A. Weiss, J. M. Giaimo, and M. R. Wasielewski. Effect of charge delocalization on radical ion pair electronic coupling. *Chemical Physics Letters*, 404:244 – 249, 2005.

[113] M. E. Rose. *Elementary Theory of Angular Momentum*. Dover Publications Inc., 1995.

[114] G. B. Arfken and Hans J. W. *Mathematical Methods for Physicists*. Harcourt Academic Press, 5 edition, 2001.

[115] K. K. Sabelfeld and I. A. Šalimova. *Spherical Means for Pdes*. V.S.P. Intl Science, 1 edition, 1997.